Establishment of a cell-based anti-prion compound screen and analysis of host response to prion infection in cerebellar organotypic slice cultures

Dissertation
zur
Erlangung des Doktorgrades (Dr. rer. nat.)
der
Mathematisch-Naturwissenschaftlichen Fakultät
der
Rheinischen Friedrich-Wilhelms-Universität Bonn

vorgelegt von

Catharina Zielinski geb. Pleschka

aus Neuss

Bonn 2019

Angefertigt mit Genehmigung der Mathematisch-Naturwissenschaftlichen Fakultät der Rheinischen Friedrich-Wilhelms-Universität Bonn

1. Gutachter: Prof. Dr. Ina Vorberg
2. Gutachter: Prof. Dr. Jörg Höhfeld

Tag der Promotion:
29.11.2018
Erscheinungsjahr: 2019

Table of contents

Summary

Prions are unconventional infectious agents that cause always fatal neurodegenerative diseases termed prion disease or transmissible spongiform encephalopathies in mammals. Prion diseases are caused by an accumulation of the misfolded, aggregated host encoded prion protein (PrP). The normal, cellular, α-helix rich isoform (PrP^{C}) is converted into the disease-associated β-sheet rich pathogenic isoform (PrP^{Sc}). PrP^{Sc} can adopt multiple conformations that likely encipher prion strain characteristics. Currently, prion therapeutic clinical trials lack success and there is an urgent need for novel therapeutics. The aim of this study was to develop a cell-based assay for high content screening of large compound libraries with an automated microscope to identify compounds that might impair prion replication. Furthermore, identified compounds should be tested on prion infected organotypic slice cultures to test whether *in vitro* detected anti-prion compounds are also effective in a more complex neuronal environment. Additionally, two promising compounds, FeTMPyP and PIM-B31, identified by our collaboration partner Emiliano Biasini (University of Trento), were tested *ex vivo*. Beside this a comparative study of host response between *ex vivo* and *in vivo* should evaluate the transferability between the two systems, as this has not been was not shown until now. In the established screen 152 compounds were tested, 84 had an inhibitory effect on PrP^{Sc} accumulation in persistently infected $N2a^{22L}$ cells and the seven strongest inhibitors were further validated by western blot analysis. The most promising candidate, PHA665752, was tested *ex vivo* and showed a reduction of PrP^{Sc} accumulation that was however not significant. FeTMPyP showed strong toxicity and PIM-B31 showed inconsistent results that depended on different concentration and strain-specificity. Beside this, pathway analysis of *ex vivo* and *in vivo* infected mouse cerebella with different strains at various time points was performed with DAVID 6.8, an online bioinformatics resource. Analysis of the 250 most significant differentially expressed genes revealed that several comparable pathways were changed due to prion infection in brain slices and brains. The calcium signaling pathways and neuroactive ligand-receptor pathways were deregulated the most by prion infection *ex vivo* as well as *in vivo*.

1 Introduction

1.1 The origin of prions

At the latest since the BSE crisis in Europe during the 1980s and 1990s a major part of the western population has heard of prions (1). But: what are prions? How do they propagate and how do prions cause prion diseases? Prions are unconventional infectious agents that cause slowly developing, always fatal neurodegenerative diseases, called prion diseases or TSEs (transmissible spongiform encephalopathies) that affect many mammalian species. Prion diseases were first documented as early as 1750 by Leopold (2), who recognized sheep suffering from this disease and already noted its infectious nature. In the following centuries different transmission routes were described and some authors suggested the coexistence of infected and non-infected animals or a spontaneous origin of the disease (2, 3). Others proposed a hereditary predisposition, transmission by asymptomatic animals and the existence of hereditary and non-hereditary forms was assumed (2, 3). In 1954, prion diseases were described as a slow-virus disease due to the remarkably long incubation time (4), though no virus could be isolated from prion diseased individuals. Additionally, the causative agent could not be inactivated by methods that were used for nucleic acid destruction like heat, nuclease treatment and UV-radiation. The unusually small size of the agent and the fact that methods that can be used to destroy proteins, namely hydrolysis and protein denaturation, were capable of destroying prions led to the suggestion that the agent might be a protein (5-7). This hypothesis was supported as Prusiner purified a protein from a prion-infected hamster brain that was not found in an uninfected hamster brain. It was described as a 27 - 30 kDa, proteinase K resistant protein. The amount of protein correlated with the titer of the agent (8). Prusiner postulated that this protein is the predominant if not sole component of the infectious particles, which he named “prion” (small **pro**teinaceous **in**fectious particle). According to the protein-only hypothesis, which states that the cellular prion protein (PrP^C) can undergo conformational changes to a misfolded isoform that then in turn serves as template for continuous conversion of prion proteins to their misfolded isoforms in the absence of any coding nucleic acid (8). For this novel finding he was awarded the Nobel Prize of medicine in 1997. Further investigation showed a more detailed description of the prion protein.

1.2 The prion protein

1.2.1 The *PRNP* gene and biosynthesis of PrP

The prion protein (PrP) is expressed in skeletal muscle, kidney, heart, secondary lymphoid organs and the central nervous system (CNS). In the CNS PrP^C is highly expressed in synaptic membranes of neurons and in astrocytes. In the periphery PrP^C is particularly expressed in lymphocytes and in follicular dendritic cells (9).

PrP is encoded by the *PRNP* gene located on chromosome 20 in humans and on chromosome 2 in mice (10). It is a highly conserved gene that shows homology of approximately 80 % from amphibians to mammals. In humans *PRNP* consists of 2 exons, whereas *PRNP* in mice is composed of 3 exons. The last exon encodes the open reading frame (ORF) and the 3´untranslated region (UTR). The ORF codes for 253 amino acid residues (aa) in humans and 254 aa in mice (11, 12) (Figure 1 A). The amino-terminus of the ORF encodes for a signal peptide (aa 1 – 22) responsible for translocation of the primary translation product to the endoplasmatic reticulum (ER) (Figure 1 B). Aa 51 – 90 contain the octapeptide repeat region, which is supposed to be important for copper binding (9) and could be involved in prion pathogenesis (13). The hydrophilic charged cluster is followed by the hydrophobic core (aa 111 – 134) that is important during conversion processes (14). The carboxy-terminus contains the membrane anchor region at aa 231 – 254.

The amino-terminus of the matured cellular prion protein (Figure 1 C) is cleaved after the signal peptide region by a signal peptidase in the ER. The amino-terminus is flexible and unstructured (aa 22-121) (15, 16). Complex carbohydrates can be linked to two asparagine residues (in humans aa 181 and 197, in mice aa 180 and 196) resulting in un-, mono- and diglycosylated PrP^C (17). Furthermore, an intramolecular disulfide bond is formed between two cysteine residues (in humans aa 179 and 214, in mice aa 178 and 213) (18). The folded domain contains three α-helixes and a short two stranded β-sheet and is linked to the membrane with a glycosylphosphatidylinositol (GPI) anchor (19, 20).

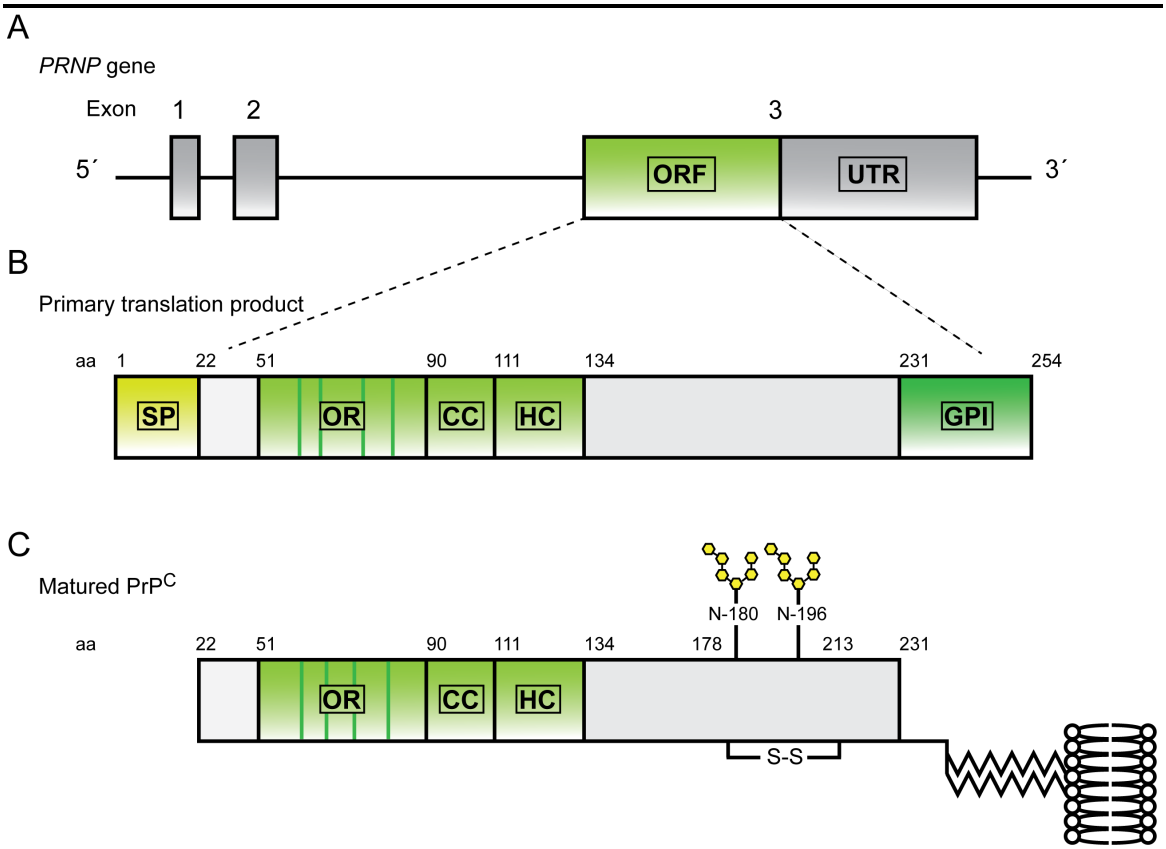

Figure 1. Structure of murine *PRNP* gene, the primary translation product and matured PrP^C. (A) The murine *PRNP* gene consists of 3 exons. Exon 1 and 2 are non-coding, exon 3 encodes for the open reading frame (ORF) and contains a 3´untranslated region (UTR). **(B)** The primary translation product contains a signal peptide (SP), the octapeptide repeat region (OR), the charged cluster (CC) and the hydrophobic core (HC), followed by a signal peptide region for attachment of the glycosylphosphatidylinositol anchor (GPI). aa = amnio acid. **(C)** In the matured PrP^C both signal peptides are cleaved (SP and GPI) and the carboxy-terminus is covalently linked to a phospholipid bilayer via a GPI anchor. Two complex carbohydrates can be linked to two asparagine residues and an intramolecular disulfide bond is formed between two cysteine residues.

PrP^C is translated on the surface of the rough ER and passes through the Golgi apparatus to the cell surface (21). Within the ER and the Golgi, the protein undergoes post-translational modification like glycosylation of two asparagine residues, formation of a disulfide bond and attachment of the GPI anchor (Figure 1 C). At the plasma membrane PrP^C is incorporated into lipid rafts and caveolae. Lipid rafts and caveolae are cholesterol and sphingolipid enriched membranes (22). Early incorporation of PrP^C into

lipid rafts appears to be crucial for correct folding of PrP^C (23). PrP^C exists as a membrane-bound, but also as an extracellular and an intracellular form. A small fraction of membrane-bound PrP^C can undergo proteolytic processing by metalloproteases, resulting in membrane-attached caboxyterminal fragments and extracellularly released aminoterminal fragments (24). Furthermore, small portions of full-length PrP^C can be released to the extracellular space either within exosomes (25) or as naked protein (26). However, PrP^C can also be found intracellularly in vesicles of the endolysosomal pathway and in multivesicular bodies (27). Beside this, a small portion of PrP^C is located in the cytosol (28) and in the nucleus, associated with chromatin (29).

1.2.2 Intracellular trafficking and physiological function of PrP^C

Membrane bound PrP^C can be readily and constitutively internalized by endocytosis induced by different external stimuli like binding of copper or stress-inducible protein 1 (STI1) (21). The internalization of PrP^C is a dynamin-dependent but GPI-anchor independent event mediated by interaction with other proteins (30). Potential interactors include laminin-receptor precursor LRP/LR, the low-density lipoprotein receptor-related protein 1 (LPR1) and glycosaminoglycans (GAGs) (31, 32). PrP^C is either directly endocytosed from lipid rafts (Figure 2 3a) (33) or it is first translocated out of the raft (Figure 2 3b) (34). Endocytosis can occur clathrin-dependently and independently. Internalized PrP^C is either transported by early endosomes (EE), before it is degraded (Figure 2 6) via the endolysosomal pathway or it is transferred rapidly and directly to recycling endosomes (RE) and transported back to the cell surface (Figure 2 5) (35).

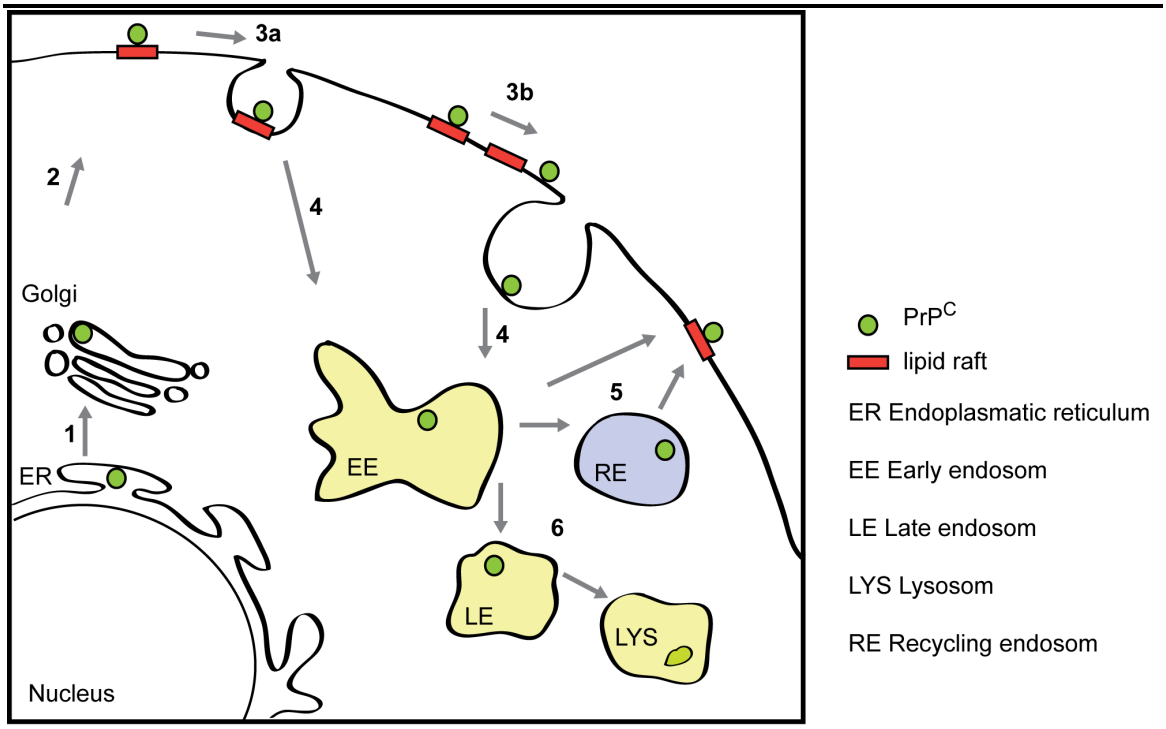

Figure 2. Endocytosis of PrP^C and intracellular trafficking. PrP^C is translated on the surface of the endoplasmatic reticulum **(1)** and passes through the Golgi apparatus **(2)** to the plasma membrane where it is incorporated into lipid rafts. Membrane-bound PrP^C is either internalized from lipid rafts **(3a)** or translocated out of the rafts and endocytosed **(3b)**. Internalized PrP^C is transported to the early endosome **(4)** and either transferred to recycling endosomes and transported back to the cell surface **(5)** or degraded by the lysosome **(6)**. Based on Grassmann et al (21).

Many physiological functions of PrP^C have been suggested, but its exact function is still elusive. PrP knockout mice do not show phenotypical deficits but are resistant to prion disease (36). However, some knockout mice show changes in circadian rhythm (37) and a mild cognitive deficit could be observed (38). PrP knockout studies also point to a possible role of PrP^C in neurotransmission (37) and showed that PrP^C is sensitive to oxidative stress (39). As PrP^C has a high affinity to metal ions the capacity of copper binding has been attributed to PrP^C (40). Furthermore, involvement in immnuoregulation, signal transduction, synaptic transmission, cell adhesion, cell cycle regulation and differentiation, microRNA metabolism and neuroprotection have been suggested (41). Neuronal apoptosis was detected in the hippocampus and cerebellum when anti-PrP

antibodies were intracranially delivered, which suggests a possible role of PrP^C in the control of neuronal survival (42). In conclusion, PrP^C might exert several functions and could be involved in diverse cellular processes. However, regardless of its physiological function, conversion of PrP^C into its pathogenic form results in neurodegeneration.

1.3 Pathogenic isoform of PrP

The key event in prion disease is the conversion of the α-helix rich cellular prion protein (PrP^C) into the β-sheet rich pathogenic isoform PrP^{Sc}. The conversion can occur sporadically, upon infectious transmission and can be due to mutations in the *PRNP* gene (43).

1.3.1 Characterization of PrP^C and PrP^{Sc}

PrP^C and PrP^{Sc} differ only in their secondary and tertiary structure, but these structural changes give PrP^{Sc} certain biochemical properties resulting finally in prion disease (Table 1) (44).

Table 1. Biochemical and structural characteristic of PrP^C and PrP^{Sc}

PrP^C	PrP^{Sc}
α-helical rich structure	β-sheet rich structure
proteinase K sensitive	proteinase K resistent
detergent soluble	detergent insoluble
no fibril formation	aggregated, fibril formation
non-infectious	infectious

PrP^C consists mainly of an α-helical structure (43 %) and only a small fraction of β-sheets (3 %), whereas PrP^{Sc} contains predominantly β-sheets and is capable of forming aggregates in contrast to PrP^C (44, 45). These structural differences are based on their biochemical differences.

PrP^C and PrP^{Sc} differ with regards to their solubility, their tendency to form fibrils and their proteinase K (PK) resistance (16). PrP^C is characterized by its solubility in detergents and it is highly susceptible to proteolysis (9). In contrast PrP^{Sc} is an insoluble protein with a partial resistance to proteolytic digestion (16, 44). PK completely degrades

PrP^C, while it is only able to cleave off the aminoterminal region of PrP^{Sc} (46). The carboxyterminal PK resistant region consists of aa 90-231. PK digestion is broadly used to discriminate between PrP^C and PrP^{Sc} by western blot analysis.

1.3.2 Replication of PrP^{Sc} and different prion strains

Several models have been proposed on how replication of PrP^{Sc} occurs, but there is growing evidence that prions replicate according to the so-called seeded-polymerization model (Figure 3) (47-50).

In the seeded-polymerization model, an equilibrium between PrP^C and an intermediate exists, with PrP^C being the dominant conformation. The intermediates are metastable and unfolded PrP molecules that can be converted into PrP^{Sc} seeds, due to mutations that destabilize PrP^C or infectious transmission (50). These seeds recruit more PrP^C monomers that turn into PrP^{Sc}. Thereby these formerly small seeds elongate and form long fibrils, a process which finally results in PrP^{Sc} aggregate formation (51). These fibrils are usually 6-12 nm in diameter, rigid and non-branching and consist of two to six protofilaments that contain β-sheets (52). The protofilaments are twisted around each other and form a supercoiled structure (53).

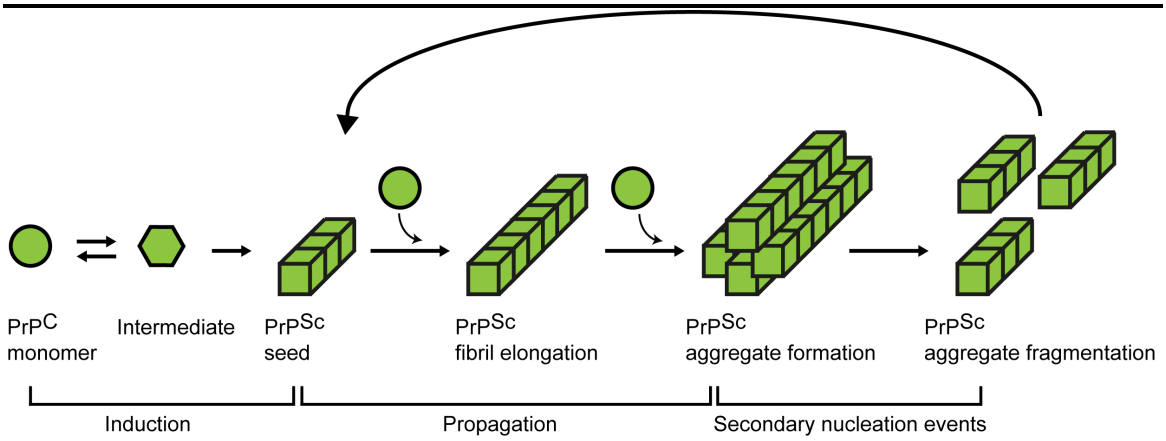

Figure 3. Replication of PrP^{Sc} according to the seeded-polymerization model. PrP^C monomers are converted to PrP^{Sc} via a PrP intermediate. By the conversion of further PrP^C monomers PrP^{Sc} seeds elongate and form aggregates. Fragmentation of aggregates produces new infectious seeds.

Formed and growing aggregates can be fragmented into smaller entities that function as new seeds for conversion of PrP^{C} monomers to PrP^{Sc} (50, 51). The underlying mechanisms of fragmentation are not fully understood to date. However, heat shock proteins and autophagy may play a role in fragmentation (54). It is hypothesized that the size of the seeds determines toxicity and infectivity. Particles comprising 14-28 PrP molecules appear to be the most infectious (55).

In the brain conversion of PrP^{C} into PrP^{Sc} induces characteristic changes consisting of neuronal vacuolation and degeneration, which gives the cerebral grey matter 'spongiform' appearance, and a reactive proliferation of astrocytes and microglia (56). Though the spongiform degeneration is frequently detected, it is not obligatory. Astrogliosis and microgliosis are more constantly observed, but they are not specific to the prion diseases. The lack of a lymphocytic inflammatory response is also an important characteristic (56-58).

Furthermore, the conversion of PrP^{C} into PrP^{Sc} can result in conformationally diverse types of PrP^{Sc}, so-called prion strains (59). Prion strains were first discovered in 1961 when goats were infected with brain homogenate of sheep suffering from prion disease. Those goats developed prion diseases with different phenotypes (60). The same phenomenon was observed later, as hamsters were infected with mink-adapted prions. The hamsters developed prion disease with different incubation times and lesion profiles (61). To study the different strains, infectious isolates from given species were transmitted to mice and passaged several times from generation to generation. The prion phenotypes remained stable, demonstrating that different strains are characterized by differences in the length of the incubation time, the neuropathological lesion profiles, the pattern of PrP^{Sc} deposition and physicochemical properties of PrP^{Sc} (61-65). The physicochemical characteristics include PK resistance, glycosylation profile, electrophoretic mobility in western blot analysis, temperature stability, difference in conformations detected by specific anti-PrP antibodies and the resistance to guanidine hydrochloride (GdnHCl) (66-69).

How different prion strains originate from the same PrP^{C} protein in the absence of nucleic acid is not understood. The strain stability in the absence of nucleic acid was demonstrated as two different mink prion strains were able to propagate in a cell-free system without any co-factors, while maintaining their specific physicochemical properties (70). This self-conformation-templating hypothesis was supported by studies on protein level with a method called protein misfolding cyclic amplification (PMCA) (71).

In this method, recombinant PrP is incubated with small amounts of isolated PrP^{Sc} from brain of infected animals. This PrP^{Sc} functions as a seed and converts the recombinant PrP into PrP^{Sc} during several repeated cycles of sonication and incubation (72). The amplified PrP^{Sc} exhibits the same distinct physicochemical properties as the starting material (71). This also proofs the protein-only hypothesis, which states that the infectious agent (PrP) solely consists of proteins which self-propagate without any nucleic acids encoded by a genetic background (8). As the genetic information is not responsible for the different prion strains, the prion strain information is likely enciphered by heritable alternative conformations of PrP^{Sc} (73). One PrP^{C} monomer can adopt multiple PrP^{Sc} conformations resulting in structurally distinct aggregate forms (PrP^{Sc} fibrils). PrP^{Sc} with distinct conformations serves as templats for conversion of adjoined PrP^{C} and thereby preserves strain-specific information (41, 74). Transmission of prions isolated from prion diseased sheep to mice led to the establishment of at least 20 different mouse-adapted strains. Two of the most established and studied mouse-adapted strains are 22L and RML. The strains display characteristic lesion profiles in different brain regions of infected C57BL/6 mice (Figure 4).

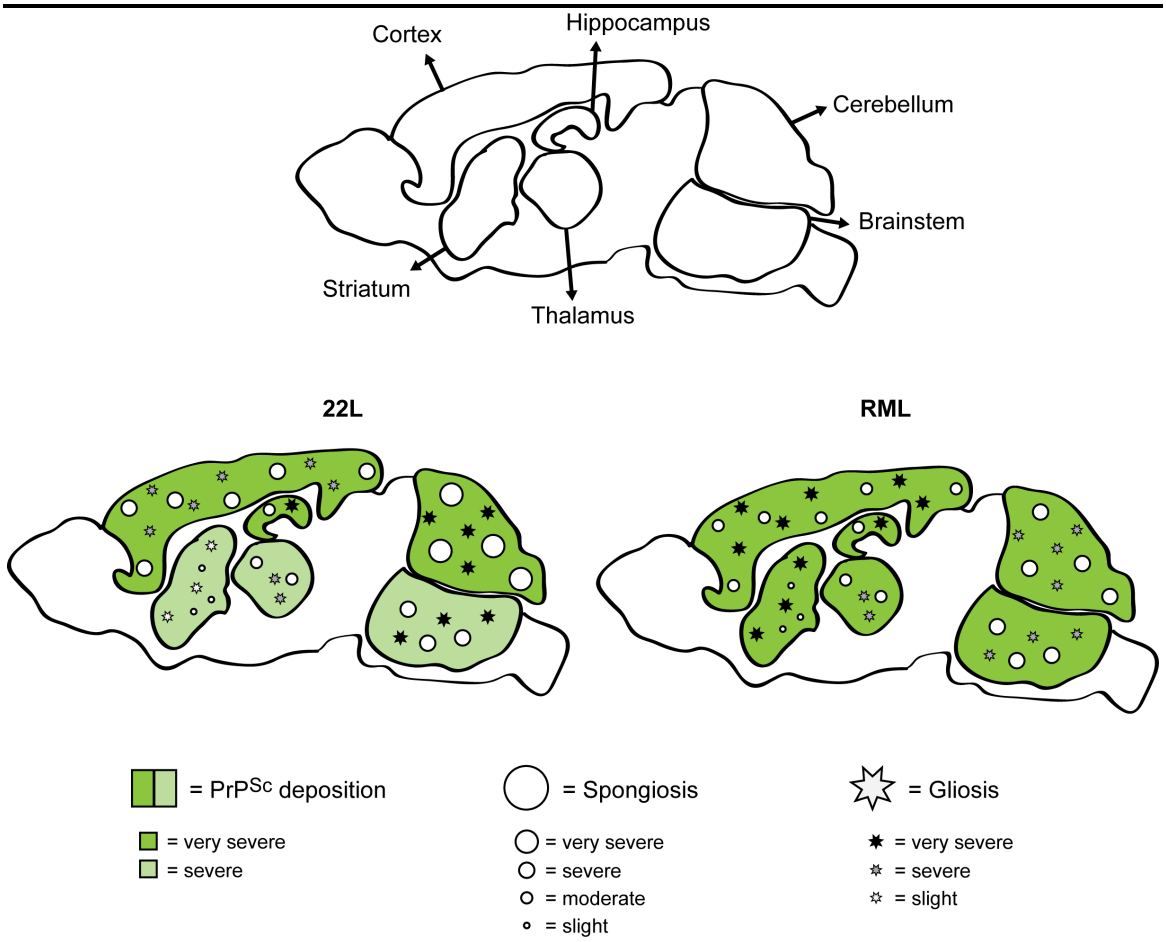

Figure 4. Strain specific pathology in 22L or RML infected C57BL/6 mouse brains. Infection of mice with prion strains 22L or RML results in distinct pathologies and lesion profiles. PrP^{Sc} deposition is shown in green, circles indicate spongiosis and stars gliosis. Severity is displayed by color and/or size of the different symbols. Figure adapted from Karapetyan et al (75).

Inoculation with 22L results in a very severe PrP^{Sc} deposition in the cortex, the hippocampus, and the cerebellum, as well as a severe deposition in the brainstem, the thalamus, and the striatum. The cerebellum is affected the strongest with a very severe spongiosis and gliosis. Also the brainstem and the hippocampus display a very severe spongiosis but only a severe to moderate gliosis. The thalamus also exhibits a moderate spongiosis but a severe gliosis. PrP^{Sc} deposition in the striatum shows the mildest lesion profile with a slight spongiosis and gliosis. In contrast, infection with prion strain RML leads to very severe PrP^{Sc} deposition in the cortex, the hippocampus, the cerebellum, the brainstem, the thalamus, and the striatum. However, less spongiosis and gliosis are found in the cerebellum and brainstem (severe). Hippocampus and thalamus show a

comparable profile to 22L concerning spongiosis and gliosis. The cortex and the striatum display a very severe gliosis, but only a moderate to slight spongiosis (75).
This example shows that different strains favor different brain regions. This might be due to different cell compositions or intracellular compartments. It is also possible that the cell specific co-factors are favored by certain PrP conformations and thereby promoting preferential propagation of one particular strain (76, 77).

1.4 The species barrier and prion disease

Different prion strains from different species are normally only transmitted within species due to the so-called species barrier. Inter-species transmission between related species is sometimes possible, but is only a rare event (78). Transmission of prions from one species to another leads to a prolonged incubation time and low attack rates in the new species (78, 79). The species barrier is mainly determined by differences in the PrP amino acid sequence between species, which results in variability in PrP structure (80). The second β-strand and the second α-helix can vary between species. This given loop mobility affects the resistance to prion disease (79). Additionally, single amino acid polymorphism within species in PrP correlate with prion susceptibility and affect the propensity of recombinant PrP to self-association into β-sheet enriched, oligomeric, and amyloid fibrils *in vitro* (79). It has been hypothesized, that also the type of prion strain influences the species barrier, as host PrP^{C} is more compatible with certain PrP^{Sc} conformations (74). On rare occasions the species barrier can be overcome and prions of one species can infect another resulting in prion disease.

Prion diseases affect many different species (Table 2). In humans they include Creutzfeldt-Jakob disease (CJD), Gerstmann-Sträussler-Scheinker syndrome (GSS), fatal familial insomnia (FFI), kuru and variant CJD (vCJD) (81). Clinical symptoms in human prion diseases can vary from progressive dementia, cerebellar ataxia, pyramidal signs, chorea, myoclonus, extrapyramidal features, pseudobulbar signs, seizures to amyotrophic features and can be seen in variable combinations (57). Bovine spongiform encephalopathy (BSE), chronic wasting disease (CWD) in deer, elk and moose and scrapie in sheep and goats are important prion diseases of mammals (82).

Table 2. Overview of prion diseases in human and mammals

Disease	Host	Etiology	Mechanism/cause
Familiar CJD	Humans	Genetic	**Mutation**: *PRNP* gene (germinal)
Iatrogenic CJD	Humans	Acquired	**Infection**: contaminated surgical equipment, blood transfusion, transplants
Variant CJD	Humans	Acquired	**Infection**: ingestion of BSE contaminated products
Sporadic CJD	Humans	Sporadic	**Mutation**: *PRNP* gene (somatic)? **Spontaneous**: conversion PrP^{C} into PrP^{Sc}?
Fatal familial insomnia	Humans	Genetic	**Mutation**: *PRNP* gene (germinal)
Gerstmann-Sträussler-Scheinker syndrome	Humans	Genetic	**Mutation**: *PRNP* gene (germinal)
Kuru	Humans	Acquired	**Infection**: cannibalism
Bovine spongiform encephalopathy	Cattle	Acquired, sporadic	**Infection**: ingestion of PrP^{Sc} contaminated bone meal; **Spontaneous** (rare)
Chronic wasting disease	Deer, elk and moose	Acquired	**Infection**: vertical and horizontal transmission
Scrapie	Sheep and goats	Acquired, sporadic	**Infection**: vertical and horizontal transmission; **Spontaneous**
Exotic ungulate encephalopathy	Exotic hoofed animals	Acquired	**Infection**: ingestion of BSE contaminated food
Feline spongiform encephalopathy	Cats and big cats	Acquired	**Infection**: ingestion of BSE contaminated food
Transmissible mink encephalopathy	Mink	Acquired	**Infection**: Ingestion of PrP^{Sc} contaminated food from sheep or cattle

Prion diseases can be divided etiologically into three forms: inherited, sporadic and acquired (83). Most human prion diseases occur sporadically (~ 85 %), with an incidence of 1 – 2 cases per million per year, equally distributed between men and women (84, 85). Over 30 autosomal dominant pathogenic mutations within the *PRNP* gene are known and cause 15 % of human prion diseases (83, 84, 86, 87). Under rare circumstances prion disease can be acquired. Iatrogenic CJD resulted from transmission of CJD prions trough treatment with pituitary hormones derived from human cadavers, implantation of dura mater grafts, corneal transplantation, blood transfusion and the use of contaminated electroencephalographic electrodes (57). The best-known acquired prion disease is kuru, resulting from ritual cannibalism among the Fore linguistic group of the Eastern Highlands in Papua New Guinea (88). More recently variant CJD was found in the United Kingdom, which distributed epidemically to Europe and later worldwide caused by the consumption of BSE contaminated products (83, 89). BSE occurred in cattle in 1986 in the United Kingdom and it was suspected to either originate from dietary intake of scrapie-infected sheep products (90, 91) or from a sporadic case (1, 92). Scrapie is the first described prion disease and can be vertically and horizontally transmitted (93). Recently, research focuses more and more on the study of chronic wasting disease (CWD), affecting deer, elk moose and reindeer. CWD occurred first in North America and Canada, later in the Republic of Korea and recently in Europe in Norway (94-97). CWD transmits naturally horizontally by uptake of prion-contaminated excretions contaminating the environment (98). Orally taken up prions are intestinally absorbed and transported via the blood and lymphoid fluids. Prions can peripherally replicate in the spleen, the appendix, tonsils or the lymphoid tissue. Afterwards they are transported primarily by peripheral nerves to the brain (99).

1.5 Models to study prion disease

A complete understanding of prion disease and the underlying pathological mechanisms are crucial to identify potential prion therapeutics. *In vitro* and *ex vivo* models provide fundamental tools to study prion biology (Table 3) (21).

Table 3. Overview of cell lines and organotypic cerebellar slices susceptible to prions. Based on Grassmann et al (21).

Agent	**Adapted to**	**Cell lines**
Human prion disease	Mouse	N2a, GT1, RK13 mouse PrP
	Human	SH-SY5Y
BSE	Mouse	MG20
	Bank vole	RK13 bank vole PrP
CWD	Mule deer elk	MDB, RK13 elk PrP
Scrapie	Mouse	N2a, GT1, RK13 mouse PrP SN56, HpL3-4 mouse PrP, CF10 mouse PrP, SMB, CAD, MG20, C2C12, L929, NIH/3T3, MSC-80, PC12
	Hamster	HaB
	Sheep/transgenic mice overexpressing ovine PrP	MovS, RK13 ovine PrP
Agent	**Adapted to**	**COCS**
BSE	Mouse	C57BL/6
Scrapie	Mouse	C57BL/6, transgenic mice

1.5.1 Prion cell culture models

The first cell culture system was already used in 1970, when cells of a mesodermal origin were isolated from a brain of a scrapie-infected mouse with clinically symptoms at the terminal stage (100). In 1980, another cell line for prion research was established, the mouse neuroblastoma cell line N2a, which is nowadays the most commonly used cell line in prion research. N2a cells are susceptible to several different mouse-adapted

scrapie strains and are able to propagate prions over many passages without cytopathic effects (101). Beside N2a cells, several other cell lines are susceptible to prions, including fibroblasts, myoblasts, epithelial and microglial cells (102-109). Exposing these cells to different prion strains of diverse origins led to persistent prion infection over several passages (107, 110). Successful infection of cells was especially achieved with prion strain 22L, RML/Chandler, ME7 and 139A (21). Primary cell culture systems including bone marrow-derived mesenchymal and neural stem cells, cerebellar neurons and astrocytes exist, but often show cytopathic effects (111-116).

However, *in vitro* research has disadvantages such as restricted susceptibility of most cell lines to prion infection, usually poor infection rates and low prion titers (117). Susceptibility of cells to chronic prions infection is influenced by genetic heterogeneity and chromosomal instability within a cell population (118, 119) and does not correlate with PrP^C expression levels (109, 118, 120), although PrP^C expression is absolutely necessary for infection (121, 122). Cloning of infected and pre-cloning of uninfected cells is a useful tool to increase the infection rate and prion titers (118, 123, 124). Additionally, persistent prion infection in cells is also highly sensitive to culture conditions and changes in growth medium conditions (117, 125).

1.5.2 Transcriptomics in prion disease

To get a more detailed understanding of the development of prion disease it is useful to utilize an approach focusing on whole pathways. Until now a detailed knowledge of the molecular processes that lead to prion disease is still missing. In this context, genomic approaches are powerful to investigate the molecular basis of prion disease. Large-scale gene expression profiling of diseased vs. healthy groups helps to identify differentially expressed genes (DEGs). These DEGs can be used to identify novel genes and pathways that are deregulated at different time points during the pathogenesis (126). Different technologies have been used to detected genes variations including cDNA libraries, genome-wide association studies, microarrays, and more recently next-generation sequencing (NGS). These studies may identify pathways, which help to gain insight within the pathogenesis of prion diseases, but also possibly may help to find biomarkers for the early detection of preclinical stages or for the identification of potential targets (126).

Several *in vivo* studies were performed and different pathways were identified. Numerous studies of prion infected brain tissues showed altered expression of genes involved in glia activation like glial fibrillary acidic protein (GFAP), lysozyme, MHC class I and II, and the chemokines CXCL10 and CXCL13 (127-129).

Analysis of mRNA levels of cortex, medulla and pons of C57Bl/6 mice infected with prion strain 139A (100, 125, 150 and 189 days post infection) revealed 114 genes with altered mRNA expression, that were mostly unknown to be involved in prion diseases. Several of these genes are involved in the inflammatory reaction and stress response, a known result of prion infection that can finally result in neuronal loss. The authors state that a limitation of the secondary inflammatory reaction may prolong survival time (130).

Comparison of gene expression between 22L and RML prion infected C57Bl/6 mouse brains at different time points showed similar inflammatory responses. Fifteen previously unreported differentially expressed genes related to inflammation or activation of the STAT signal transduction pathway were identified. The endogenous interleukin-1 receptor antagonist (IL-1Ra), an inflammatory marker, was newly identified as increasing preclinically and could possibly be used for early detection of the disease (131).

As described, a lot of transcriptomic studies analyze different kinds of inflammatory responses, due to the prominent microgliosis and astrogliosis in prion disease. To examine molecular changes unique to neurons, RNA isolation of the CA1 hippocampus region is useful as this region is particularly dense of neurons. Analysis of RNA expression in this distinct brain region of RML prion infected mice at different time points showed a bi-phasic response. During early prion disease neuronal protective mechanisms were up-regulated, while this protection was subsequently diminished at late stages of infection, in line with the clinical manifestation. The authors claim that these findings demonstrate the ability of neurons to mount an initial neuroprotective response to prions that could be exploited for therapy development (132).

Hood et al performed a large comprehensive transcriptome analysis in brains of mice infected with eight different strains at 8 – 10 different time points. They identified 333 core genes that appeared to play a central role to prion disease. Of these, 178 had not previously been reported to change in prion-infected mice. They generate a complex hypothetical dynamic protein network that could be associated with known pathological events in disease progression, including pathways like GAG metabolism, androgen metabolism, cholesterol homeostasis and sphingolipid metabolism (133).

These examples of studies of the transcriptomic changes in prion diseases show the broad range of possible field of applications. These genomic approaches could help to find biomarkers, to understand complex processes during symptom and disease development and may identify possible sites of actions for therapeutics.

1.5.3 *Ex vivo* prion model

To investigate prion infection in a complex neuronal environment, organotypic slice culture represents an important tool. This *ex vivo* model largely recapitulates the *in vivo* cellular environment (134). Organotypic cultures were used to study a variety of different brain areas including the hippocampus and the cerebellum (134). In 2008 cultured organotypic cerebella slices (COCS) of neonatal mice were used for the first time in prion research (135). COCS are incubated with prion-containing inoculum as free-floating sections (135) and are subsequently grown on membrane inserts (136). COCS are susceptible to a mouse-adapted BSE strain and different mouse-adapted scrapie strains like 22L, RML and ME7 (137). In COCS PrP^{Sc} amplifies five times faster than *in vivo*. Prion infection of COCS recapitulates important hallmarks of prion pathology like deposition of PrP^{Sc}, vacuolation, neuronal loss, astro- and microgliosis (137, 138) and a decrease in Purkinje cell dendritic spine density (139). With all these features, COCS provide a powerful tool to study prion diseases. Beside western blot analysis and immunofluorescent staining of COCS, recent analysis of the transcriptome in COCS is a tool to study prion infection in slices (140) . However, the *in vivo* transferability concerning differential expressed genes and deregulated pathways was not tested until now.

1.5.4 Role of *in vitro* and *ex vivo* models in prion disease

In vivo and *ex vivo* models can be used to identify avenues of therapeutic intervention of prion diseases. Compounds that increase survival times in scrapie-infected mice are usually also inhibitors of PrP^{Sc} levels in cell culture (117). Pentosan polysulfate, one of the most active anti-scrapie compounds *in vivo* (141) strongly inhibits PrP^{Sc} formations in cells (142). Amphotericin B (143) and some other porphyrins (144, 145) with known anti-scrapie activity reduce PrP^{Sc} formation also *in vitro*. This clearly demonstrates that screening of compounds that effectively inhibit PrP^{Sc} formation in cell culture is a good alternative for the expensive and time-consuming process of testing drugs against

scrapie *in vivo*. Identification of anti-prion compounds *in vitro* is currently accomplished by low-throughput assays that detect PrP^{Sc} levels by immunofluorescence staining or western blot analysis. Additionally, a high-throughput screening method exists that allows the identification of PrP^{Sc} inhibitory compounds on TSE-infected cells by a dot-blot apparatus (117). In this assay, chronically infected cells are treated with compounds on a 96-well plate for distinct time periods. Before cells are lysed, toxic effects are determined by light microscopy. Proteinase K treated lysates are transferred to a PVDF membrane by a dot-blot apparatus. Subsequently, PrP^{Sc} can be detected by antibodies (117, 146). However, this assay has several limitations. It is not possible to relate the effect of a drug to the cell number analyzed, it delivers no information on PrP^{Sc} levels on single cell basis and it cannot be used to identify cellular mechanisms that might be inhibiting PrP^{Sc} formation (117).

Ex vivo models also provide a good tool to study compound effects on prion disease as COCS provide a complex environment with interaction between highly diverse cell types including neurons, astrocytes and microglia (147). COCS can also be used to test the compound effects on the establishment of infection as well as on persistently infected slices. As this method is relative time consuming it is reasonable to examine only *in vitro* pretested compounds. To date, COCS were already successfully used to study the pharmacological inhibition of a persistent prion infection with known anti-prion compounds (137).

1.6 Objectives

Currently, prion therapeutic clinical trials have lacked success and there is an urgent need for novel therapeutics that can prevent, slow down, and ultimately stop prion disease progression (148). Several compounds have been identified that interfere with the prion conversion process, alter prion protein trafficking, or enhance prion degradation (148-152). However, only pentosan polysulfate and quinacrine were tested clinically and failed to reduce the clinical signs of prion disease (153, 154). Therefore, the aim of this study was to develop a cell-based assay for high content screening of compound libraries to identify compounds that might impair prion replication. Persistently prion strain 22L infected, compound treated N2a cells should be analyzed by automated high-throughput confocal microscopy. In contrast to already existing methods, this allows automated analysis and evaluation of thousands of cells on a single cell basis. Such an

assay would provide a powerful tool to identify compounds that reduce levels of PrP^{Sc} in single cells and can be further analyzed *ex vivo* or *in vivo*. Furthermore, identified compounds should be tested on prion infected organotypic slice culture to test whether *in vitro* detected anti-prion compounds are also effective in a more complex neuronal environment. Such a compound would present a perfect candidate for *in vivo* analysis and may finally result in a new therapeutically approach.

Beside this, a comparative study of host response between *ex vivo* and *in vivo* should evaluate the transferability between the two systems, as this was not shown until now. To address this, organotypic slice culture from C57BL/6 pups (*ex vivo*) and C57BL/6 mice (*in vivo*) should be infected with 22L- and RML-prions and after different incubation times a comparative RNA sequencing analysis should be performed. This analysis should show if prion infection results in comparable deregulated pathways *ex vivo* and *in vivo* and should help to assess the value of organotypic slice culture in prion research.

2 Materials and methods

2.1 Biological safety

Prion work was accomplished under biosafety level 2 according to the lab operating instructions and to the German *Gentechnikgesetz* (August 31st, 2015). Solid and liquid waste were autoclaved for 60 min at 134 °C. Prion contaminated liquids were inactivated with 1 M NaOH (final concentration) for at least 24 h.

2.2 Cell biological methods

All cell culture work was performed under a laminar flow cabinet (Scanlaf, Mars Safety Class 2, Labogene, Lynge, Denmark) and hands, bench and all instruments were disinfected or sterilized. To prevent contamination with prions, two pairs of gloves and protective sleeves were worn.

2.2.1 Cell Lines

DMEM + GlutaMAX-I	Dulbecco's Modified Eagle Medium (1x) + 4.5 g/L Glucose, - Pyruvat Invitrogen, Darmstadt, Germany
F – 12 Nutrient Mixture	Kaighn's Modification of Hams F – 12 Nutrient Mixture (1x) + L-Glutamine Invitrogen, Darmstadt, Germany
Fetal calf serum	PAA Laboratories, Pasching, Austria
Penicillin/streptomycin solution (PenStrep)	10,000 units/mL Penicillin 10,000 µg/mL Streptomycin Invitrogen, Darmstadt, Germany

Cell lines were stored in liquid nitrogen. Cell culture media were stored at 4 °C and pre-warmed to 37 °C in a water bath (GFL, Burgwedel, Germany) before use.

Table 4. Cell lines

Cell line	Description	Cultivation
L929 15.9	Murine fibroblast cell line L929 (ECACC, L929 (NCTC), Cat. No. 85103115) subclone highly susceptible to mouse-adapted prion strains 22L and RML. Produced by Romina Bester by two rounds of limiting dilution cloning	DMEM 10 % FCS 1 % PenStrep
L929 ^{22L}	L929 15.9 cell line persistently infected with mouse-adapted scrapie strain 22L	DMEM 10 % FCS 1 % PenStrep
N2a	Murine neuroblastoma cell line (ATCC CCL 131)	DMEM 10 % FCS 1 % PenStrep
N2a ^{22L}	N2a cell line persistently infected with mouse-adapted scrapie strain 22L	DMEM 10 % FCS 1 % PenStrep

2.2.2 Thawing of cells

Cells were stored at -170 °C in liquid nitrogen and thawed at 37 °C in a water bath. 5 mL of appropriate pre-warmed cell culture medium was added to the cells and they were pelleted at 1,200 g (Heraeus™ Multifuge™ X3R, Thermo Scientific, Rockford, USA) for 5 min at room temperature (RT). The cell pellet was resuspended in 3 mL medium and transferred to a cell culture flask containing medium.

2.2.3 Cultivation of cells

Phosphate buffered saline (PBS)	Invitrogen, Darmstadt, Germany
0.25 % Trypsin-EDTA	Invitrogen, Darmstadt, Germany

Cells were grown in either T25 or T75 flasks at 37 °C with 90 % air humidity and 5 % CO_2 (Incubator: HERAcell 240i, Thermo Scientific, Rockford, USA). At a confluency of 80 – 90 %, cells were rinsed with pre-warmed PBS and detached by incubating them with 500 µL – 1 mL of Trypsin-EDTA for 2 – 3 min at RT. Cells were resuspended by pipetting them up and down in 4 – 6 mL of fresh cell culture medium. An appropriate

volume of cell suspension was diluted into a new flask containing cell culture medium. Cells were split every 3 - 4 days at a ratio of 1:8 to 1:10.

2.2.4 Cryoconservation of cells

Dimethyl sulfoxide (DMSO) Sigma-Aldrich, Steinheim, Germany

Nearly confluent monolayers were harvested as described in 2.2.3. Cells were counted and pelleted at 1,200 g for 5 min at 4 °C. The supernatant was discarded and the pellet was resuspended in an appropriate volume of cell culture medium containing 10 % DSMO. Cells were either diluted to 3.5 x 10^5 cells in 500 µL or 1 x 10^6 in 1 mL and frozen in cryotubes at -80 °C in a box containing 100 % isopropanol for gentle reduction of the temperature. After 24 - 48 h, cryotubes were transferred to liquid nitrogen.

2.2.5 Determination of the cell number

0.4 % Trypan Blue Solution Sigma-Aldrich, Steinheim, Germany

The number of cells in a cell suspension was determined using an automated cell counter (TC20, BioRAD, Hercules, USA). To distinguish between vital and dead cells, the cell suspension was diluted 1:2 with trypan blue and transferred to a cell counting chamber. The cell counter determined the amount of vital and dead cells and the total amount of cells per mL cell suspension.

2.2.6 Preparation of brain homogenates

Opti-MEM-I (1 X) + GlutaMAX-I Reduced serum medium
Invitrogen, Darmstadt, Germany

Homogenates were prepared from brains of C57BL/6 mice infected with scrapie strains 22L and RML. Scrapie-infected mouse brains were kindly provided by Prof. Dr. M. Groschup, Friedrich-Löffler-Institut, Bundesforschungsinstitut für Tiergesundheit, Isle of Riems, Germany and by Dr. Deborah McKenzie, Department of Biological Science, University of Alberta, Canada. A 10 % brain homogenate was prepared by homogenizing infected mouse brains with a glass dounce homogenizer (Homogenisator potter S, Sartorius, Göttingen, Germany) in Opti-MEM. As negative control, Mock brain

homogenates were prepared from prion uninfected C57BL/6 mice. Brain homogenate was centrifuged at 872 g (Heraeus™ Multifuge™ X3R, Thermo Scientific, Rockford, USA) for 5 min at 4 °C to remove the cell debris. Aliquots of the supernatant were stored at -80 °C.

2.2.7 Infections of cells with scrapie strains 22L or RML

Persistently infected cells were generated by incubating cells with brain homogenates. Therefore, 2 x 10^4 cells were seeded in a 24-well plate (Sigma-Aldrich, Steinheim, Germany) and 24 h after seeding, the medium was replaced by growth medium with supplements containing 1 % (v/v) brain homogenate. After five hours, the brain homogenate was diluted 1:3 with cell culture medium. The medium was replaced by cell culture medium approximately 24 h after infection

2.2.8 Treatment of cells with different compounds

DMSO Sigma-Aldrich, Steinheim, Germany

Cells were seeded and grown for two hours. Compounds were diluted in DMSO or H_2O_{bidest} according to manufacturer`s protocol. For treatment of the cells, compounds were added to cell culture medium at different concentrations. As control DMSO or H_2O_{bidest} without any compound were added to the cells. Cells were treated for 44 h.

2.3 Primary slice culture methods

All primary slice culture methods were based on a modified protocol for the prion organotypic slice culture assay (POSCA) from Falsig and Aguzzi (135).

2.3.1 Mouse husbandry

Female C57BL/6JRj mice with pups were ordered from Janvier (St. Berthevin Cedex, France) and housed in cages at a 12:12 light:dark cycle. Food and water were available *ad libidum*. All animal experiments were approved by the *Landesamt für Natur, Umwelt und Verbraucherschutz NRW* and conducted according to the institutional animal care committee guidelines and German animal protection laws.

2.3.2 Preparation of organotypic cerebellar brain slices

100 mM Kynurenic acid stock solution	in H_2O_{bidest}, pH 7.2 – 7.4 Sigma-Aldrich, Steinheim, Germany
Grey's balanced salt solution (GBSS)	Sigma-Aldrich, Steinheim, Germany
D-(+)-glucose solution (45 %)	Sigma-Aldrich, Steinheim, Germany
GBSSK	6.662 mL D-(+)-glucose solution (45 %) 5 mL 100 mM Kynurenic acid stock solution in 500 mL GBSS
2 % LMP agarose solution	UltraPure Low-melting-point agarose Invitrogen, Darmstadt, Germany in GBSSK
Glue	Glue Roti coll1, Carl Roth, Karlsruhe, Germany

Cerebellar brain slices were prepared by decapitation of 9 - 13 days old pups of C57BL/6JRj mice. Heads were kept on ice and the skin was removed. The skull was opened and the brain was dissected. Brains were kept on ice cold GBSSK and the cerebella were dissected from the brains under a stereoscopic microscope. Cerebella were imbedded into 2 % low melting agarose in an upright position in a plastic container (Ø 22 mm, 7 mL, Carl Roth, Karlsruhe, Germany). Blocks containing the cerebellum were cut and glued on the disc of the vibratome (VT1200S, Leica, Biosystems, Wetzlar, Germany). The disc was fixed in the inner chamber of the vibratome, filled with ice cold GBSSK and the inner chamber was placed into the ice filled outer chamber. A blade (VALET AutoStrop, England, UK) was fixed to the slicing arm and 350 µm thick cerebellar brain slices were prepared with a speed of 0.24 mm/s and an amplitude of 1.00 mm. Slices were transferred into an ice cold GBSSK filled 6 cm dish and remaining agarose was removed from the slices under a stereoscopic microscope. Cerebellar brain slices were either directly transferred to a membrane insert for cultivation (2.3.4) or infected with prions as described in 2.3.3.

2.3.3 Infection of cerebellar brain slices with scrapie strain 22L or RML

Cerebellar slices were exposed to prion-infected brain homogenate (2.2.6) under a laminar flow cabinet (Scanlaf, Mars Safety Class 2, Labogene, Lynge, Denmark) according to the safety instructions. Up to 10 brain slices were transferred to a 24-well plate (BD Biosciences, Heidelberg, Germany) containing GBSSK. Cerebellar brain slices were exposed to 20 mg/mL prion-infected brain homogenate or, as negative control, to uninfected Mock brain homogenates for 1 h at 4 °C under permanent shaking. To remove brain homogenate, slices were washed three times with ice cold GBSSK in a 6-well plate. Cerebellar brain slices were transferred to a membrane insert for cultivation.

2.3.4 Cultivation of cerebellar brain slices

Minimal essential medium (MEM)	Invitrogen, Darmstadt, Germany
Basal medium Eagle (BME)	Invitrogen, Darmstadt, Germany
Horse serum	Heat inactivated
	Invitrogen, Darmstadt, Germany
GlutaMAX-I	100X
	Invitrogen, Darmstadt, Germany
Penicillin/streptomycin solution	10,000 units/mL Penicillin
	10,000 µg/mL Streptomycin
	Invitrogen, Darmstadt, Germany
D-(+)-glucose solution (45 %)	Sigma-Aldrich, Steinheim, Germany
2x MEM	1.922 g MEM
	0.44 g NaHCO3
	Sigma-Aldrich, Steinheim, Germany
	In 100 mL in H_2O_{bidest}
Slice culture medium	100 mL 2x MEM
	100 mL BME
	100 mL Horse serum
	4 mL GlutaMAX-I
	4 mL Penicillin/streptomycin
	5.5 mL D-(+)-glucose solution (45 %)
	86.5 mL in H_2O_{bidest}
	pH 7.2 – 7.4

Up to five infected or uninfected cerebellar brain slices were transferred to membrane inserts. Membrane inserts were placed in a 6-well plate containing slice culture medium. Cerebellar brain slices were cultured up to 12 weeks at 37 °C with 90 % air humidity and 5 % CO_2 (Incubator: HERAcell 240i, Thermo Scientific, Rockford, USA). Every 2 - 3 days medium was replaced by fresh medium.

2.3.5 Treatment of cerebellar slices with different compounds

DMSO	Sigma-Aldrich, Steinheim, Germany

Cerebellar slices were infected with 22L or RML prion brain homogenate (2.3.3) and grown for two weeks. Compounds were diluted in DMSO or H_2O_{bidest} according to manufacturer`s protocol. For treatment of the cerebella slices, compounds were added to the slice culture medium at different concentrations. As control DMSO or H_2O_{bidest} without any compound were added to the cells. Cerebellar slices were treated for up to five weeks.

2.3.6 Propidium iodide (PI) staining

Propidium iodide solution	10 mg/mL Sigmal-Aldrich, Steinheim, Germany
Hydrogen peroxide solution (H_2O_2)	8.8 µM Sigmal-Aldrich, Steinheim, Germany
Staurosporine	5 µM Enzo, Lausen, Switzerland
GBSS	Sigma-Aldrich, Steinheim, Germany

The tissue viability was tested by PI incorporation into dead cells of cerebellar slices. 10 µg/mL PI was added to slices culture medium and slices were incubated for 2 h at 37 °C. Slices were washed three times with GBSS for 10 min. As a positive control slices were treated for two days with slice culture medium containing 8.8 mM H_2O_2. PI incorporation was detected by an inverse epifluorescence microscope (Axio observer Z1, Zeiss, Jena, Germany). The exposure time was adjusted in the positive control slices and kept constantly during the whole experiment.

2.4 Injection of mice with brain homogenate

2.4.1 Mouse husbandry

Female and male C57BL/6JRj mice from Janvier (St. Berthevin Cedex, France) were housed in cages at a 12:12 light:dark cycle. Food and water were available *ad libidum*. All animal experiments were approved by the *Landesamt für Natur, Umwelt und Verbraucherschutz NRW* and conducted according to the institutional animal care committee guidelines and German animal protection laws.

2.4.2 Intracranial injection and tissue dissection

Isoflurane FORENE	100% AbbVie, North Chicago, USA
Rimadyl Cattle	50 mg/mL Solution Pfizer, New York, USA

Mouse work was performed in collaboration with Walker Jackson and Melvin Schleif (DZNE, Bonn). Six weeks old mice were anesthetized with 3 – 5 % isoflurane and 20 µL of 0.1 % 22L- or RML prion brain homogenate (2.2.6) were injected intracranially into the right brain hemisphere at the bregmatic suture. Injection depth was 3 mm starting at the outer mouse head skin. As negative control mice were injected with Mock brain homogenate. The wound was cleaned with 70 % ethanol (EtOH) and mice were carefully observed until full recovery from anesthesia. All injections were done on the same day. An analgesic (Rimadyl) was administered within the next 72 h according to the manufacturer's instructions.

Mice were sacrificed 10, 14 and 18 weeks post injection by CO_2 inhalation. Brains were dissected, the two hemispheres were separated and each one snap frozen for mRNA isolation and stored at -80 °C.

2.5 Indirect immunofluorescence staining of proteins

2.5.1 Indirect immunofluorescence staining of cells

Table 5. Primary antibodies

Antibody	Origin	Specificity	Application	Reference
4H11	mouse, monoclonal	anti- PrP (C-terminal end)	WB 1:10000 IF 1:10 (cells), 1:5 (cerebellar slice)	Dr. Elisabeth Kremmer (155), Helmholtz Center Munich, Germany
PrPA	mouse, monoclonal	anti- PrP (N-terminal end, amino acid 23 - 30)	WB 1:10000	Dr. Elisabeth Kremmer, Helmholtz Center Munich, Germany
PrPB	mouse, monoclonal	anti- PrP (amino acid 89 - 109)	WB 1:10000	Dr. Elisabeth Kremmer, Helmholtz Center Munich, Germany
Saf32	mouse, monoclonal	anti- PrP (oktapeptide repeat region)	WB 1:10000	Cayman Chemicals, Michigan, USA
p-Met	rabbit, monoclonal	Anti-phosphorylated Met	IF 1:200 (cerebellar slice)	Cell Signaling Technology, Leiden, Netherlands
Lamp-1	rat, monoclonal	Lamp-1 of NIH/3T3 mouse embryo fibroblast tissue culture cell membranes	IF 1:200 (cerebellar slice)	Diagnostics, Freiburg, Germany
β-3-tubulin	rabbit, polyclonal	epitope in microtubules	IF 1:250 (cerebellar slice)	Diagnostics, Freiburg, Germany

Table 6. Secondary antibodies

Antibody	Origin	Specificity	Application	Reference
Alexa Fluor 488-conjugated anti-Mouse IgG	goat	mouse IgG	IF 1:300 (cells and cerebellar slices)	Life Technologies, Darmstadt, Germany
Alexa Fluor 647-conjugated anti-Mouse IgG	goat	rat IgG	IF 1:300 (cells)	Life Technologies, Darmstadt, Germany
Horseradish peroxidase-conjugated anti-Mouse IgG	goat	mouse IgG	WB 1:10000	Dianova, Hamburg, Germany

PBS	Invitrogen, Darmstadt, Germany
4 % PFA	Paraformaldehyde Sigma-Aldrich, Steinheim, Germany in PBS, pH 7.2 – 7.4
0.1 % Triton X-100	Roth, Karlsruhe, Germany in PBS
6 M GdnHCl	Guanidine hydrochloride Sigma-Aldrich, Steinheim, Germany in PBS
0.2 % Gelatine	from cold water fish skin Sigma-Aldrich, Steinheim, Germany in PBS
Hoechst 33342	Molecular Probes, Eugene, Oregon, USA

For detection of specific proteins, 2 x 10^4 cells were seeded in 24-wells (BD Biosciences, Heidelberg, Germany) on coverslips. Cells were cultured for 3 d and washed with PBS. After fixation with 4 % PFA for 20 min at room temperature (RT), cells were rinsed at least 3 times with PBS. Cells were permeabilized with 0.1 % Triton X-100 for 10 min and washed 3 times with PBS. For specific detection of PrP^{Sc} proteins were denatured with 6

M guanidine hydrochloride for 10 min at RT and rinsed 5 times with PBS. After blocking the cells with 0.2 % gelatine for 1 h at RT, primary antibody (Table 5) in blocking solution was added for 1 h at RT and cells were rinsed 3 times with PBS. The fluorophore-conjugated secondary antibodies (Table 6) were added to the cells, incubated for 1 h at RT and removed by three washing steps with PBS. Nuclei were visualized with 1 µg/mL Hoechst 3342 DNA (Deoxyribonucleic acid) staining in PBS for 10 min at RT, followed by 3 washing steps with PBS and one final washing step with H_2O. Cover slips were transferred to glass object slides (25 x 75 x 1.0 mm, Menzel-Gläser, SuperFrost Plus, Thermo Scientific, Braunschweig, Germany) and mounted with Aqua-Poly/Mount (Polysciences, Eppelheim, Germany), dried for at least 1 h at RT and stored at 4 °C until microscopic analysis was carried out. Confocal microscopy was performed using the LSM 700 (Zeiss, Jena, Germany) or the upright LSM 700 (Zeiss, Jena, Germany).

2.5.2 Indirect immunofluorescence staining of cells for high-throughput screen

PBS	Invitrogen, Darmstadt, Germany
4 % PFA	Paraformaldehyde Sigma-Aldrich, Steinheim, Germany in PBS, pH 7.2 – 7.4
0.1 % Triton X-100	Roth, Karlsruhe, Germany in PBS
6 M GdnHCl	Guanidine hydrochloride Sigma-Aldrich, Steinheim, Germany in PBS
0.2 % Gelantine	from cold water fish skin Sigma-Aldrich, Steinheim, Germany in PBS
Hoechst 33342	Molecular Probes, Eugene, Oregon, USA
HCS CellMask Blue stain	Molecular Probes, Eugene, Oregon, USA

For the high-throughput screen, 5 x 10^3 cells were seeded per well on a 96-well plate (µclear-plate, Black, Greiner bio one, Frickenhausen, Germany). Cells were stained following the protocol described in 2.5.1. In contrast to staining in 24-well plates, the

whole 96-well plate was immersed in 6M guanidine hydrochloride for 10 min to inactivated prions. Additionally, cytoplasm was visualized with HCS CellMask Blue stain (1:5000) for 10 min followed by 3 washing steps with PBS, after Hoechst treatment. Thereby, cell borders were defined and intracellular PrP^{Sc} detection was possible. 96 well plates could be stored at 4°C, if all wells were covered with sufficient amount of PBS or plates were directly analyzed. Cells were analyzed with an automatic confocal microscope (Cell Voyager 6000, Yokogawa, Tokyo, Japan). Image analysis was performed using the Columbus Image Data Storage and Analysis System.

2.5.3 Indirect immunofluorescence staining of cerebellar slices

PBS	Invitrogen, Darmstadt, Germany
4 % PFA	Paraformaldehyde Sigma-Aldrich, Steinheim, Germany in PBS, pH 7.2 – 7.4
0.5 % Triton X-100	Roth, Karlsruhe, Germany in PBS
6 M GdnHCl	Guanidine hydrochloride Sigma-Aldrich, Steinheim, Germany in PBS
5 % BSA	Albumin from bovine serum Fluka, Sigma-Aldrich, Steinheim, Germany in PBS
Hoechst 33342	Molecular Probes, Eugene, Oregon, USA

For indirect immunofluorescence staining of cerebellar slices, slices were washed with PBS and fixed with 4 % PFA at RT for 2 h, followed by three washing steps with PBS for 10 min. Slices were permeabilized with 0.5 % Triton X-100 at 4 °C for 18 h. After three times washing with PBS slices were incubated with 6 M guanidine hydrochloride for 3 h at RT for PrP^{Sc} detection (147). Slices were thoroughly rinsed three times with PBS. To avoid unspecific binding of the antibodies, slices were blocked with 5 % BSA for three days at 4 °C. Afterwards, cerebellar slices were cut out of the membrane inserts with biopsy punch (8,0 mm, Stiefel, Offenbach am Main, Germany) and transferred to a 24-well plate (BD Biosciences, Heidelberg, Germany). Primary antibodies (Table 5) diluted

in 5 % BSA were incubated at 4 °C for three days, slices were rinsed four times with PBS and the fluorophore-conjugated secondary antibody (Table 6) diluted in 5 % BSA was added for 3 days at 4 °C. Afterwards, slices were washed four times with PBS and nuclei were stained with Hoechst diluted 1:10,000 in PBS for 10 min at RT, followed by four washing steps with PBS. Slices were transferred on top of a drop PBS on a glass object slide (25x75x1.0 mm, Menzel-Gläser, SuperFrost Plus, Thermo Scientific, Braunschweig, Germany) to help smoothening of the membrane. PBS was removed, a drop of Aqua-Poly/Mount (Polysciences, Eppelheim, Germany) was added and slices were mounted with a cover slip (high precision, No 1.5 H, 12 mm Ø, Marienfeld, Lauda-Könighofen, Germany). The samples were dried for 1 h at RT and stored at 4 °C until microscopic investigation was conducted. Cerebellar brain slices were analyzed with an inverse epifluorescence microscope (Axio observer Z1, Zeiss, Jena, Germany).

2.6 Protein biochemical methods

2.6.1 Preparation of post nuclear cell lysates

PBS	Invitrogen, Darmstadt, Germany
Lysis buffer	100 mM NaCl
	Roth, Karlsruhe, Germany
	100 mM Tris/HCl, pH 7.5
	Roth, Karlsruhe, Germany
	100 mM EDTA
	Fluka, Sigma-Aldrich, Steinheim, Germany
	0.5 % Desoxycholate acid sodium salt
	Roth, Karlsruhe, Germany
	in H_2O_{bidest}
TNE buffer	50 mM Tris/HCl, pH 7.5
	Roth, Karlsruhe, Germany
	150 mM NaCl
	Roth, Karlsruhe, Germany
	5 mM EDTA
	Fluka, Sigma-Aldrich, Steinheim, Germany
	in H_2O_{bidest}
1 % Pefabloc SC (AEBSF)	Roche, Mannheim, Germany

	in H_2O_{bidest}
100 % Methanol	Roth, Karlsruhe, Germany
3x SDS sample buffer (SEB)	90 mM Tris/HCl
	Roth, Karlsruhe, Germany
	7 % SDS
	Roth, Karlsruhe, Germany
	0.01 % Bromphenol blue
	Merck, Darmstadt, Germany
	30 % Glycerol
	Roth, Karlsruhe, Germany
	20 % β-Mercaptoethanol
	Sigma-Aldrich, Steinheim, Germany
	in H_2O_{bidest}

Cells were lysed for western blot analysis. Therefore, grown cells were rinsed with PBS and incubated for 10 min with lysis buffer at RT. Cell lysates were centrifuged at 10,817 g (Eppendorf Centrifuge 5417R, Hamburg, Germany) for 1 min at 4 °C to remove the cell debris. The total amount of protein in the lysates was detected as described in 2.6.3. For detection of total PrP and other proteins, lysate containing 10 µg of total protein was treated with 0.02 % Pefabloc and mixed with 3x SEB. By boiling the samples for 10 min at 95 °C, proteins were denatured. Boiled samples were either stored at -20 °C or directly loaded onto a NuPAGE Novex 4 – 12 % Bis-Tris Midi gel for western blot analysis.

For the detection of PrP^{Sc} lysates were digested with proteinase K prior to Pefabloc treatment (2.6.4). Boiled samples were either stored at -20 °C or directly loaded onto a NuPAGE Novex 4 – 12 % Bis-Tris Midi gel for western blot analysis.

2.6.2 Preparation of cerebellar brain slice lysates

PBS	Invitrogen, Darmstadt, Germany
Brain slice lysis buffer	0.5 % Desoxycholate acid sodium salt
	Roth, Karlsruhe, Germany
	0.5 % Nonidet P40 substitute
	Sigma-Aldrich, Steinheim, Germany

	In PBS
1 % Pefabloc SC (AEBSF)	Roche, Mannheim, Germany
	in H_2O_{bidest}
NuPAGE LDS sample buffer	4X
	Invitrogen, Darmstadt, Germany

For protein extraction from cerebellar brain slices, inserts were washed once with PBS and brain slice lysis buffer was added. Brain slices were scraped off the inserts and two brain slices were pooled. Lysis of tissue was performed by three freeze and thaw cycles. One cycle consisted of freezing the lysates for 20 min at -80 °C, followed by thawing and sonication (Sonoplus HD3200, Bandelin Sonorex Technik, Berlin, Germany) for 30 s. After lysis, samples were cleared by low speed centrifugation at 1,152 g (Eppendorf Centrifuge 5417R, Hamburg, Germany) for 3 min at 4 °C. Pellets were discarded and the protein concentration was determined (2.6.3). For specific detection of PrP^{Sc}, 20 µg protein was digested with proteinase K as described in 2.6.5, whereas 10 µg protein was used to detect total PrP or other proteins. Those samples were directly mixed with 0.02 % Pefabloc SC and NuPAGE LDS sample buffer and boiled for 5 min at 95 °C. Samples were loaded onto a NuPAGE Novex 4 – 12 % Bis-Tris Midi gel (Invitrogen, Darmstadt, Germany) or stored at -80 °C.

2.6.3 Determination of protein concentration

Quick Start Bradford Assay	BioRAD, Hercules, USA
Quick Start Bovine Serum Albumin	BioRAD, Hercules, USA

The protein concentration of cell lysates was determined by the Bradford protein assay. 5 µL of the sample, in duplicate, a BSA standard dilution series (62.5 – 2000 µg/mL) and a lysis buffer blank control were transferred to a clear 96-well plate and 250 µL Bradford reagent was added. Samples were incubated for 5 min and absorbance was measured at 595 nm with the plate reader (FLUOstar Omega, BMG Labtech, Offenburg, Germany). A standard curve was generated using MARS data analysis software and protein concentration could be determined. If necessary samples were diluted 1:5 or 1:10 in H_2O_{bidest} , in that case H_2O_{bidest} served as blank control.

2.6.4 Proteinase K digestion of post nuclear cell lysates

1 % proteinase K (PK)	Carl Roth, Karlsruhe, Germany in H_2O_{bidest}
1 % Pefabloc SC (AEBSF)	Roche, Mannheim, Germany in H_2O_{bidest}
Blue DEXTRAN 2000	GE Healthcare, Uppsala, Sweden In lysis buffer

For detection of PrP^{Sc} post nuclear cell lysates (2.6.1) were incubated with 20 µg/mL PK for 30 min at 37 °C. Proteinase inhibitor Pefabloc SC (0.02 %) was added to stop the reaction. Blue DEXTRAN was added to the sample for detection of the cell pellet. Lysates were centrifuged at 20,817 g (Eppendorf Centrifuge 5417R, Hamburg, German) for 1 h at 4 °C and the supernatant was discarded. The pellet was resuspended in TNE buffer and 3x SDS sample buffer. Samples were boiled at 95°C for 10 min and loaded onto a NuPAGE Novex 4 – 12 % Bis-Tris Midi gel (Invitrogen, Darmstadt, Germany) or stored at -80 °C.

2.6.5 Proteinase K digestion of cerebellar brain slice lysates

1 % proteinase K (PK)	Carl Roth, Karlsruhe, Germany in H_2O_{bidest}
NuPAGE LDS sample buffer	4x Invitrogen, Darmstadt, Germany

Cerebellar brain slice lysates were supplemented with 62.5 µg/mL PK and incubated for 30 min at 37°C. The PK treatment was stopped by adding NuPAGE LDS sample buffer. After boiling the samples for 5 min at 95 °C, they were either stored at – 80 °C until use or loaded onto a NuPAGE Novex 4 – 12 % Bis-Tris Midi gel (Invitrogen, Darmstadt, Germany).

2.7 Sodium dodecyl sulfate polyacrylamide gel electrophoresis (SDS-PAGE)

NuPAGE MOPS SDS running buffer	20x Invitrogen, Darmstadt, Germany
Protein ladder	PageRuler Plus Prestained Protein Ladder Thermo Scientific, Rockford, USA

Proteins were separated by their molecular weight in an electrical field using denaturing SDS-PAGE. A NuPAGE Novex 4 – 12 % Bis-Tris Midi gel (Invitrogen, Darmstadt, Germany) was placed into an electrophoresis chamber (XCell4 Surelock Midi-Cell, Invitrogen, Darmstadt Germany). The chamber was filled with 1x NuPAGE MOPS SDS running buffer. Protein lysates and protein ladder were loaded onto the gel and electrophoresis was performed under a current of 30 mA per gel for 2.5 h.

2.8 Western blot analysis

100 % Methanol	Roth, Karlsruhe, Germany
Wet blotting buffer	192 mM Glycin Roth, Karlsruhe, Germany 25 mM Tris Roth, Karlsruhe, Germany 0.01 % SDS Roth, Karlsruhe, Germany 20 % Methanol Roth, Karlsruhe, Germany in H_2O_{bidest}
10 x TBST	0.5 % Tween-20 Roth, Karlsruhe, Germany 1.5 M NaCl, pH 8.0 Roth, Karlsruhe, Germany in H_2O_{bidest}
Blocking solution	5 % milk powder Roth, Karlsruhe, Germany In 1x TBST buffer

Amersham ECL Prime	Solution A : Solution B (1:1) GE Healthcare, Buckinghamshire, UK
Pierce ECL solution	Solution A : Solution B (1:1) Thermo Scientific, Rockford, USA
SuperSignal™ West Femto Maximum Sensitive Substrate	Solution A : Solution B (1:1) GE Healthcare, Buckinghamshire, UK

Western blot analysis was performed to electrically transfer proteins, separated by SDS-PAGE (2.7), onto a polyvinylidene difluoride (PVDF) membrane (Amersham Hybon-P, GE Healthcare, Buckinghamshire, UK) for the subsequent detection of proteins by specific antibodies. Proteins were transferred onto a methanol activated PVDF membrane using a wet blot chamber with a constant power of 30 V for approximately 17 h at 4 °C. The membrane was blocked with 5 % milk powder (MP) in TBST for 1 h to saturate unspecific binding sites. Primary antibody was incubated either for 1 h at RT or over night at 4 °C in 1 % MP in TBST (Table 5). After removing excess antibody by five washing steps for 6 min with TBST, the membrane was incubated with secondary antibodies coupled to horseradish peroxidase for 1 h at RT in 1 % MP in TBST (Table 6). The membrane was washed five times in TBST and incubated for 1-5 min in ECL solution according to manufacturers protocol. The horseradish peroxidase coupled to the secondary antibody catalyzed the conversion of the chemiluminescence substrate. The chemiluminescence was detected by the Stella Imaging System (Raytest Isotopenmessgeräte, Straubenhardt, Germany).

For detection of other proteins with a similar size on the same membrane, the membrane was stripped to remove the antibodies. The membrane was washed with H_2O_{bidest} for 10 min and incubated twice for 20 min with 1 x Re-Blot Plus Strong Solution (1:10 in H_2O_{bidest}). The membrane was carefully rinsed five times and blocked again for 30 min with 5 % MP. Afterwards the membrane was stained as described above.

2.9 Molecular biological methods

2.9.1 RNA isolation of cerebellar brain slices

PBS	Invitrogen, Darmstadt, Germany
Guanidine-isothiocyanate	4M in RLT buffer diluted 1:2 with 35 % EtOH Roth, Karlsruhe, Germany

RNA of cerebellar brain slices was isolated with the RNeasy Plus Mini Kit (Qiagen, Hilden, Germany). The manufacturer's protocol was adapted to the specific need of the experiments. Briefly, cerebellar brain slices were washed once with PBS. Afterwards, cerebellar slices were cut out of the membrane inserts with a biopsy punch (8.0 mm, Stiefel, Offenbach am Main, Germany) and slices were homogenized in highly denaturing guanidine-isothiocyanate-containing Buffer RLT Plus, that protected the RNA against degradation, using a dounce homogenizer (Homogenisator potter S, Sartorius, Göttingen, Germany). One lysate was split and transferred to two gDNA Eliminator spin columns to remove DNA in the samples. After centrifugation, the supernatant was mixed with 70 % ethanol (1:2) to provide appropriate binding conditions and passed through a RNeasy spin column. Additionally, 4 M guanidine-isothiocyanate in RLT buffer diluted 1:2 with 35 % EtOH was applied to the RNeasy spin column and incubated for 30 min to guaranty inactivation of PrP^{Sc}. After incubation, samples were centrifuged and the supernatant was loaded a second time to minimize the loss of RNA. After several washing steps with different washing buffers according to the manufacturer's protocol, RNA was eluted by adding H_2O to the column. The RNA concentration was determined as described in 2.9.3 and isolated RNA was stored at -80 °C.

2.9.2 RNA isolation of cerebella

Guanidine-isothiocyanate	4M in RLT buffer diluted 1:2 with 35 % EtOH Roth, Karlsruhe, Germany

RNA of cerebella isolated with the RNeasy Plus Mini Kit (Qiagen, Hilden, Germany). The cerebella were cut into two halves and manufacturer's protocol was adapted to the specific need of the experiments. Cerebella were homogenized with a glass

homogenizer in 1.5 mL highly denaturing guanidine-isothiocyanate-containing Buffer RLT Plus. The following steps were accomplished as described in 2.9.1. The RNA concentration was determined as described in 2.9.3 and isolated RNA was stored at -80 °C.

2.9.3 Determination of RNA concentration

Qubit® RNA Reagent	Thermo Scientific, Rockford, USA
Qubit® RNA Buffer	Thermo Scientific, Rockford, USA

The total amount of isolated RNA was determined by using Qubit® RNA Assay Kit (Thermo Scientific, Rockford, USA) according to the manufacturer's protocol. The kit is based on measurements of fluorescence signals. Samples were added to a prepared working solution and incubated for 15 min at RT after vortexing. The working solution was produced by diluting RNA reagent in RNA buffer (1:200). The RNA reagent has extremely low fluorescence until it binds to RNA. The fluorescent signal was measured by the Qubit® fluorometer (Thermo Scientific, Rockford, USA) and the RNA concentration in the samples was calculated using a reference curve of *E. Coli* rRNA concentration.

2.9.4 Next generation sequencing

RNA- TruSeq RNA sample preparation 2 Kit	Illumina, San Diego, USA
Transcriptor high fidelity cDNA synthesis Kit	Roche Applied Science, Mannheim, Germany
TruSeq SBS Kit 3-HS	Illumina, San Diego, USA
TruSeq SR Cluster Kit 3-cBot-HS	Illumina, San Diego, USA
Qubit® dsDNA HS Assay Kit	Thermo Scientific, Rockford, USA

RNA-sequencing was done at the DZNE in Göttingen (AG Bonn). Each individual RNA sample was checked for quality and RNA integrity number using Nanodrop 2000 (Thermo Scientific, Rockford, USA) and Agilent 2100 Bioanalyzer (Agilent, Santa Clara, USA), respectively. For each condition two individual samples were pooled. RNA was converted to cDNA using the Transcriptor High Fidelity cDNA synthesis Kit. RNA-

sequencing libraries were prepared using the TruSeq RNA Sample Preparation 2 Kit. The library quality was checked using an Agilent 2100 Bioanalyzer and concentration was measured by a Qubit® dsDNA HS Assay Kit and adjusted to 2 nM before sequencing (single end, 50 bp) on a HiSeq 2000 Sequencer using TruSeq SR Cluster Kit 3-cBot-HS and TruSeq SBS Kit 3-HS according to the manufacturer's instructions.

2.9.5 Polymerase chain reaction (PCR)

iScript reaction mix	5x Biorad, Hercules, USA
iScript reverse transcriptase	Biorad, Hercules, USA

For generation of cDNA iScript PCR kit was used according to the manufacturer's instructions. RNA samples were kept on ice all the time and were adjusted to 50 ng in 15 µL water and mixed with 4 µL iScript reaction mix and 1 µL iScript reverse transcriptase. The reaction was run as followed: 5 min at 25 °C; 30 min at 42 °C, 5 min at 85 °C and held on 4 °C (Biorad T100 Thermal Cycler, Hercules, USA). Concentration of generated cDNA was measured (2.9.7) and stored at -20 °C.

2.9.6 Real time PCR (qPCR)

Table 7. TagMan probes

Gene	Species	Amplicon length	Label
Met	Mouse	74	FAM
Apc	Mouse	85	FAM
Hgf	Mouse	85	FAM
SYT1	Mouse	81	FAM
Slc17a7	Mouse	55	FAM
Stx1b	Mouse	92	FAM
Cxcl10	Mouse	59	FAM
Gfap	Mouse	75	FAM
Snap25	Mouse	66	FAM
Actb	Mouse	143	VIC

TaqMan gene expression master mix	Thermo Scientific, Rockford, USA
TaqMan gene expression assay	Thermo Scientific, Rockford, USA

Generated cDNA was diluted in water (200 ng/8 µL). A master mix was prepared containing 10 µL of TaqMan gene expression master mix, 1 µL TagMan gene

expression assay (target genes) and 1 µL housekeeping gene (actin) (Table 7). TaqMan gene expression assays consist of a pair of unlabeled PCR primers and a TaqMan probe with an FAM (target genes) or VIC (actin) dye label on the 5' end and minor groove binder and nonfluorescent quencher on the 3' end. Master mix solution was pipetted into a PCR 96-well plate (TW-MT-Plate, Biozym, Hessisch Oldendorf, Germany) and 8 µL of the sample was added. The plate was covered with a plastic sheet and centrifuged at 300 g for 1 min. The samples were placed into the qPCR machine (Applied Biosystems StepOnePlus Realtime PCR System, California, USA) and incubated for 2 min at 50 °C, followed by 10 min at 95 °C. 40 cycles of 15 s denaturing at 95 °C and 1 min annealing and extending at 60 °C were performed.

2.9.7 Quantification of DNA concentration

Single stranded DNA concentration was determined by measuring the absorbance in the samples at a wavelength of 260 nm (A260) with the NanoDrop spectrophotometer (NanoDrop2000). H_2O_{bidest} severed as blank control. An absorbance of 1 at 260 nm equals a concentration of 50 µg/ml DNA. Possible protein concentration was measured at an absorbance of 280 nm (A280). A ratio of A260/A280 lower 1.8 indicates protein contamination, whereas a higher value confirms a good quality of the samples.

2.10 Data analysis and statistics

2.10.1 Image editing

Confocal images captured with the LSM 700, upright LSM 700 (Zeiss, Jena, Germany) or inverse epifluorescece microscope (Axio observer Z1, Zeiss, Jena, Germany) were processed using Zen 2010 (black edition) or Zen 2012 (blue edition) software (Zeiss, Jena, Germany).

2.10.2 Image data analysis with Columbus software

Image analysis of the high-throughput screen was performed in collaboration with Christoph Möhl (DZNE, Bonn) using Columbus 2.4.1. Briefly, the input data consisted of two different channels: Nucleus/Cytoplasm marker (C0) and aggregate marker (C1). Nuclei were detected in the C0 channel with "Find Nuclei" (method A, common threshold 0.4, area > 70 µm2, split factor 7, individual threshold 0.4, contrast 0.1). The cytoplasm

region was detected in C0 with “Find Cytoplasm” (method A, individual threshold 0.15). With a feature analysis two sensitive features were selected for successfully PrP^{Sc} detection within cells: Haralick Contrast 1px and Haralick Sum Variance 1px. Haralick features contain information about the textural characteristics of an image (156). The contrast feature measures the local variation of intensity between two pixels. Cells with HaralickContrast > 0.04 and HaralickSumVariance > 0.17 should be classified as PrP^{Sc} infected cell.

2.10.3 Image data analysis with Cell Voyager Analysis support software

$L929^{15.9}$ and $L929^{22L}$ images analyzed by an automatic confocal microscope (Cell Voyager) were further assessed by the Cell Voyager support software. An image analysis routine was developed for single-cell segmentation and aggregate identification (Yokogawa Inc.). The total number of cells was determined by nuclei detection based on the Hoechst signal, and morphology properties. The corresponding cytoplasm was identified based on intensity levels of HCS CellMask Blue stain. Cells touching the borders of an image were excluded. The spot detection module was used for detection of PrP^{Sc} puncta. The algorithm was carefully trained using specific morphology parameters and intensity characteristics. Uninfected control cells served as PrP^{C} background signals. If PrP^{Sc} puncta were linked to single cells, this cell was considered to be infected. The total number of infected and uninfected cells was counted and percentage of infected cells per well was calculated.

2.10.4 RNA-sequencing data analysis

RNA sequencing data analysis was performed in collaboration with Melvin Schleif (AG Jackson, DZNE Bonn). Raw RNA-Sequencing data was imported into the CLC Genomics Workbench (8.5.1), quality checked, trimmed and mapped to the mouse genome (NCBI GRCm38.82). The trimming parameters were ambiguous trim limit = 2; quality trim limit = 0.05; minimum number of nucleotides in reads = 30. The mapping parameters were maximum number of hits for a read = 1; strand specific = both; similarity fraction = 0.8; length fraction = 0.9; mismatch cost = 2; insertion cost = 3; deletion cost = 3. Mapped sequence data were compared to each other with CLC (Mock vs. RML od Mock vs. 22L). Differential expression analysis was carried out using UER

counts from CLC with DESeq1 package (1.9.12) in R-Project Bioconductor (3.1.2). The following workflow was run:

```
> datafile = system.file("Data/XXX.txt", package="DESeq")
> CountTable = read.table(datafile, header=TRUE, row.names=1)
> #not run
> condition = factor(c("Group1", "Group2"))
> library("DESeq")
> cds =newCountDataSet(CountTable, condition)
> cds = estimateSizeFactors(cds)
> sizeFactors(cds)
> cds = estimateDispersions(cds, method="blind", sharingMode="fit-only")
> res = nbinomTest(cds, "Group1", "Group2")
> write.csv(res, file="XXX.csv")
```

2.10.5 Evaluation of qPCR

For evaluation of qPCR results the obtained C_T values of the housekeeping genes was subtracted from C_T values of the genes of interest (ΔC_T). ΔC_T of Mock samples was subtracted from ΔC_T 22L or RML samples and multiplied by -1 ($-\Delta\Delta C_T$). The power of this value was calculated ($2^{-\Delta\Delta C_T}$) (157).

2.10.6 Statistical analysis

Statistical analysis was performed using Graph Pad Prism 6 (Graph Pad software, La Jolla, CA, USA). Statistical analysis of data was performed using the unpaired two-tailed Student´s t-test for single comparisons or one-way ANOVA with Dunnett's multiple comparisons test. Error bars represent the standard deviation (SD) and the sample size was at least three. A p-value less than 0.05 was considered as statistically significant (*$p \leq 0.05$, **$p \leq 0.01$, ***$p \leq 0.001$, ****$p \leq 0.0001$).

3 Results

The central event in prion disease is the conversion of an α-helix-rich PrP^{C} into a misfolded β-sheet-rich, pathogenic and infectious isoform PrP^{Sc} (158). Stabilization of native PrP^{C} without blocking of the normal function, interruption of the conversion of PrP^{C} into PrP^{Sc} or reduction of already existing PrP^{Sc} aggregates could be possible ways to intervene with prion disease. Although there are several compounds known to inhibit prion accumulation in cell culture systems (146, 155, 159, 160), a therapeutic compound is still missing. We wanted to test a promising anti-prion compound candidate and a novel synthesized compound in an *ex vivo* system as this method provides a more complex cellular system, which increases the probability that a compound shows similar effects *in vivo*. For this purpose the iron-containing cationic alkylpyridyl porphyrin FeTMPyP was chosen. FeTMPyP is a compound, which previously was shown to bind to PrP^{C}, and is capable of inhibitiing PrP^{C}-mediated toxicity and is known to inhibit the replication of multiple prion strains *in vitro* (161). Beside this PIM-B31 was tested. This drug was provided in collaboration with Emiliano Biasini (University of Trento) who synthesized it as a potential anti-prion compound.

3.1 *Ex vivo* analysis of compounds

For *ex vivo* analysis, the prion organotypic slice culture assay (POSCA) was used, as it is an advanced model for prion studies (138). Slice cultures from neonatal mouse cerebella can be infected with different prion strains, including prion strains 22L and RML (137, 138). Cerebellar organotypic cultures (COCS) present a complex cell environment with interactions among highly diverse cell types including neurons, astrocytes and microglia. In contrast to *in vivo* models, the blood-brain barrier, which can display an obstruction for drug application is lacking in COCS, but at the same time the *in vivo* microenvironment is largely retained (162). Therefore COCS represents a powerful tool to study the effectively of anti-prion compounds.

3.1.1 Experimental setup to study anti-prion compounds *ex vivo*

For studying the effect of FeTMPyP and PIM-B31 *ex vivo* the following experimental setup was designed. COCS were prepared from 9 - 13 days old pups of C57BL/6JRj mice (2.3.2), infected with 22L prions (2.3.3) and grown for 2 weeks (2.3.4) to allow establishment of the infection (Figure 5). Two weeks post infection (p.i.), COCS were treated with diverse compounds at different concentrations replacing the normal culture medium with compound-containing culture medium for five weeks. COCS were analyzed seven weeks p.i. by either immunofluorescence staining, western blot analysis, propidium iodide staining or a combination of those methods. For specific detection of PrP^{Sc} by immunofluorescent staining, fixed samples were treated with guanidine hydrochloride. GdnHCl reduces PrP^{C} background staining, while drastically increasing the immunoreactivity of PrP^{Sc} (147). Due to the proteinase K resistance of PrP^{Sc}, PK treatment of lysates can be used to discriminate between PrP^{Sc} and PrP^{C} by western blot analysis (16).

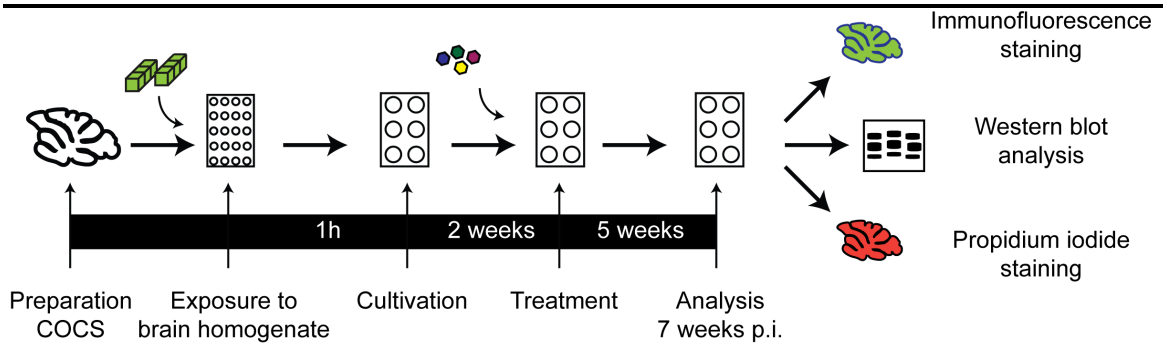

Figure 5. Experimental setup for compound treatment of 22L or RML prion infected cerebellar organotypic cultures. Cerebella were dissected from 9 - 13 days old C57BL/6JRj pups and organotypic slices were produced. After incubation for one hour with 20 mg/mL 22L/RML prion-infected brain homogenate, slices were grown for 2 weeks until treatment with compound via culture medium started. Slices were treated for 5 weeks followed by immunofluorescence staining, western blot analysis and/or propidium iodide staining. As negative control COCS were exposed to uninfected brain homogenate (Mock).

3.1.2 FeTMPyP shows a strong toxicity on COCS

First the toxicity of FeTMPyP on COCS was evaluated. The viability of slices was investigated using propidium iodide (PI) that incorporates into dead cells. Therefore, COCS were grown for one day and FeTMPyP (solved in water) at six different concentrations (100 µM, 50 µM, 25 µM, 12.5 µM, 6.25 µM and 3.75 µM) was added. After two weeks of treatment, PI staining was performed. As a positive control for PI staining, untreated COCS were incubated with 5 µM staurosporine for 2 days.

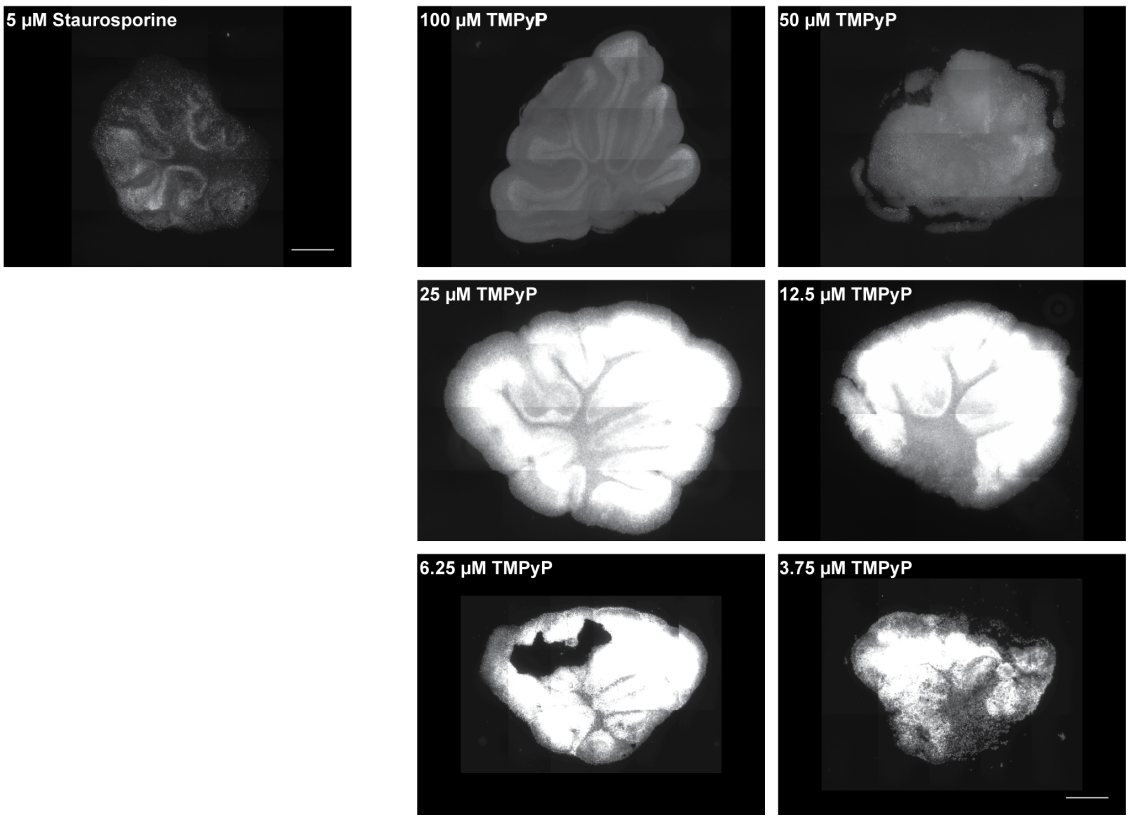

Figure 6. FeTMPyP-treated COCS showed massive PI incorporation. Uninfected cerebellar slices were cultured for 1 day followed by treatment with FeTMPyP for 2 weeks. Slices were incubated with 10 µg/mL PI for 2 h to stain dead cells. **(A)** COCS treated with 5 µM Staurosporine for 2 days served as positive controls for the staining method. **(B)** PI incorporation by COCS treated with 3.75 – 100 µM. Samples were analyzed by epifluorescence microscopy with a magnification of 10x using tile scanning function with identical imaging settings. Scale bar: 500 µm.

FeTMPyP decreased the viability of cerebellar slices (Figure 6 B). At concentrations from 25 µM to 3.75 µM, massive PI incorporation was observed and COCS started to shrink, indicative of compound toxicity. Treatment with FeTMPyP was even more toxic than the positive control with 5 µM Staurosporine (Figure 6 A). Strikingly, at higher concentrations (100 µM and 50 µM), PI incorporation decreased, potentially due to precipitation of the drug. For further experiments, a concentration below the tested ones was chosen (1 µM).

To test if FeTMPyP is effective against persistent 22L and RML infection in COCS, slices were prepared and exposed to 22L or RML prions for 1 h. Starting 2 weeks post infection cerebellar slices were continuously exposed to culture medium containing 1 µM FeTMPyP. As visual inspection of slices showed strong toxicity, samples were analyzed by immunofluorescence staining 5 weeks p.i..

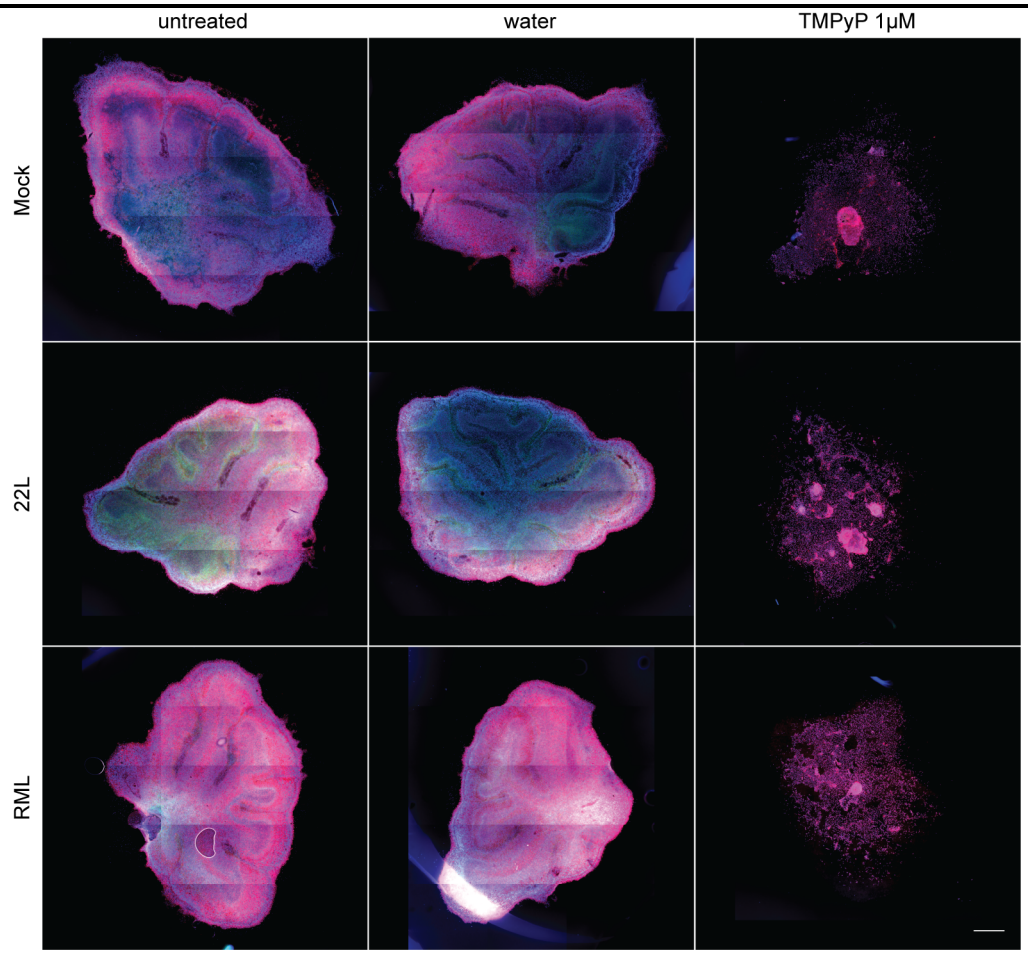

Figure 7. Treatment with 1 µM FeTMPyP was toxic for cerebellar slices. Mock brain homogenate, 22L or RML prion exposed COCS were cultured for 2 weeks. At that time point, the treatment with 1 µM FeTMPyP or water was started. Three weeks p.i., PrP^{Sc} was specifically stained with mAb 4H11 following GdnHCl treatment of fixed cells (green). Neurons were detected with pAb β -3-tubulin (red) and lysosomes were labeled with mAb Lamp-1 (magenta). Nuclei were counterstained with Hoechst (blue). Cerebellar slices exposed to (uninfected) mock brain homogenate served as controls. Samples were analyzed by epifluorescence microscopy with a magnification of 10 using tile scanning function with identical imaging settings. Scale bar: 500 µm.

Unfortunately, the treatment of infected COCS with 1 µM FeTMPyP for 3 weeks was extremely toxic and led to a nearly complete dissolution of the COCS (Figure 7). Therefore, drug treatment with FeTMPyP was discontinued.

3.1.3 Treatment of COCS with PIM-B31 is non-toxic, but has variable effects on PrP^{Sc} accumulation

Parallel to experiments with FeTMPyP, the compound PIM-B31 was tested on COCS with the same experimental setup. To identify a concentration of PIM-B31 on COCS that is not toxic, slices grown for one day before treatment for two weeks with different concentrations of PIM-B31 (3.75 - 100 µM) and PI staining was performed. Slices treated with 5 µM Staurosporine for 2 days served as positive control of PI incorporation.

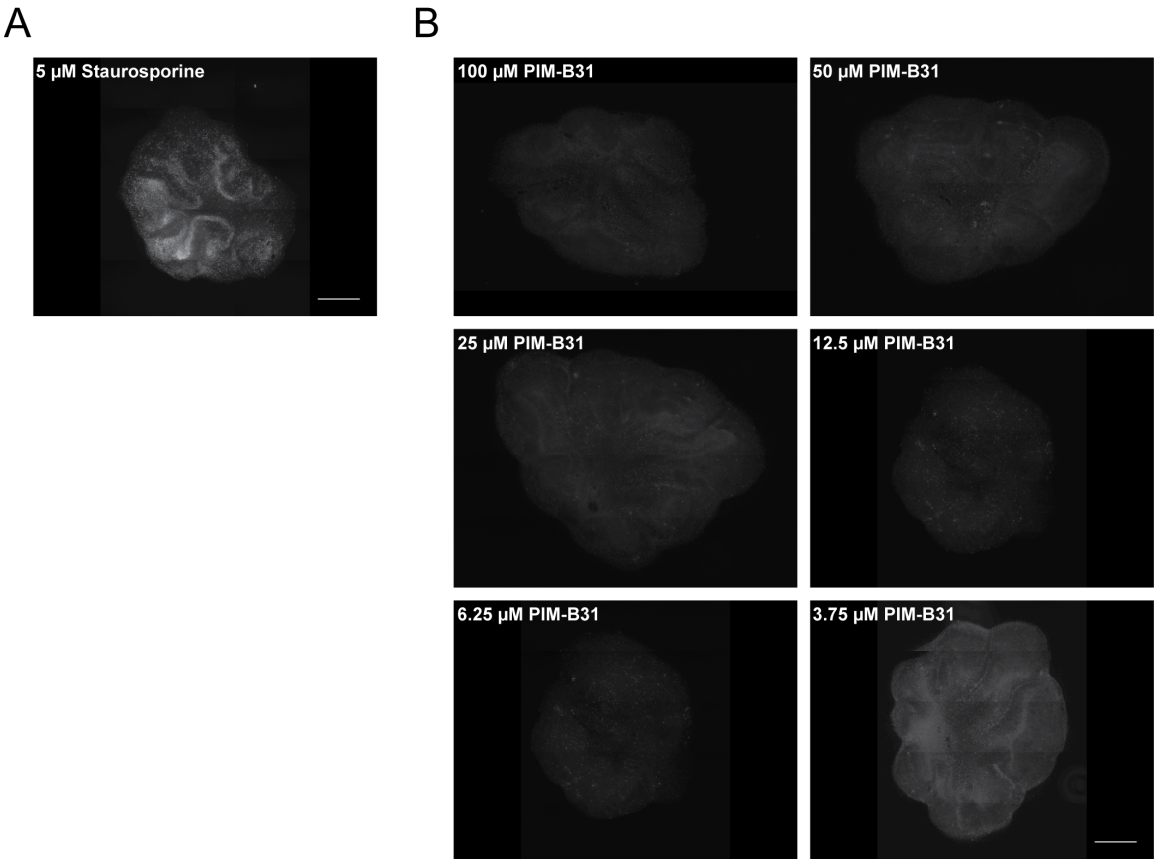

Figure 8. Treatment with PIM-B31 did not result in increased PI incorporation into COCS. Uninfected cerebellar slices were cultured for 1 day and subsequently treated with PIM-B31 for 2 weeks. Slices were incubated with 10 µg/mL PI for 2 h to visualize dead cells. **(A)** As positive control COCS were treated with 5 µM Staurosporine for 2 days. **(B)** Treatment of COCS with different concentrations (100, 50, 25, 12.5, 6.25, or 3.75 µM) of PIM-B31 on COCS. Samples were analyzed by epifluorescence microscopy with a magnification of 10x using the tile scanning function and identical imaging settings. Scale bar: 500 µm.

Treatment of cerebellar slices with PIM-B31 for 2 weeks showed almost no toxic effect, independent of the concentration (Figure 8). Therefore, a low concentration (10 µM) and a high concentration (50 µM) of PIM-B31 were chosen to test the influence of PIM-B31 on 22L or RML infected COCS. Two weeks p.i. COCS were treated with culture medium containing 50 µM and 10 µM PIM-B31. At week 5 p.i., samples were analyzed and western blot analysis, immunofluorescence staining and propidium iodide staining were performed. Treatment of 22L infected slices with 10 µM or 50 µM PIM-B31 for 3 weeks showed almost no effect on viability (Fig. 6). This time treatment with 8.8 µM H_2O_2 served as a positive control, as 5 µM Staurosporine led to little PI incorporation (Figure 9).

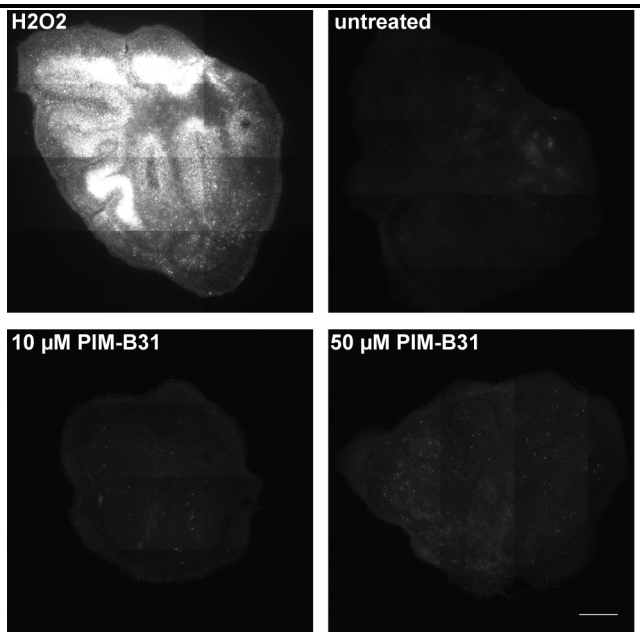

Figure 9. Treatment with PIM-B31 showed no toxicity, as no PI incorporation into infected COCS could be observed. Infected COCS were cultured for 2 weeks followed by treatment with PIM-B31 (50 and 10 µM) for 3 weeks. Slices were incubated with 10 µg/mL PI for 2 h to stain dead cells. COCS treated with 8.8 µM H_2O_2 for 1 days served as positive controls. Samples were analyzed by epifluorescence microscopy with a magnification of 10x using the tile scanning function and identical imaging settings. Scale bar: 500 µm.

Western blot analysis was conducted (Figure 10) to reveal successful infection of slices. In Mock treated COCS, no signal for PrP^{Sc} was detected. Infection with 22L and RML prions led to a strong signal of PrP^{Sc} in DMSO-treated controls. Signal intensity of PrP^{Sc}

changed in response to PIM-B31 treatment. Treatment of RML prion infected slices showed variable results; there appeared to be a reduction in PrP^{Sc} signal at 10 µM and 50 µM, but the variation was very high (Figure 10 A, C). The variation might originate from technical problems during sample preparation or western blot procedure. It was therefore decided to repeat the experiment. Treatment of 22L prion-infected cerebellar slices with 50 µM PIM-B31 led to a reduction of the PrP^{Sc} signal in western blot analysis, whereas treatment with 10 µM PIM-B31 led to a slight increase in signal (Figure 10 A, B).

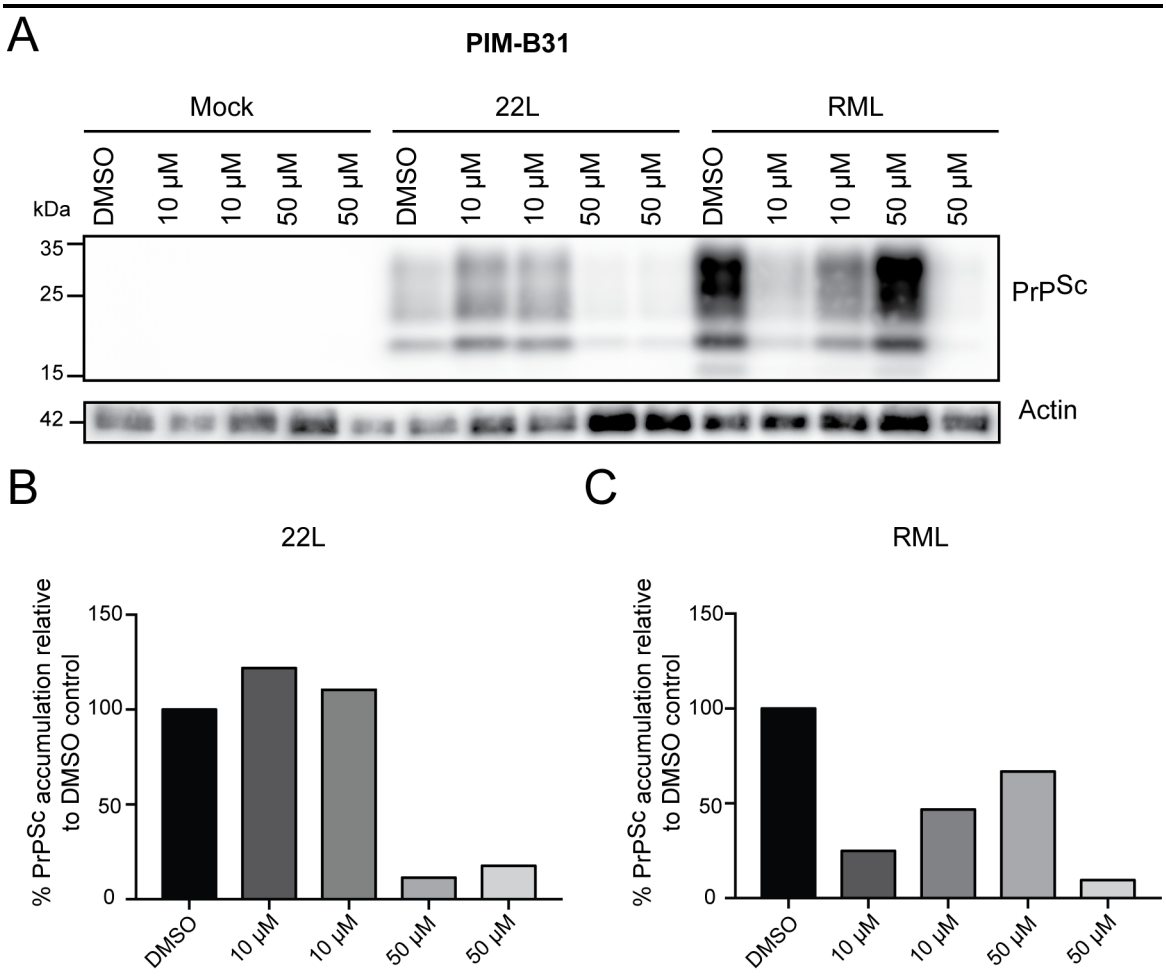

Figure 10. Influence of PIM-B31 on PrP^{Sc} levels in cerebellar slices during persistent infection with 22L or RML. COCS exposed to Mock brain homogenate, 22L or RML prions were cultured for 2 weeks. Subsequently, COCS were continuously exposed to 10 µM or 50 µM SM31. COCS were lysed at week 5 p.i. for western blot analysis **(A)** For one lysate two slices were pooled. PK-resistant PrP (PrP^{Sc}) was detected using mAb 4H11. Actin was detected in –PK samples as loading control. **(B – C)** Quantification of PrP^{Sc} signals normalized to actin. Experiments were performed in duplicate. One bar represents one experiment.

Comparable results were observed when 22L infected COCS were stained for immunofluorescence analysis (Figure 11). RML infected COCS were not analyzed by immunofluorescence staining, because we were not capable to develop a staining protocol detecting RML prions in COCS with a quality suitable for analysis.

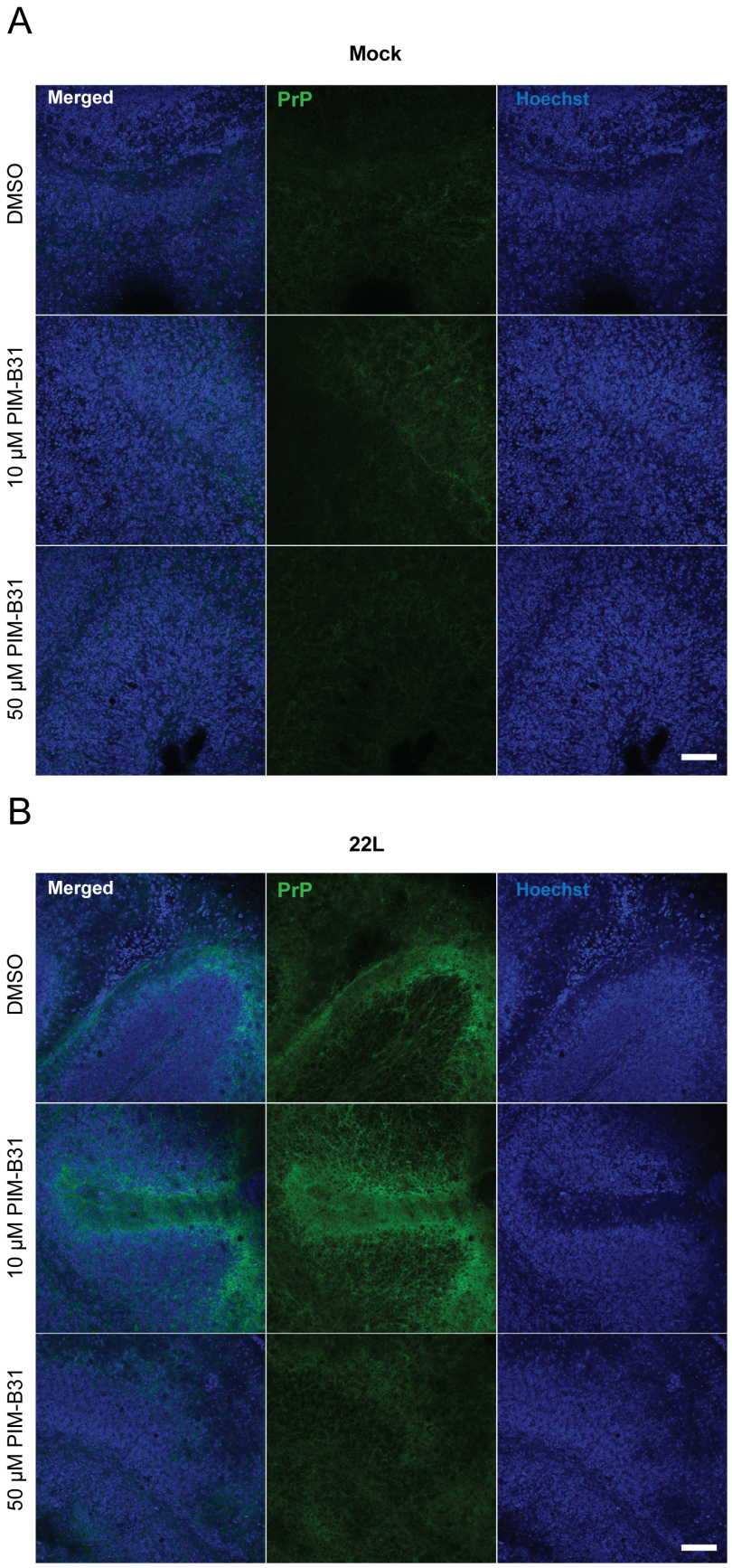
A
Mock
Merged
PrP
Hoechst
DMSO
10 µM PIM-B31
50 µM PIM-B31
B
22L
Merged
PrP
Hoechst
DMSO
10 µM PIM-B31
50 µM PIM-B31

Figure 11. Reduction of PrP^{Sc} levels upon treatment with 50 µM PIM-B31 in 22L infected COCS during persistent 22L infection. Mock brain homogenate **(A)** or 22L prion exposed **(B)** cerebellar slices were cultured for 2 weeks. At that time point, the treatment with DMSO or PIM-B31 was started. At 5 weeks p.i., COCS were fixed and PrP^{Sc} was specifically stained with mAb 4H11 following GdnHCl treatment. Nuclei were counterstained with Hoechst. Cerebellar slices exposed to (uninfected) Mock brain homogenate served as controls. Samples were analyzed by confocal microscopy with identical imaging settings. Scale bar: 50 µm.

Untreated cerebellar slices demonstrated successful infection with 22L prions. The signal intensity of PrP^{Sc} showed no noticeable changes after treatment with 10 µM PIM-B31 (Figure 11 B middle panel), but treatment with 50 µM PIM-B31 led to a decrease in the PrP^{Sc} signal (Figure 11 B lower panel).

To validate the results, PIM-B31 was tested again on COCS persistently infected with 22L or RML. Therefore, freshly prepared cerebellar slices were exposed to 22L or RML prions or Mock brain homogenate and were treated as described above. As the compound batch used in the previous experiment was almost depleted COCS were treated with a freshly synthesized batch of PIM-B31 this time. Additionally, COCS were analyzed seven instead of five weeks p.i. by western blot analysis and immunofluorescence staining as we expected that a longer treatment might lead to more significant results.

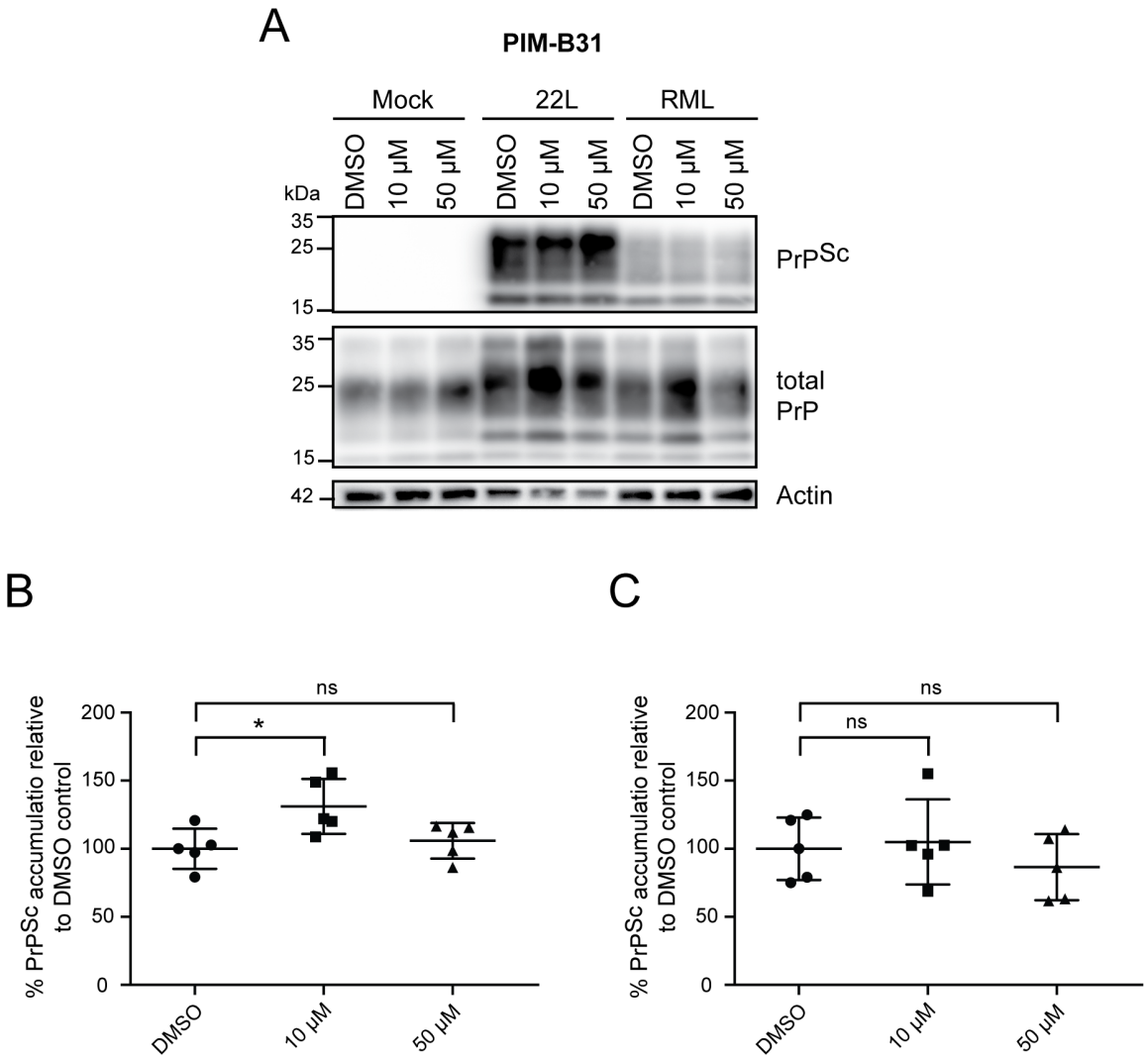

Figure 12. Influence of PIM-B31 on levels of PrP^{Sc} in cerebellar slices during persistent 22L and RML infection. COCS, exposed to Mock brain homogenate, 22L or RML prions were cultured for 2 weeks. Subsequently, treatment with 10 or 50 µM PIM-B31 was started and slices were lysed 7 week p.i.. **(A)** Western blot analysis. PrP^{Sc} was detected in PK treated samples using mAb 4H11. Actin and total PrP were detected in –PK samples as loading controls. Experiments were performed in quintuplicates. **(B – C)** Quantification of western blot analysis. PrP^{Sc} accumulation was normalized against actin and PrP^{Sc} accumulation in compound-treated samples was compared to PrP^{Sc} accumulation in DMSO-treated samples, which were set to 100 %. A single dot represents one experiment, the line the mean and the whiskers the standard deviation. One-way ANOVA with Dunnett´s multiple comparisons test was used to statistically analyze the data. Asterisks display significant changes (*p ≤ 0.05, ns= not significant).

Quantification of western blot analysis revealed successful infection of COCS with 22L and RML prions, although the signal intensity of PrP^{Sc} was stronger in 22L infected COCS. Treatment with 10 µM PIM-B31 of 22L infected led to slightly significant increase of PrP^{Sc} accumulation, as found in the previous experiment. Surprisingly and in contrast to the experiment with the old batch of the compound, treatment with 50 µM showed no significant changes in PrP^{Sc} accumulation in 22L infected COCS. Results for RML-infected PIM-B31 treated COCS were also contradictory to the experiment with the old batch. This time no significant changes in signal intensity could be observed at both concentrations.

It was possible that the lack of compound activity was due to the new batch of compound that was used in the repeat experiment. To exclude this possibility, a comparative experiment of the anti-prion activity of the old and new batch of PIM-B31 was performed. Emiliano Biasini had shown that PIM-B31 successfully reduces PrP^{Sc} accumulation in N2a cells infected with prion strain 22L (unpublished data). Therefore, the old and new batch of PIM-B31 were tested on persistently infected $N2a^{22L}$ cells, comparable to his protocol. For testing this, $N2a^{22L}$ cells were treated with 50 µM PIM-B31 of the old and the new batches of the drug and PrP^{Sc} accumulation was analyzed by western blot (Figure 13 A).

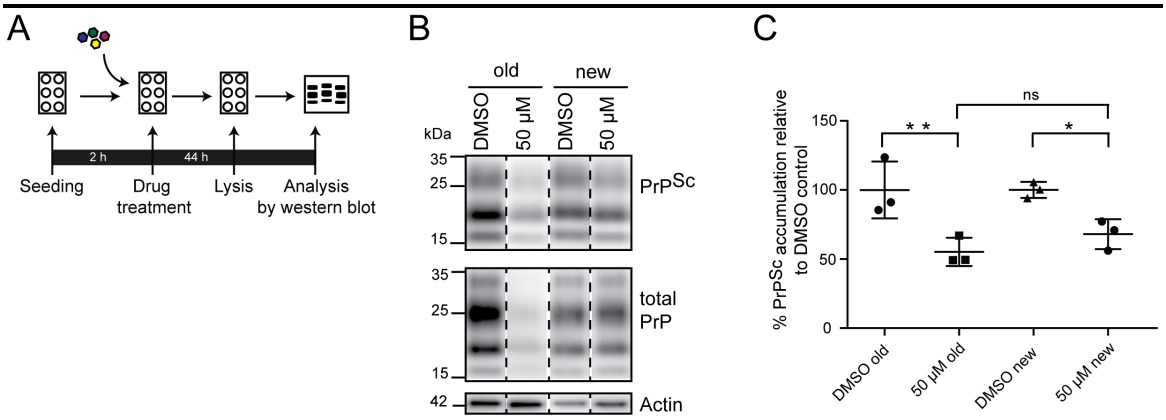

Figure 13. Influence of two different batches PIM-B31 on levels of PrP^{Sc} in persistently 22L prion infected cells. (A) Persistently infected $N2a^{22L}$ cells were seeded on 6-well plates and treated for 44 h with 50 µM PIM-B31. **(B)** PrP^{Sc} was detected in PK treated samples using mAb 4H11. Actin and total PrP was detected in –PK samples as loading control. Experiments were performed in triplicates. For presentation purposes empty lanes were cut out, indicated by the dotted line. **(C)** Quantification of western blot analysis. A single dot represents one experiment, the line the mean and the whiskers the standard deviation. One-way ANOVA with Dunnett´s multiple comparisons test was used to statistically analyze the data. Asterisks display significant changes (*$p \leq 0.05$, ns= not significant).

Treatment of $N2a^{22L}$ cells with 50 µM PIM-B31 of the old and new compound batch led to a significant reduction of PrP^{Sc} accumulation. The signal intensity of PrP^{Sc} of cells treated with the old batch of PIM-B31 decreased to 55 % compared to DMSO-treated cells. The reduction of PrP^{Sc} accumulation was less if cells were treated with the new batch of PIM-B31 (68 %). However, the difference between both batches was not significant (Figure 13 C).

In summary, treatment with PIM-B31 of RML infected COCS showed diverse effects on PrP^{Sc} accumulation with the first compound batch. Treatment with the second batch of PIM-B31 resulted in no changes in PrP^{Sc} accumulation in RML infected COCS. Signal intensity of PrP^{Sc} in 22L infected COCS treated with 10 µM PIM-B31 increased slightly with both batches, whereas treatment with 50 µM PIM-B31 with the first batch of drug led to a strong decrease of PrP^{Sc} accumulation, but no effect could be detected with the second batch of PIM-B31, maybe due to technical errors. No toxicity of PIM-B31 could be observed in COCS or cells.

3.2 Identification of compounds effective against 22L mouse adapted prions in a cell culture high-throughput screen

Testing of FeTMPyP, a known *in vitro* anti-prion compound and PIM-B31, a novel synthesized potential anti-prion compound on prion-infected COCS unfortunately did not reveal suitable candidates for further *in vivo* analysis. Therefore, we aimed to discover new candidates that are capable of reducing already existing PrP^{Sc} aggregates. For this purpose a cell culture based high-throughput screen on persistently prion strain 22L infected cells was established.

3.2.1 Assay development for PrP^{Sc} detection in prion-infected cells in a 96-well format

The assay was established in a 96-well format for uninfected L929 cells ($L929^{15.9}$) and persistently 22L prion infected cells ($L929^{22L}$), a subclone highly susceptible to mouse-adapted scrapie strains 22L and RML (Table 4). Cells were seeded to be approximately 90 % confluent at the time of fixation, so that proper separation of cells by the image analysis routine was possible and to avoid different cell numbers in each of the imaged positions per well. To identify whether different cultivation times affect the percentage of infected cells, $L929^{15.9}$ and $L929^{22L}$ cells were seeded on three different 96-well plates (5000 cells/well, 30 wells per cell line) and fixed after 24 h, 48 h and 72 h. Plates were stained as described in 2.5.2. Due to biosafety regulations of the screening facility a method to inactivate the prion containing plate was established. The whole 96-well plate was immersed in 6M guanidine hydrochloride and cells were washed with PBS. The external surface was carefully rinsed with water and EtOH. Cells were analyzed with an automatic confocal microscope (Cell Voyager 6000) with a 10x objective. Image analysis was performed with the Cell Voyager Analysis support software and an image analysis routine was developed for single-cell segmentation and aggregate identification (2.10.3). If at least one aggregate was detected per cell, this cell was counted as positive. Per condition and cell type, at least 27,000 cells were analyzed. The percentage of PrP^{Sc} containing cells changed only slightly over the time course of 24 – 72 h (Figure 14).

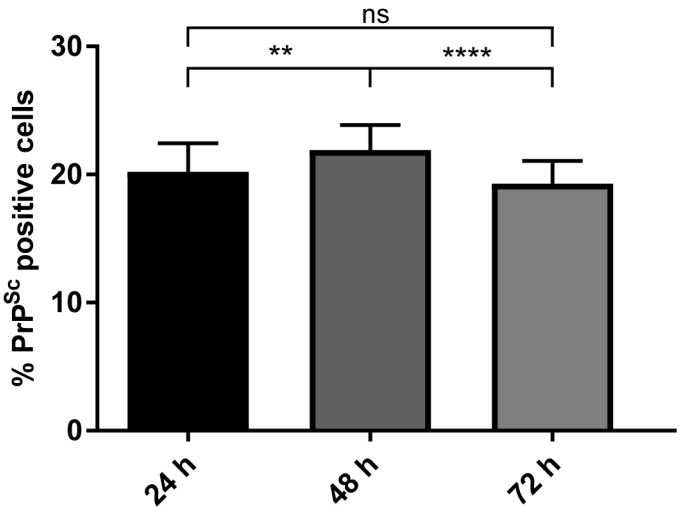

Figure 14. Cells cultured for 48 h showed the highest percentage of infected cells in contrast to cells cultured for 24 h or 72 h. 5000 cells per well of $L929^{15.9}$, which served as background control for PrP^{C} , and $L929^{22L}$ were seeded on three 96-well plates and grown for 24, 48 or 72 h. Plates were fixed and immunofluorescence staining followed by GdnHCl treatment was performed. PrP^{Sc} was detected by mAb 4H11, nuclei were detected by Hoechst and cytoplasm by CellMask. Plates were analyzed by an automatic confocal microscope (Cell Voyager 6000) with a 10x objective and PrP^{Sc} infected and uninfected cells were detected by Cell Voyager Analysis support software. At least 27,000 cells were analyzed per condition per cell type. One-way ANOVA with Dunnett's multiple comparisons test was performed. Bars represent mean values ± SD (**p ≤ 0.01, ****p ≤ 0.0001, ns: not significant).

After 48 hours of cultivation the percentage of PrP^{Sc} positive cells was the highest (22 %). The differences between 24 hours (20 % PrP^{Sc} positive cells) and 72 hours (19 % PrP^{Sc} positive cells) of cultivation were only marginal. Thus, each cultivation time would be suitable for further experiments. Due to practical reasons and for optimal workflow 46 h hours of cultivation were chosen for future experiments.

3.2.2 Establishment of a cell-based high-throughput screen for PrP^{Sc} detection in chronically prion-infected N2a cells using automated microscopy

After successful development of an assay for PrP^{Sc} detection in L929 cells in a 96-well format, a high-throughput screen was established to find potential drug targets for prion disease. For the high-throughput screen N2a cells were used instead of L929 cells. N2a

cells are a murine neuroblastoma cell line. N2a cells have been extensively used to study neuronal differentiation, axonal growth and signaling pathways (163). They are fast growing and are capable of differentiating into cells displaying certain properties of neurons (163). Several studies of neurodegenerative diseases, like Alzheimer´s disease (164) and Creutzfeldt-Jakob disease (123), are based on N2a cell culture work. Furthermore, N2a cells are capable of being persistently infected with prions and the reproducibility of productive infection in N2a cells was demonstrated (165). For those reasons, the developed assay protocol was optimized for uninfected N2a cell ($N2a^{uninfected}$) and 22L infected N2a cells ($N2a^{22L}$).

Several parameters needed to be adapted: the cell number was changed to 4,000 cells per well and a different image analysis was applied. Due to specific characteristics of the N2a cells analysis with Cell Voyager Analysis support software was not as accurate as it was for L929 cells. Either increased numbers of false positive (detection of putative PrP^{Sc} in cells that are not infected) or false negative cells (cells were considered as not infected although they were PrP^{Sc} positive) were identified. A refined analysis was performed by the Columbus software in collaboration with Christoph Möhl (DZNE, Bonn). The Columbus system is an internet-based, universal high-volume image data storage and analysis system that is compatible with Cell Voyager 6000 imaging data. Nuclei were detected by Hoechst signal and cytoplasm by CellMask. With a complex analysis of in total 62 features, two sensitive features were selected that successfully detected cells with PrP^{Sc} as described in 2.10.2 (Haralick Contrast 1px and Haralick Sum Variance 1px). Haralick features characterize the textural characteristics of an image. The contrast feature measures the local variation of intensity between two pixels.

For a high-throughput screen $N2a^{22L}$ cells were seeded on 96-well plates in 60 wells. $N2a^{uninfected}$ cells were seeded every plate for detection of the PrP^{C} background signal. (Figure 15).

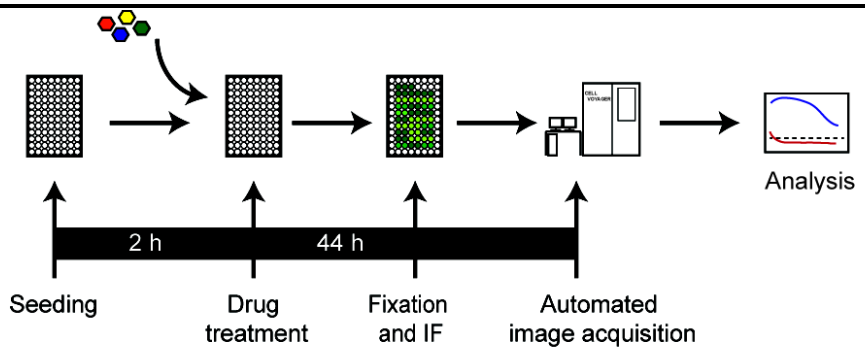

Figure 15. Experimental setup for the high-throughput screen. N2a and N2a^{22L} cells were seeded on 96-well plates. After 2 h drugs were added to the plates and cells were grown for 44 h. For detection of PrP^{Sc} with mAB 4H11 immunofluorescence staining following GdnHCl treatment was performed. Nuclei were detected by Hoechst and cytoplasm by CellMask. Plates were analyzed by an automatic confocal microscope (Cell Voyager 6000) with a 10x objective.

A yeast-based screen identified molecules reducing protein aggregation that were found to be also efficient in promoting mammalian prion clearance in an *in vitro* system (166). Therefore, 152 compounds from a preselected library that originated from our unpublished screen based on cell-to-cell propagation of the yeast prion Sup35NM (167) performed by Shu Liu (DZNE Bonn) were tested. In this assay, donor mouse neuroblastoma N2a cells containing aggregated HA-tagged Sup35NM and recipient N2a cells expressing soluble GFP-tagged Sup35NM were cocultured for 12 hours. After staining with anti-HA antibody and image acquisition, NM-HA aggregates in donor cells and NM-GFP aggregates in recipient cells were quantified. 4,050 compounds (from Tocris, Selleckchem and Lopac commercially available bioactive compound libraries) were tested for their effect on both donor cells for preexisting aggregates and recipient cells for intercellular aggregate transmission or aggregate *de novo* generation. 152 hits were identified that affected NM aggregates in donor cells. These hits were tested in the present screen in three different concentrations (10, 1 and 0.25 µM) in duplicate to analyze their effects on PrP^{Sc} aggregates. N2a^{uninfected} cells and three wells with N2a^{22L} cells remained untreated and only DMSO without any compound was added in duplicates at the respective concentration to six wells of N2a^{22L} cells (DMSO control). As positive controls three known compounds, that are capable of reducing the percentage of PrP^{Sc} infected cells, were chosen. Gallotannin is a known inhibitor of PrP^{Sc} levels in

cells and was used as a control at 2 µM. At a concentration of 100 nM it reduces PrP^{Sc} levels to 50 % in 22L and RML infected N2a cells analyzed by dot-blot if treated for 5 days (146). Chlorpromazine, used at 2 µM, is known to dose-dependently decrease proteinase K resistant PrP levels, detected by western blotting of 22L prion-infected N2a cell lysates (160). In this experiment cells were infected with 22L containing brain homogenate and passaged for 5 times and then treated for 4 days with Chlorpromazine. A concentration of 3 µM lead to reduction of PrP^{Sc} levels to 50 % (160). The third control was Imatinib (5 µM). The tyrosine kinase inhibitor showed to be highly effective against PrP^{Sc} accumulation at concentration of 1 µM. Western blot analysis showed that incubation for 3 days reduced PrP^{Sc} levels to 50 % (155). The three control compounds were added in duplicates. 44 hours after drug treatment cells were fixed and stained for PrP^{Sc} following GdnHCl treatment (2.5.2). Cells were imaged as above and image analysis was performed using the Columbus software (2.10.2). The analysis demonstrated that in the DMSO control approximately ~ 18 % of cells were PrP^{Sc} positive. Imatinib (16 % infected cells) and Chlorpromazine (19 % infected cells) led to a weak or no reduction in numbers of infected cells, whereas Gallotannin reduced the percentage of infected cells to 5 % if analyzed by immunofluorescence staining. The effects of the 152 tested compounds were classified based on their toxicity and were categorized as inhibitor or activator (Table 8).

Table 8. Categorization of compound effects compared to DMSO treated control

	Toxicity	Inhibitor	Activator
Strong	Survival of cells treated with 0.25 µM of a compound < 75 %	Reduction of PrP^{Sc} positive cells ≥ 50 %	Increase of PrP^{Sc} positive cells ≥ 50 %
Poor	Survival of cells treated with 1 µM of a compound < 75 %	Reduction of PrP^{Sc} positive cells <50 % and >25 %	Increase of PrP^{Sc} positive cells <50 % and >25 %
Weak	Survival of cells treated with 10 µM of a compound < 75 %	Reduction of PrP^{Sc} positive cells ≤ 25 %	Increase of PrP^{Sc} positive cells ≤ 25 %
No	Survival of cells treated with 10 µM of a compound ≥ 75 %		

This categorization led to the identification of 83 inhibitors and 104 activators (Figure 16). 63 compounds had dual effects, which means that the percentage of PrP^{Sc} positive cells increased or decreased depending on the concentrations. The toxic effect of

treatment with 28 compounds was classified as strong, thus no reliable conclusion concerning the number of PrP^{Sc} positive cells could be drawn, as the high rate of dead cells could have distorted the ratio of PrP^{Sc} positive to negative cells.

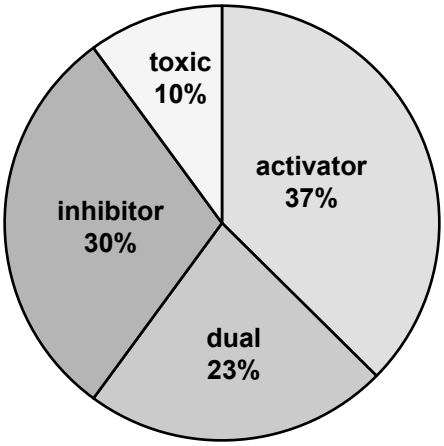

Figure 16. Evaluation of anti-prion compounds identified by high-throughput screen. 152 compounds were tested in a N2a cell-based screen. $N2a^{22L}$ and $N2a^{uninfected}$ cells, which served as background control for PrP^{C} were seeded on 96-well plates and treated for 44 h with different concentrations of compounds starting 2 h after seeding. After antigen retrieval with GdnHCl and staining of PrP^{Sc} with mAb 4H11 antibody, plates were imaged with an automated microscope and PrP^{Sc} positive cells were quantified by Columbus software.

3.2.3 Identification of seven compounds that strongly reduce the percentage of PrP^{Sc} infected cells

The evaluation of the screen data led to the identification of 84 compounds with potentially inhibitory properties on PrP^{Sc} levels in cells infected with 22L prions. From this list, seven compounds were selected for further analysis. Those seven selected Food and Drug Administration (FDA) approved compounds or approved drug candidates were strong inhibitors with poor or no toxicity. Their effects on prions were so far unknown, except for Quinacrine dihydrochloride. The screen successfully identified quinacrine dihydrochloride as positive control as it is a known inhibitor of PrP^{Sc} accumulation. It is a non-selective monoamine oxidase A/B (MAO-A/B) inhibitor. Incubation of persistently

22- or RML-infected neuroblastoma cells with Quinacrine induced the clearance of PrP^{Sc} (159, 168, 169). In the present screen Quinacrine dihydrochloride reduced the percentage of PrP^{Sc} positive cells about 64 % (Figure 17 A). Three of the inhibitors can be grouped as dopamine, norepinephrine and serotonin uptake inhibitors: at 10 µM Indatraline hydrochloride reduced the percentage of positive cells about 70 %, Maprotiline hydrochloride reduced the signal of PrP^{Sc} positive cells about 68 % at a concentration of 10 µM and treatment with 1 µM Methiothepin mesylate led to a reduction to 53 % (Figure 17 B-D). AEE788 is a potent inhibitor of EGFR and HER2 and led to a reduction of PrP^{Sc} positive cells about 70 % at a concentration of 10 µM (Figure 17 E). The strongest inhibitory compounds were SB590885 (- 90 %) and PHA665752 (- 71 %) at a concentration of 1 µM (Figure 17 F, G). SB590885 is a potent B-Raf inhibitor and PHA-665752 is a potent, selective and ATP-competitive c-Met inhibitor.

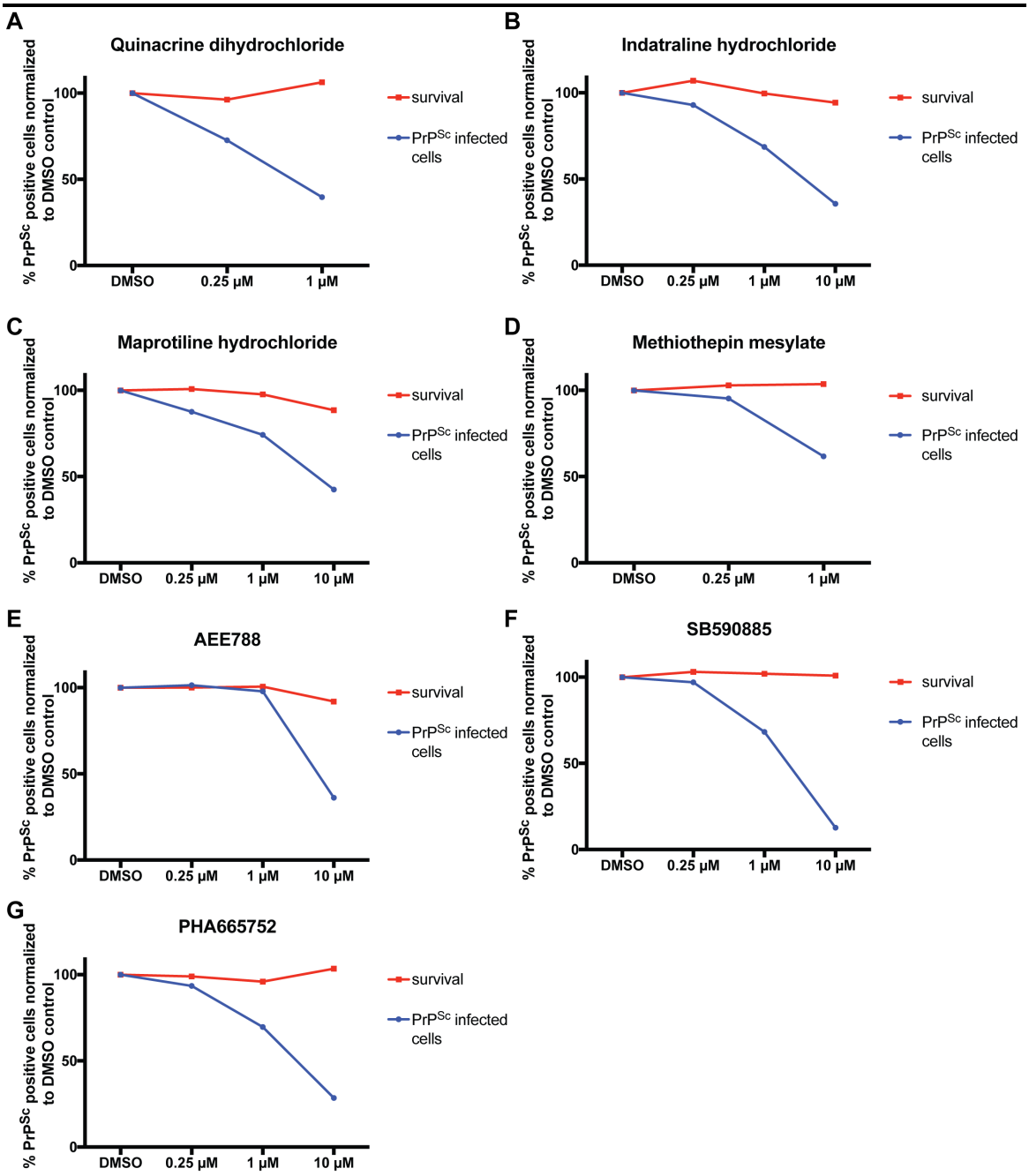

Figure 17. The cell-based high-throughput screen identified seven strong inhibitors. Image analysis of data generated by Cell Voyager 6000 revealed seven compounds, capable of reducing the percentage of PrP^{Sc} positive N2a cells after incubated for 44 h **(A – G)**. Cells were stained for aggregates and microscopy images were analyzed by the Columbus software. The red line indicates the survival of cells in percent normalized against DMSO treated cells. Percent of PrP^{Sc} positive cells normalized against DMSO is illustrated in blue. Values for three different concentrations of compounds are shown; if one concentration is missing it indicates that the survival is below 75 %. Mean values of two independent wells are shown (~ 2,500 cells/well).

3.2.4 Assessment of anti-prion efficacy of identified compounds by western blot analysis

To confirm the results generated by the cell-based high-throughput screen, a second detection method for PrP^{Sc} detection in infected cells was performed. For the detection of PrP^{Sc} by western blot analysis, aliquots of cell lysates were either incubated with PK (2.6.4) or processed without any PK addition. In the PK treated lysates only PK resistant proteins, like PrP^{Sc}, can be detected. Other proteins like actin can be detected in the PK untreated lysate. The signal intensity for PrP^{Sc} by western blot analysis is often low. To detect the changes in intensity levels of PrP^{Sc}, due to the drug treatment, it is essential to detect a strong and stable signal for PrP^{Sc}. Therefore, we performed limited dilution cloning of the $N2a^{22L}$ cells used in the screen to generate a high number of PrP^{Sc} positive cells. Infection of cloned cells was tested by detection of PrP^{Sc} by immunofluorescence staining. To guarantee a stable, highly 22L infected N2a cell line a second round of cloning was conducted with the 10 most infected cell clones from first round of cloning. This led to the generation of a highly infected $N2a^{22L}$ cell line with ~ 80 % positive cells that was used for further experiments (Figure 18).

For western blot analysis, cells were seeded and treated with seven compounds for 44 h (Figure 19 A). Cells were treated with all concentrations that showed no toxic effect in the screen, including 10 µM, 1 µM and 0.25 µM or just 1 µM and 0.25 µM. At the same time cells were also seeded and immunofluorescence staining was conducted without any compound treatment to confirm that $N2a^{22L}$ cells were infected (Figure 18 A). Immunofluorescence staining revealed a strong infection of $N2a^{22L}$ (Figure 18 B) and western blot analysis was conducted.

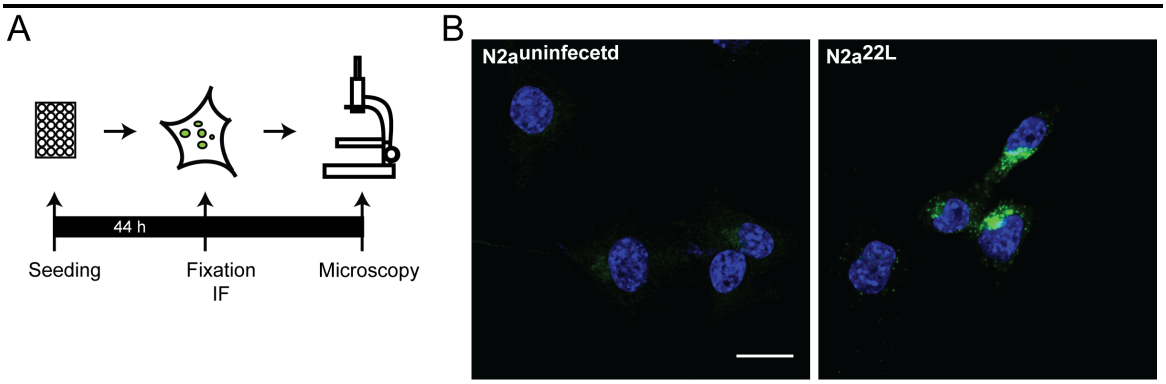

Figure 18. Immunofluorescence staining indicated a strong N2a^{22L} infection. (A) Experimental setup of immunofluorescence staining of N2a^{uninfected} and N2a^{22L}. **(B)** Confocal microscopy analysis of the subclone of N2a cells. PrP^{Sc} was detected with mAb 4H11 (green). Nuclei were stained with Hoechst (blue). Scale bar: 20 µm.

Accumulation of PrP^{Sc} in compound or DMSO-treated cells was detected in PK digested lysates (+PK). 240 µg of total protein were PK-treated and loaded per well, whereas for detection of total PrP and actin untreated (-PK) lysates were used (10 µg were loaded). Analysis of western blots accumulation of PrP^{Sc} in compound-treated N2a^{22L} cells was calculated in relation to the PrP^{Sc} signal in DMSO control, which was set to 100 %. Signal intensities of PrP^{Sc} in DMSO and compound treated cells were normalized to the corresponding actin signal. The experiment was repeated three times, one representative blot is shown (Figure 19 B – H). Treatment with Quinacrine dihydrochloride (Figure 19 B), Indatraline hydrochloride (Figure 19 C) Maprotiline hydrochloride (Figure 19 D) and AEE788 (Figure 19 F) showed no significant reduction of PrP^{Sc} accumulation. In contrast to the screen, treatment with Quinacrine dihydrochloride and AEE788 displayed even a slightly but not significant increase in PrP^{Sc} accumulation compared to the DMSO control. The accumulation of PrP^{Sc} decreased if cells were treated with Indatraline hydrochloride at all concentrations, as well as if they were treated with 10 µM of Maprotiline hydrochloride (Figure 19 D). Considering the western blot image this effect appeared to be drastic, but after statistical analysis the reduction of PrP^{Sc} accumulation was not significant, likely due to the high standard deviation between the different experiments. The accumulation of PrP^{Sc} after treatment with Methiothepin mesylate, SB590885 and PHA665752 confirmed the results found in the screen. Methiothepin mesylate treatment decreased the PrP^{Sc} accumulation significantly at 10 µM to 60 % compared to DMSO (100 %). Treatment with 1 µM of

Methiothepin mesylate led to a PrP^{Sc} accumulation of 73 % (not significant), whereas 0.25 µM showed no effect on PrP^{Sc} accumulation.

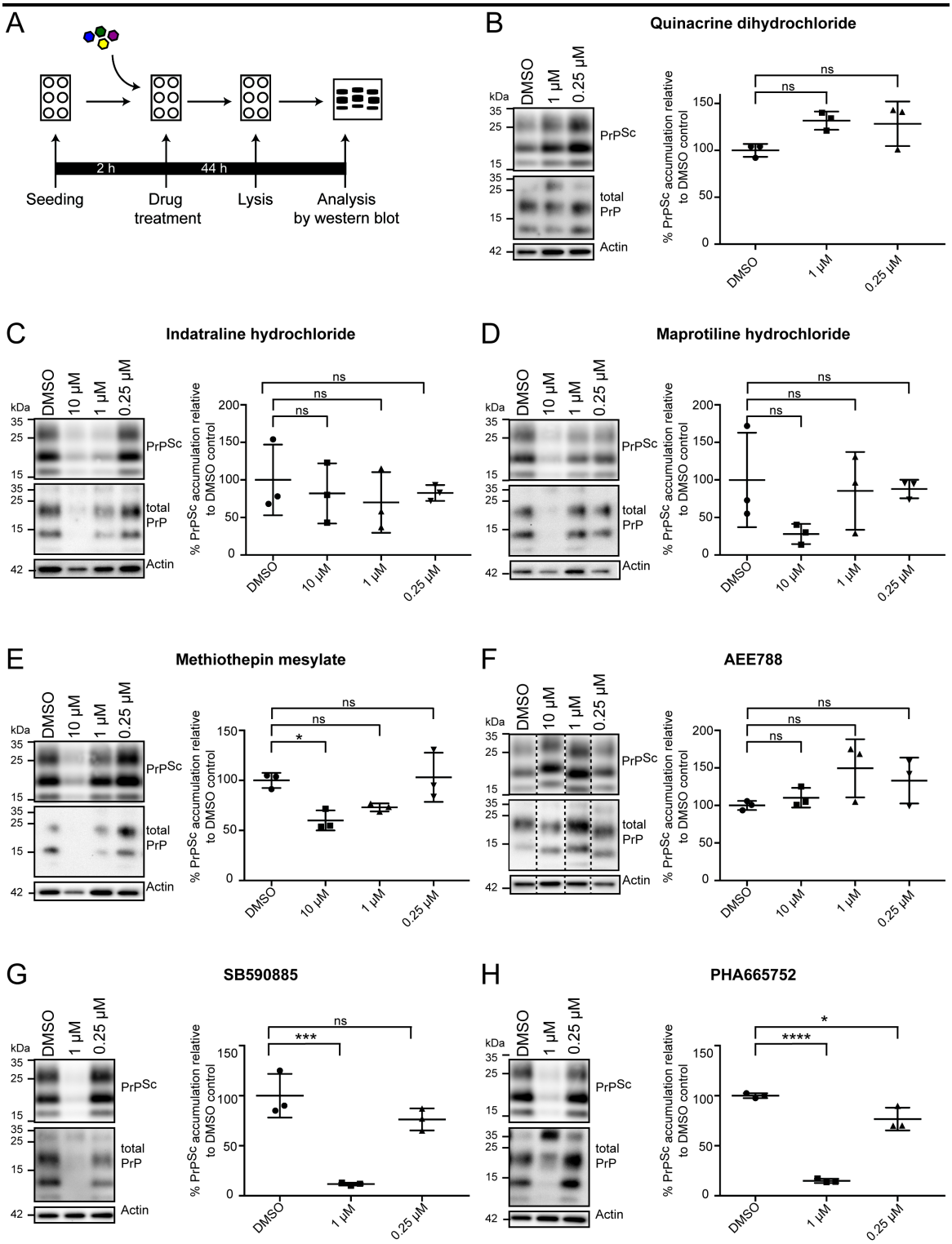

Figure 19. Validation of the compounds' inhibitory effect on PrP^{Sc} accumulation identified by the high-throughput screen in persistently 22L infected N2a cells. (A) Experimental setup. $N2a^{22L}$ were seeded and treated with seven identified strong inhibitors at different concentrations for 44 hours. Cells were lysed and western blot analysis was conducted. **(B – H)** Accumulation of PrP^{Sc} was detected in proteinase K treated lysates using mAb 4H11. Total PrP was revealed by mAb 4H11 in PK untreated lysates. This blot was reprobed with anti-Actin Ab as a loading control. PrP^{Sc} accumulation was normalized against actin and PrP^{Sc} accumulation in compound-treated cells was compared to PrP^{Sc} accumulation in DMSO-treated cells, which was set to 100 %. The experiment was done in triplicates. A single dot represents one experiment, the line the mean and the whiskers the standard deviation. One-way ANOVA with Dunnett´s multiple comparisons test was used to statistically analyze the data. Asterisks display significant changes (*$p \leq 0.05$, **$p \leq 0.01$, ***$p \leq 0.001$, ****$p \leq 0.0001$, ns= not significant).

The strongest and most significant effects on PrP^{Sc} accumulation could be observed after treatment with SB590885 and PHA665752 (Figure 19 G – H). As those compounds had a toxic effect at 10 µM in the screen, only 1 µM and 0.25 µM were tested. Treatment with 1 µM of SB590885 led to a decrease of PrP^{Sc} accumulation of 89 % ($p \leq 0.001$) and treatment with 1 µM PHA665752 decreased PrP^{Sc} accumulation to only 15 %, even more significantly (****$p \leq 0.0001$). PHA665752 was also the only compound that showed a significant reduction of PrP^{Sc} accumulation at 0.25 µM. Here the signal was reduced by 23 % with a p value of $p \leq 0.05$ (Figure 19 H).

As two independent methods demonstrated that Methiothepin mesylate, SB590885 and PHA665752 were able to reduce the number of persistently prion infected N2a cells, those promising compounds were further characterized and analyzed. A dose response analysis was performed to determine the half maximal inhibitory concentration (IC_{50}). For this purpose, $N2a^{22L}$ cells were seeded and either treated with drugs (Figure 19 A) or immunofluorescence staining was performed (Figure 18 A). As immunofluorescence staining revealed that $N2a^{22L}$ cell were still infected, western blot analysis was continued. Data analysis was performed as mentioned before, but experiments were performed four times (n = 4) (Figure 20).

Methiothepin mesylate

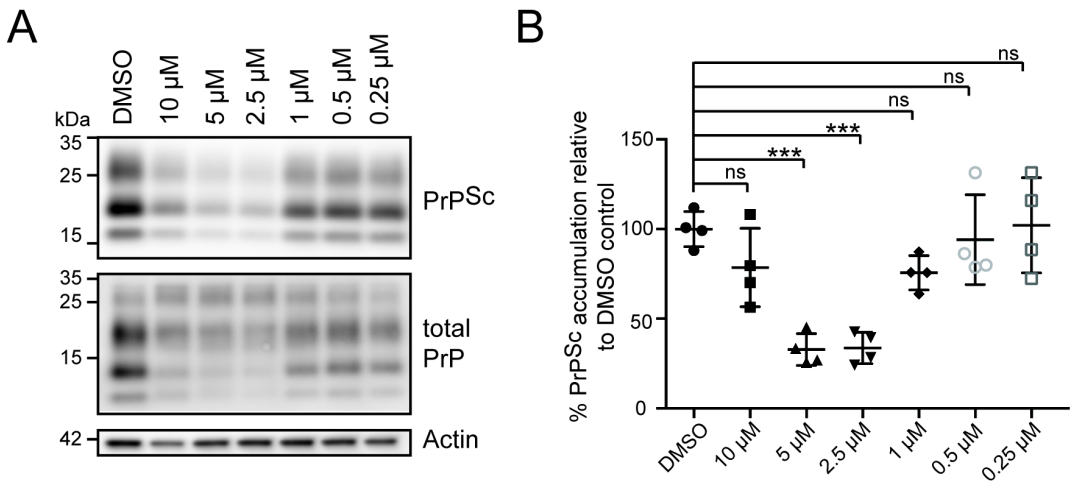

SB590885

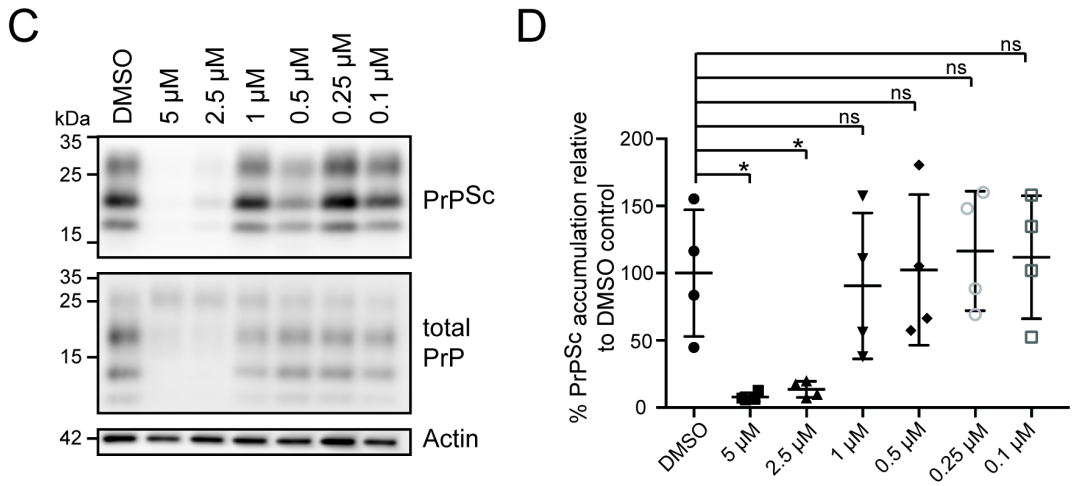

PHA66575

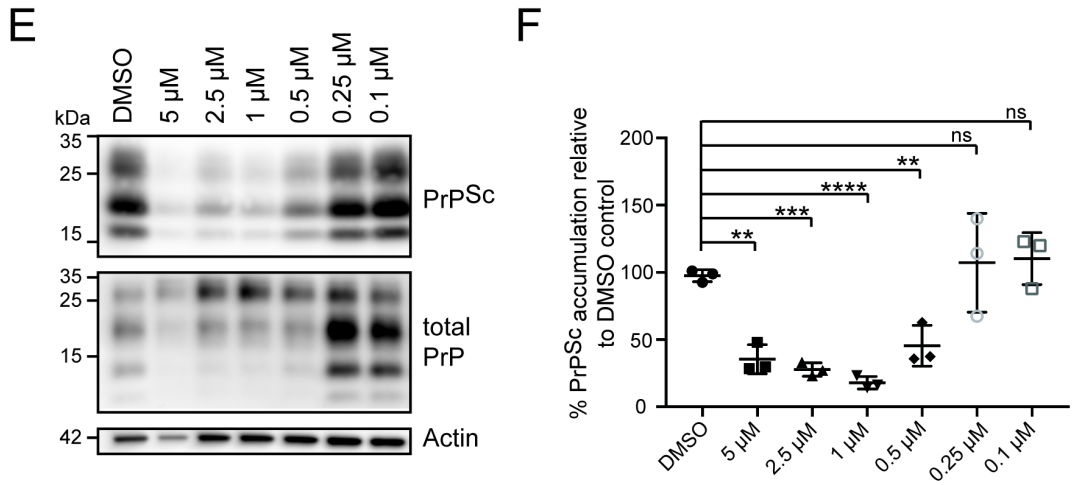

Figure 20. Treatment of N2a^{22L} with Methiothepin mesylate, SB590885 and PHA665752 at six concentrations demonstrated the inhibitory effect on PrP^{Sc} accumulation. (A, C and E) Western blot analysis. Accumulation of PrP^{Sc} was detected in +PK samples using mAb 4H11, whereas total PrP (mAb 4H11) and actin (mAb anti-actin) were analyzed in –PK samples. Actin served as a loading control. **(B, D and F)** Quantification of western blot analysis. PrP^{Sc} accumulation was normalized against actin and PrP^{Sc} accumulation in compound-treated cells was compared to PrP^{Sc} accumulation in DMSO-treated cells, which was set to 100 %. Experiments were performed four times. A single dot represents one experiment, the line the mean and the whiskers the standard deviation. One-way ANOVA with Dunnett´s multiple comparisons test was used to statistically analyze the data. Asterisks display significant changes (*p ≤ 0.05, **p ≤ 0.01, ***p ≤ 0.001, ****p ≤ 0.0001, ns= not significant).

Methiothepin mesylate was tested at six different concentrations (10, 5, 2.5, 1, 0.5 and 0.25 µM). Treatment with 5 µM and 2.5 µM led to a significant reduction of PrP^{Sc} accumulation to 30 % (Figure 20). Surprisingly, treatment with 10 µM of Methiothepin mesylate had a milder effect on PrP^{Sc} reduction (79 %). The difference between DMSO control and 10 µM Methiothepin mesylate was statistically not significant. Treatment with concentration < 2.5 µM had no significant effect on PrP^{Sc} accumulation. Analysis of the dose response curve displays an IC_{50} of 1.02 µM (Figure 21 A).

SB590885 and PHA665752 were also tested at six concentrations; the highest examined concentration was lower than for Methiothepin mesylate due to toxicity detected in previous experiments (5, 2.5, 1, 0.5, 0.25 µM and 0.1 µM). SB590885 has an IC_{50} of 1.38 µM (Figure 21 B) and showed a significant decrease of PrP^{Sc} accumulation at 5 µM (8 %) and 2.5 µM (13 %) (Figure 20 B). Incubation of SB590885 at lower concentration did not significantly reduce PrP^{Sc} accumulation. Treatment of N2a^{22L} cells with PHA665752 had the best inhibitory effect. It led to significant reduction of PrP^{Sc} accumulation at four different concentrations (5, 2.5, 1 and 0.5) as well as the most significant reduction tested with a p value ≤ 0.0001 at 1 µM and an IC_{50} of 0.42 µM (Figure 21 B). The strongest reduction of PrP^{Sc} accumulation was also at 1 µM with a total accumulation of 23 % compared to DMSO control. Treatment of N2a^{22L} cells with 0.25 µM and 0.1 µM PHA665752 did not significantly reduce PrP^{Sc} accumulation. Due to consistent inhibitory effects of PHA665752 in the screen, western blot validation and dose response analysis, PHA665752 was chosen for further *ex vivo* analysis.

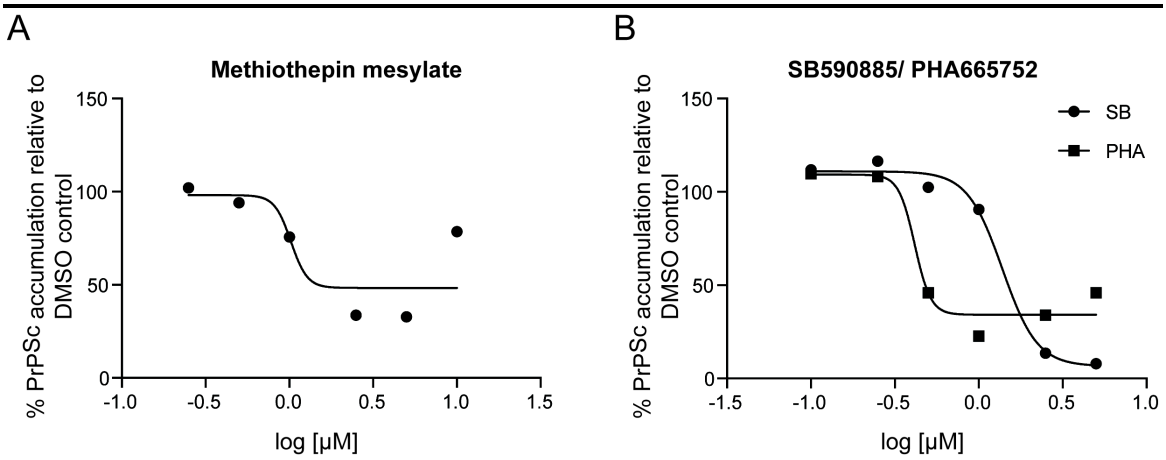

Figure 21. Dose response curve of Methiothepin mesylate, SB590885 and PHA665752. Dose response curves were generated by plotting the percentage of PrP^{Sc} accumulation in compound-treated cells relative to PrP^{Sc} accumulation in DMSO-treated cells and normalized to actin against the logarithm of drug concentrations in µM. Cells were either treated with Methiothepin mesylate **(A)**, SB590885 or PHA665752 **(B)**. Each dot represents the mean value of four experiments.

3.2.5 Treatment of 22L prion infected cerebellar slices with PHA665752 leads to a weak but insignificant decline in PrP^{Sc} accumulation

The performed high-throughput compound screen and our western blot analysis of PrP^{Sc} accumulation identified PHA665752 as a compound with anti-prion efficacy in a cellular prion model. Therefore, the effect of PHA665752 on prion accumulation was tested in COCS. The potential target for PHA665752 is the receptor c-Met (170). To test if c-Met is expressed in COCS infected with 22L prions, immunofluorescence staining with mAB c-Met was performed (2.5.3).

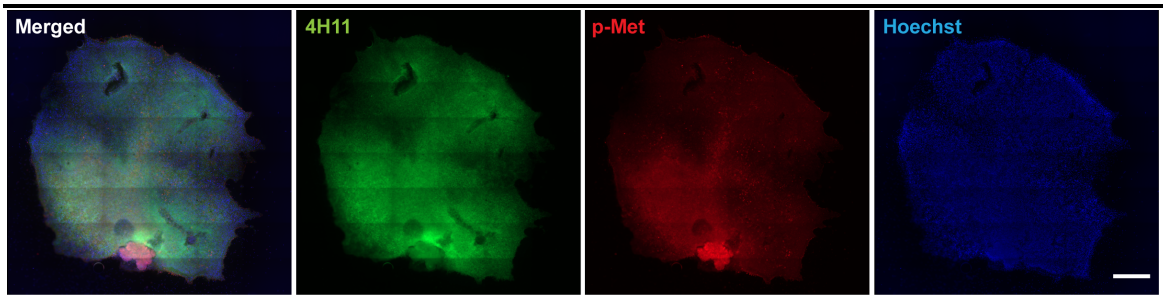

Figure 22. Immunofluorescence staining reveals c-Met expression in COCS. 22L prion exposed COCS were cultured for 7 weeks. At that time point, immunofluorescence staining was performed. PrP^{Sc} was specifically stained with mAb 4H11 following GdnHCl treatment (green) and c-Met with mAb anti-c-Met (red). Nuclei were counterstained with Hoechst. Samples were analyzed by epifluorescence microscopy using the tile scanning function and identical imaging settings. Scale bar: 500 µm.

Immunofluorescence staining revealed the expression of c-Met in COCS (Figure 22). Next, PHA665752 was tested for its anti-prion efficacy in COCS at a concentration of 1 µM. This concentration was chosen because it was non-toxic in cell culture and showed *in vitro* a strong reduction of PrP^{Sc} accumulation in 22L infected N2a (Figure 20 F). COCS were infected with 22L prion- and Mock brain homogenate. Two weeks p.i. treatment with 1 µM PHA665752 started and seven weeks p.i, COCS were analyzed by western blot analysis and immunofluorescence staining for PrP^{Sc} accumulation (Figure 23).

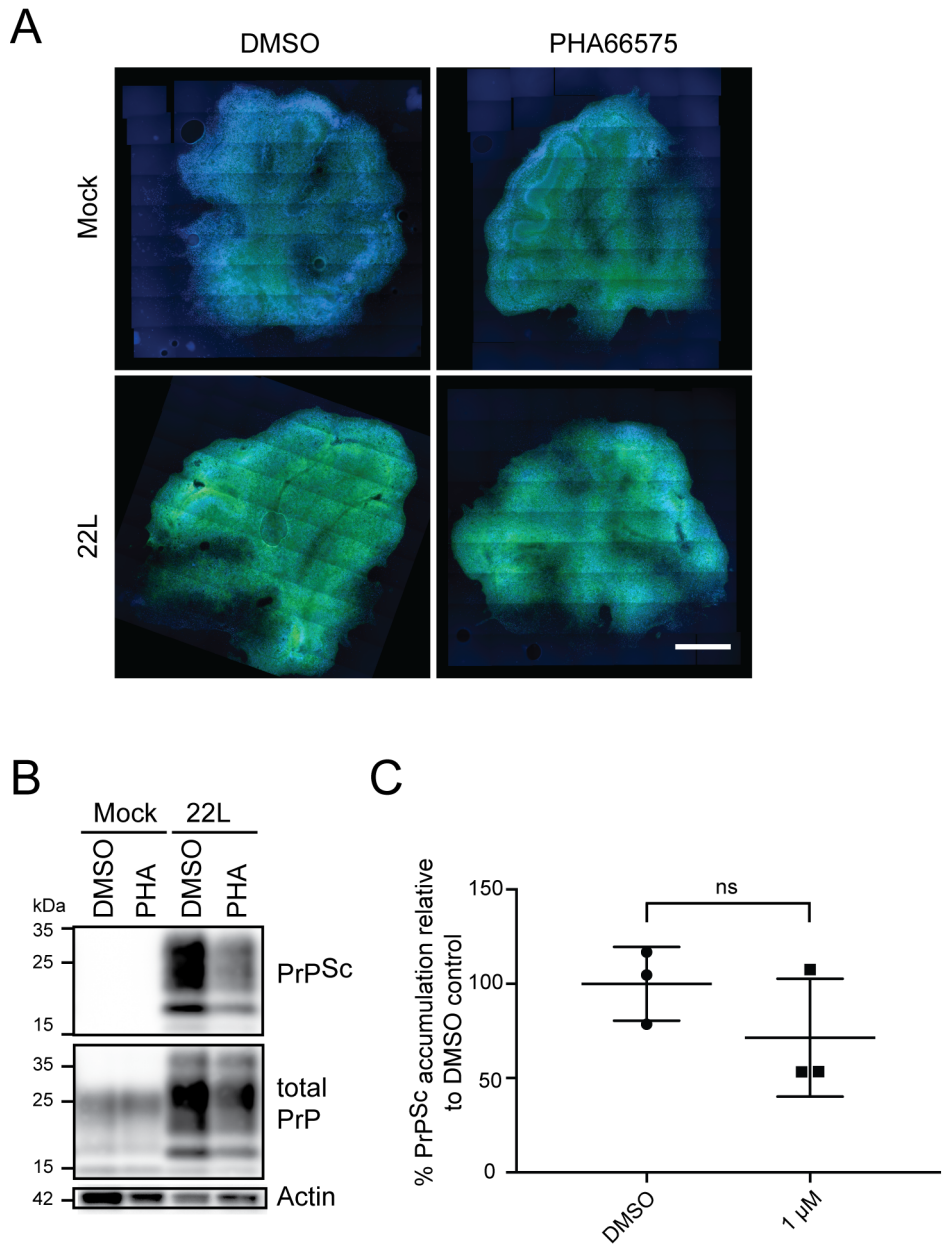

Figure 23. Treatment of infected COCS with PHA665752 led to a weak reduction in PrP^{Sc} accumulation. COCS were treated with 1 µM of PHA665752 or DMSO for five weeks starting two weeks post 22L infection. **(A)** Immunofluorescence staining of COCS. PrP^{Sc} was detected with mAb 4H11 following GdnHCl treatment and nuclei were visualized with Hoechst. Slices were imaged with identical image settings with an epifluorescence microscope with a magnification of 20x using the tile scanning function. Scale bar: 500 µm. **(B)** Detection of accumulation of PrP^{Sc} by western blot analysis. For one lysate two slices were pooled. PrP^{Sc} was detected in +PK samples with mAb 4H11. Total PrP (mAb 4H11) and actin (mAb anti-actin) were analyzed in –PK samples. Actin served as a loading control. **(C)** For quantification of the western blot analysis PrP^{Sc} accumulation was normalized against actin. PHA665752 treated COCS were compared to DMSO

treated COCS, which were set to 100 %. The experiment was done in triplicates. A single dot represents one experiment, the line the mean and the whiskers the standard deviation. Unpaired t test was used to statistically analyze the data (ns= not significant).

Immunofluorescence staining revealed the successful infection of COCS with 22L prions. Infected slices showed a strong signal of PrP^{Sc} (green) (Figure 23 A right panel) and only a weak PrP^{C} background staining was detected in Mock infected COCS (Figure 23 A left panel). Treatment with PHA665752 was not overtly toxic to COCS as visual inspection showed no signs of toxicity like holes within the slices, changes in shape or frayed borders of the slices. However, PHA665752 treated COCS showed a weak not distinct difference in signal intensity between DMSO and PHA665752 treatment (Figure 23 A). Western blot analysis confirmed the infection of COCS with 22L prions (Figure 23 B). The PrP^{Sc} signal intensity in 22L infected PHA665752 treated COCS was reduced compared to the signal in DMSO treated COCS. This reduction was, however, not significant (Figure 23 C). To sum up, treatment of 22L prion infected COCS for five weeks with 1 µM PHA665752 led to a weak, but not significant reduction of PrP^{Sc} accumulation.

Beside these findings, western blot analysis of uninfected COCS revealed a molecular weight for PrP^{C} lower than expected. Uninfected prion protein presents itself in western blot analysis normally with the first diglycosylated band at the height of approximately 27 kDa, the monoglycosylated band at approximately 23 kDa and the unglycosylated band at approximately 19 (171). However, the first band was recognized at approximately 23 kDa (Figure 23, B) in uninfected COCS. Therefore a comparative western blot analysis between COCS and brain lysates with two different antibodies was performed. First uninfected COCS and brain lysate were stained with monoclonal antibody 4H11 and compared. The binding site for 4H11 is at the C-terminal region, where complex carbohydrates can be linked to two asparagine residues (in mice PrP aa residues 180 and 196), resulting in un-, mono- and diglycosylated PrP^{C}. In brain lysate three bands were detected (Figure 24 A). The highest band at approximately 30 kDa likely presented diglycosylated PrP, the following band at 23 kDa monoglycosylated PrP and the lowest band unglycosylated PrP at approximately 19 kDa. Interestingly, in COCS the diglycosylated band is visible, but the signal was fainter. Beside the three typical bands the 4H11 antibody also detects a smear. In the cell the prion protein is proteolytically

processed. The three main cleavage events are α-cleavage, β-cleavage, and ectodomain shedding at the N-terminal part of the PrP, which result in different sizes for truncated PrP (172) which might also be detected by the 4H11 antibody. The staining with monoclonal antibody 4H11 was compared to a staining with the commonly used monoclonal antibody Saf32, which recognizes the octa-repeat region, located in the N-terminal part of PrP (Figure 24, B). Staining of uninfected brain with Saf32 showed a signal between 30 and 27 kDa, which likely comprised the di- and monoglycosylated PrP and an additional band for unglycosylated PrP. It is difficult to distinguish between di- and monoglycosylated PrP with Saf32 staining, however the overall signal intensity is lower in COCS (exposed for 5 min) compared to brain lysate.

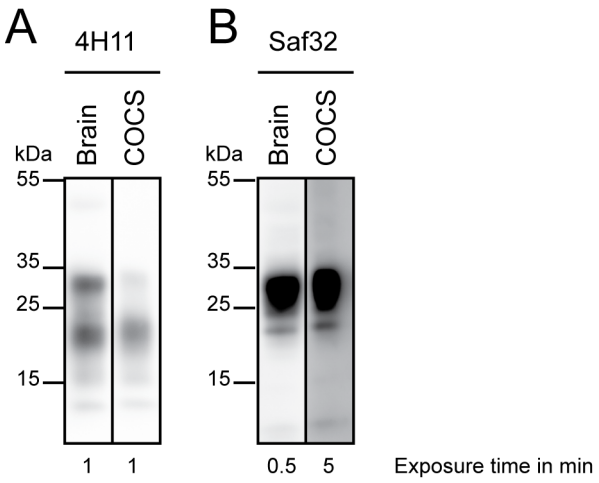

Figure 24. Saf32 bind to the N-terminal part of PrP and detects also truncated PrP. Lysates of uninfected COCS (10 µg per lane) and brain samples (2 µg per lane) were prepared for western blot analysis and total PrP was detected by 4H11 **(A)** and Saf32 **(B)**.

3.3 Identification of pathways deregulated in prion infection in *ex vivo* cerebellar slices and *in vivo* in mice

Organotypic cerebellar slice cultures are currently analyzed by a broad range of different techniques, for example western blot analysis, immunofluorescent staining and different biochemical methods (137, 147). Beside this, molecular biological methods like RNA analysis by qPCR or genome linkage analysis are used to study prion disease in COCS (138, 173). However, the comparability of the host response between the *in vivo* prion

infected mice and *ex vivo* prion infected of cerebellar slices is unknown. Therefore, the next part of the presented thesis focuses on the analysis of the host response of 22L and RML prion-infected COCS by RNA sequencing analysis and differences and similarities between ex vivo and *in vivo* experiments are analyzed. *In vivo* sequencing data were provided by Dr. Melvin Schleif (DZNE, Bonn).

For the *in vivo* experiments, 6 weeks old C57BL/6 mice were intracranially injected with brain homogenate that originated from brains of mice infected with prion strain 22L, RML or uninfected mice (Mock control). Mice were sacrificed 10, 14 and 18 weeks post injection (Figure 25). Ten weeks of incubation represent, in our experiments, a very early stage of prion disease with first signs of prion pathology in the brain. After 14 weeks, as an intermediate time point, prion pathology has established in the brain, whereas 18 weeks post injection represents a late stage of the disease with all signs of prion disease in the brain, but mice just start to develop physically impairments (174).

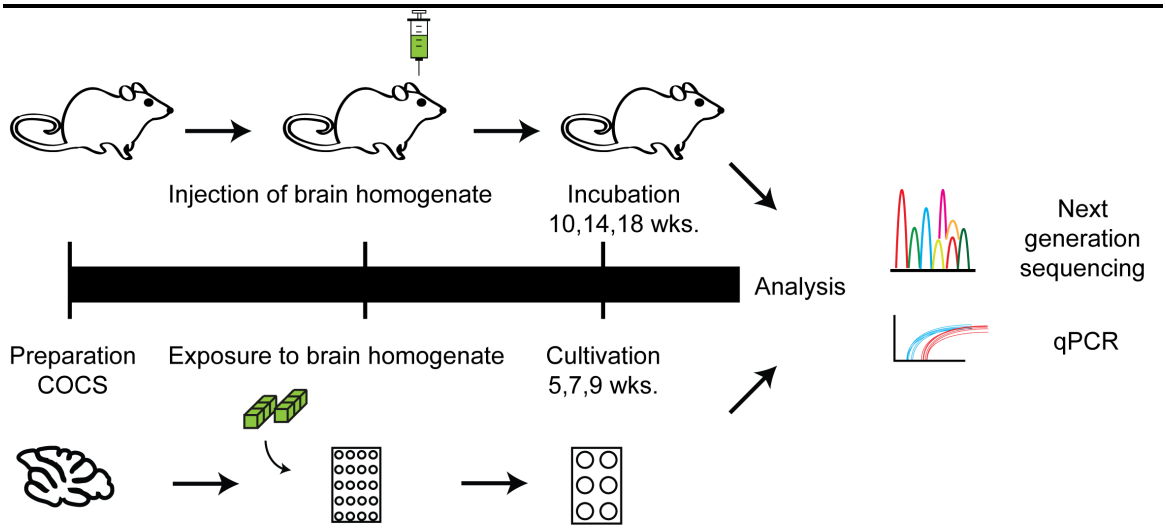

Figure 25. Experimental setup for the comparative *in vivo* / *ex vivo* transcriptome analysis. Six weeks old C57BL/6 mice were intracranially injected with 0.1 % brain homogenate and incubated for 10, 14 and 18 weeks. COCS were prepared, exposed for 1 h to 1 % brain homogenate and grown for five, seven and nine weeks. Isolated RNA of cerebella and COCS were analyzed by next generation sequencing and qPCR.

To compare the gene expression profile of prion infected COCS to mice cerebella, slices were prepared and exposed to the same brain homogenates (22L, RML and Mock).

COCS were grown for five, seven and nine weeks (Figure 25). Five weeks p.i. is comparable to an early stage of disease as western blot of those samples reveals an infection of the slice, whereas western blot analysis with shorter incubations do not necessarily reveal an infection with prions (135, 147). Incubation of slices for nine weeks was taken as a correspondence to 18 weeks incubation *in vivo*, as slices show a strong infection without any impairment of viability like shrinking or holes. Seven weeks was chosen as intermediate time point, to analyze the disease progression and the accompanied transcriptomic changes. Pooled isolated RNA of mice cerebella and COCS was sent to Stefan Bonn (DZNE, Göttingen) for next generation sequencing. Successful prion infection of COCS was detected by western blot analysis (Figure 26). The longer COCS were grown the more PrP^{Sc} accumulation could be detected, which reveals the progression of the disease in the slices.

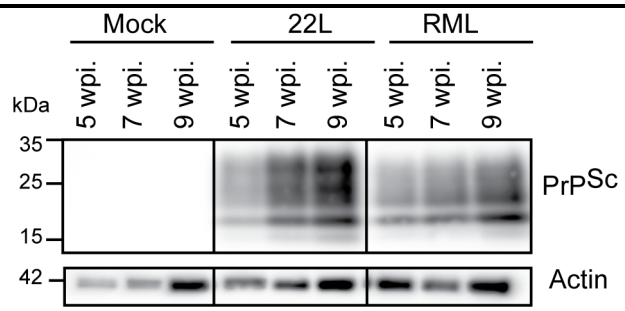

Figure 26. 22L and RML infected COCS revealed an increase in PrP^{Sc} accumulation over time. COCS were prepared, exposed for 1 h to 1 % brain homogenate and grown for five, seven and nine weeks. COCS lysates were PK-digested (20 µg/mL). PrP^{Sc} was detected using mAb 4H11. Actin was detected in –PK samples (5 µg of total protein of the lysate) and served as loading control.

3.3.1 RNA sequencing analysis reveals differences in transcriptomic changes between *in vivo* and *ex vivo*, but also some similar differential expressed genes

Generated sequencing data were analyzed (2.10.4) and gene expression of 22L or RML samples was compared to expression in Mock samples. The list of genes was ordered by p value. Differentially expressed genes with a p value ≤ 0.05 were sorted by log2 fold change. The 250 most differential expressed genes at each time point and condition (Appendix Table 13, Table 14) were further analyzed. Amongst these 250 genes some

similar DEGs between *in vivo* and *ex vivo* were found. Infection with 22L prions led to the identification of six similar DEGs at early time point, two at intermediate and four similar DEGs at late time point (Figure 27, Table 9). Surprisingly, these DEGs were not necessarily regulated in the same direction. Some of them, e.g. *Dnd* were downregulated in COCS 5 wpi and upregulated in *in vivo* infected cerebellum 10 wpi. Only three genes were comparably regulated *in vivo* and *ex vivo*. *Myo5B* and *Met* were upregulated at early respectively at late time points, whereas *Dlk1* was down regulated at the intermediate time point (Table 9).

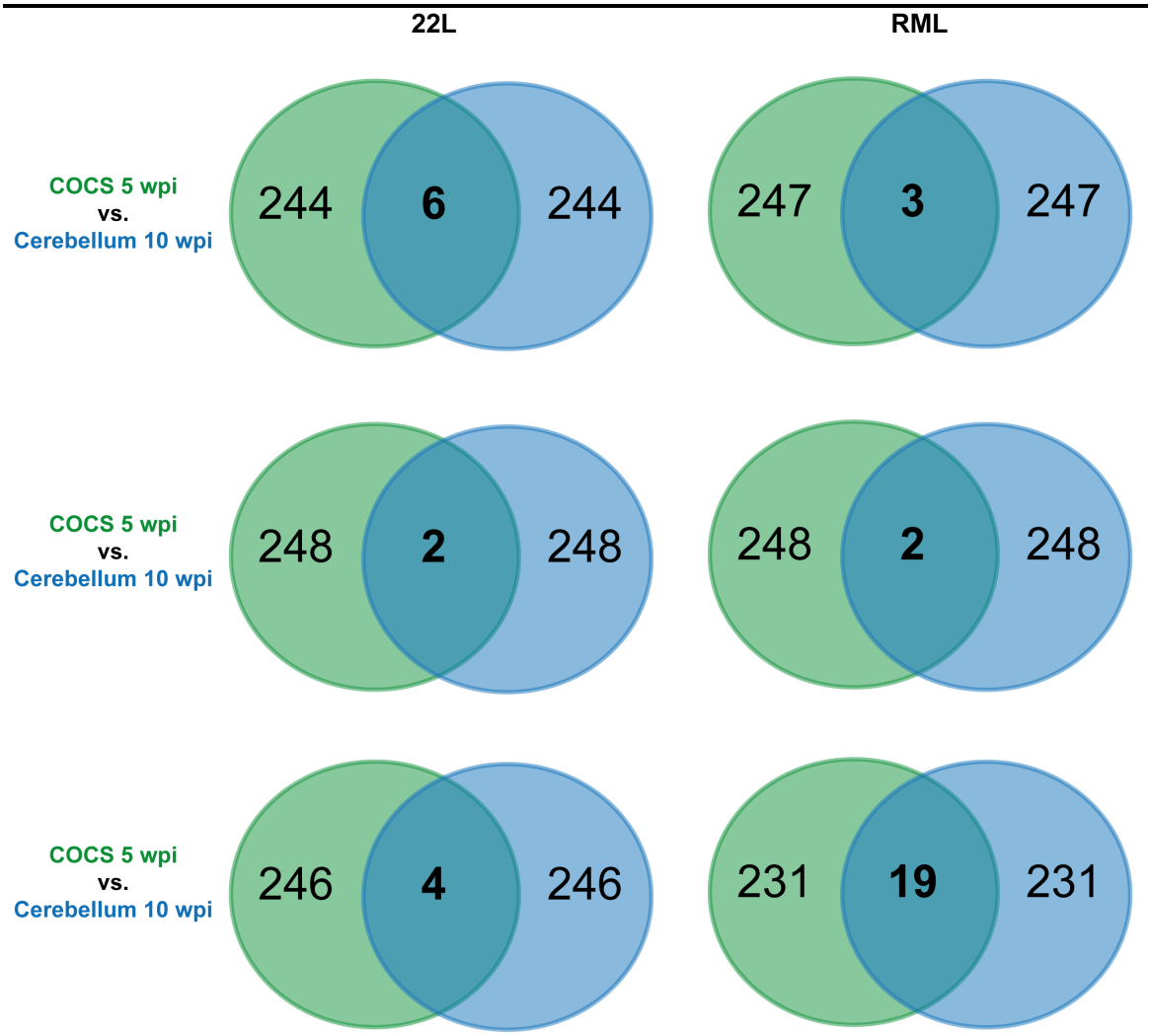

Figure 27. Comparison of gene expression between prion infected brain slices and mouse cerebella. COCS were prepared from C57BL/6JRj pups and infected with 22L or RML prions. Six weeks old C57BL/6JRj mice were injected with the same prion strains. RNA was isolated at three time points and sequencing analysis was performed. Unpaired t test was used to statistically analyze the data. Differentially expressed genes with a p value ≤ 0.05 were sorted by log2 fold change. The 250 DEGs with the highest log2 fold change were compared to each other. wpi = weeks post infection.

Comparison of RML infected COCS to RML infected mice cerebellar showed more similarities than 22L infected COCS and cerebella. At early time there were just three and at intermediate time point two DEGs found, but at late time point 19 DEGs *in vivo* and *ex vivo* were deregulated (Figure 27). However, just two genes were regulated in the same way, *Dlk1* and *Serpina3n* were down regulated at the late time point (Table 9).

Table 9. Genes differentially expressed in cerebellum and COCS infected with 22L or RML prions at a different time point

				COCS		Mouse cerebellum	
Strain	**Time point**	**Gene**	**Description**	**Log2 fold change**	**P value**	**Log2 fold change**	**P value**
22L	**early**	*Ddn*	Dendrin	-3.99	0.0002	2.04	0.0000
		Fam19a2	Family with sequence similarity 19, member A2	-1.64	0.0188	1.14	0.0004
		Lars2	Leucyl-tRNA synthetase, mitochondrial	1.88	0.0000	0.94	0.0184
		Lcn2	Lipocalin 2	-0.96	0.0005	1.44	0.0024
		Miat	Myocardial infarction associated transcript	-1.60	0.0474	1.45	0.0000
		Myo5b	Myosin	1.36	0.0416	1.37	0.0000
	inter-mediate	*Dlk1*	Delta-like 1 homolog	-0.97	0.0000	-1.96	0.0000
		Th	Tyrosine hydroxylase	-1.58	0.0001	1.21	0.0003
	late	*Ccl6*	Chemokine (C-C motif) ligand 6	-0.89	0.01	3.15	0.0000
		Met	Met proto-oncogene	1.68	0.02	2.05	0.0000
		Postn	Periostin, osteoblast specific factor	-0.99	0.00	1.81	0.0000
		Th	Tyrosine hydroxylase	-5.38	0.00	2.88	0.0000
RML	**early**	*Camkv*	CaM kinase-like vesicle-associated [	-2.41	0.0104	2.19	0.0000
		Ddn	Dendrin	-4.38	0.0000	2.82	0.0000
		Ecel	Endothelin converting enzyme-like 1	-2.95	0.0006	1.56	0.0039
	inter-mediate	*Dlk1*	Delta-like 1 homolog	-3.51	0.0000	-1.74	0.0000
		Serpina3n	serine (or cysteine) peptidase inhibitor, clade A, member 3N	0.50	0.0212	1.04	0.0002
	late	*Abca4*	ATP-binding cassette, sub-family A (ABC1), member 4	-1.86	0.0004	1.44	0.0000
		Aqp1	Aquaporin 1	-1.99	0.0000	2.03	0.0001
		Car12	Carbonic anyhydrase 12	-1.91	0.0000	2.33	0.0000
		Cldn1	Claudin 1	-1.91	0.0000	1.42	0.005
		Cldn2	Claudin 2	-1.68	0.0000	1.71	0.0000
		Col8a1	Collagen, type VIII, alpha 1	-1.59	0.0000	1.55	0.0000
		Col8a2	Collagen, type VIII, alpha 2	-1.59	0.0000	1.25	0.0049
		En1	Engrailed 1	-1.57	0.0025	1.11	0.0004
		Folr1	Folate receptor 1 (adult)	-1.94	0.0000	1.16	0.0288
		Gm853	Predicted gene 853	-2.75	0.0510	1.45	0.0065
		Krt18	Keratin 18	-2.56	0.0000	1.25	0.0182
		Mfrp	Membrane-type frizzled-related protein	-1.65	0.0009	1.71	0.0000
		Npr3	Natriuretic peptide receptor 3	-1.88	0.0000	2.00	0.0000
		Slc4a5	Solute carrier family 4, sodium bicarbonate cotransporter, member 5	-1.88	0.0000	1.75	0.0000
		Sostdc1	Sclerostin domain containing 1	-1.54	0.0001	1.38	0.0083
		Steap1	Six transmembrane epithelial antigen of the prostate 1	-1.63	0.0234	1.67	0.0000
		Th	Tyrosine hydroxylase	-2.49	0.0000	1.59	0.0000
		Tmem72	Six transmembrane epithelial antigen of the prostate 1	-2.32	0.0000	1.68	0.0007
		Wdr86	WD repeat domain 86	-2.03	0.0047	1.37	0.0005

+ Only genes that were deregulated in cerebella as well as COCS are shown
++ Time point: early: COCS 5 wpi vs. cerebellum 10 wpi; intermediate: COCS 7 wpi vs. cerebellum 14 wpi; late: COCS 9 wpi vs. cerebellum 18 wpi

3.3.2 Comparison of *in vivo* ad *ex vivo* transcriptomes suggest that the calcium signaling pathways and the neuroactive ligand receptor interactions are strongly deregulated

To identify pathways and genes of interest that were deregulated, the 250 most DEGs were additionally analyzed by DAVID 6.8, an online bioinformatics resource, based on the KEGG pathway library. Over 100 pathways were deregulated, but only a few showed similarities between *in vivo* and *ex vivo* at a distinct time point. Prion infection of COCS and mice cerebella with 22L prions resulted in changes in the Ras signaling pathway, insulin secretion, cAMP signaling pathway, calcium signaling pathway and neuroactive ligand-receptor interaction at early time point. After 7/14 wpi changes in cocaine addiction, retrograde endocannabinoid, nicotine addiction, and also calcium signaling pathway and neuroactive ligand-receptor interaction were observed. At the late time point only three pathways were deregulated, namely regulation of actin cytoskeleton, proteoglycans in cancer and chemokine signaling pathways (Figure 28). However, in these pathways the kind of the gene, as well as the number of genes that were deregulated varied (Table 10). RML infection resulted in fewer shared pathways compared to 22L infected mice and COCS. 10/5 weeks post infection serotonergic synapse calcium signaling pathway and neuroactive ligand-receptor interaction were changed. At the intermediate time point RML infection led to changes in morphine addiction, Chagas disease, nicotine addiction and calcium signaling pathways. At the late time point the only changes were observed in the cell adhesion molecules pathway *in vivo* and *ex vivo* (Figure 28).

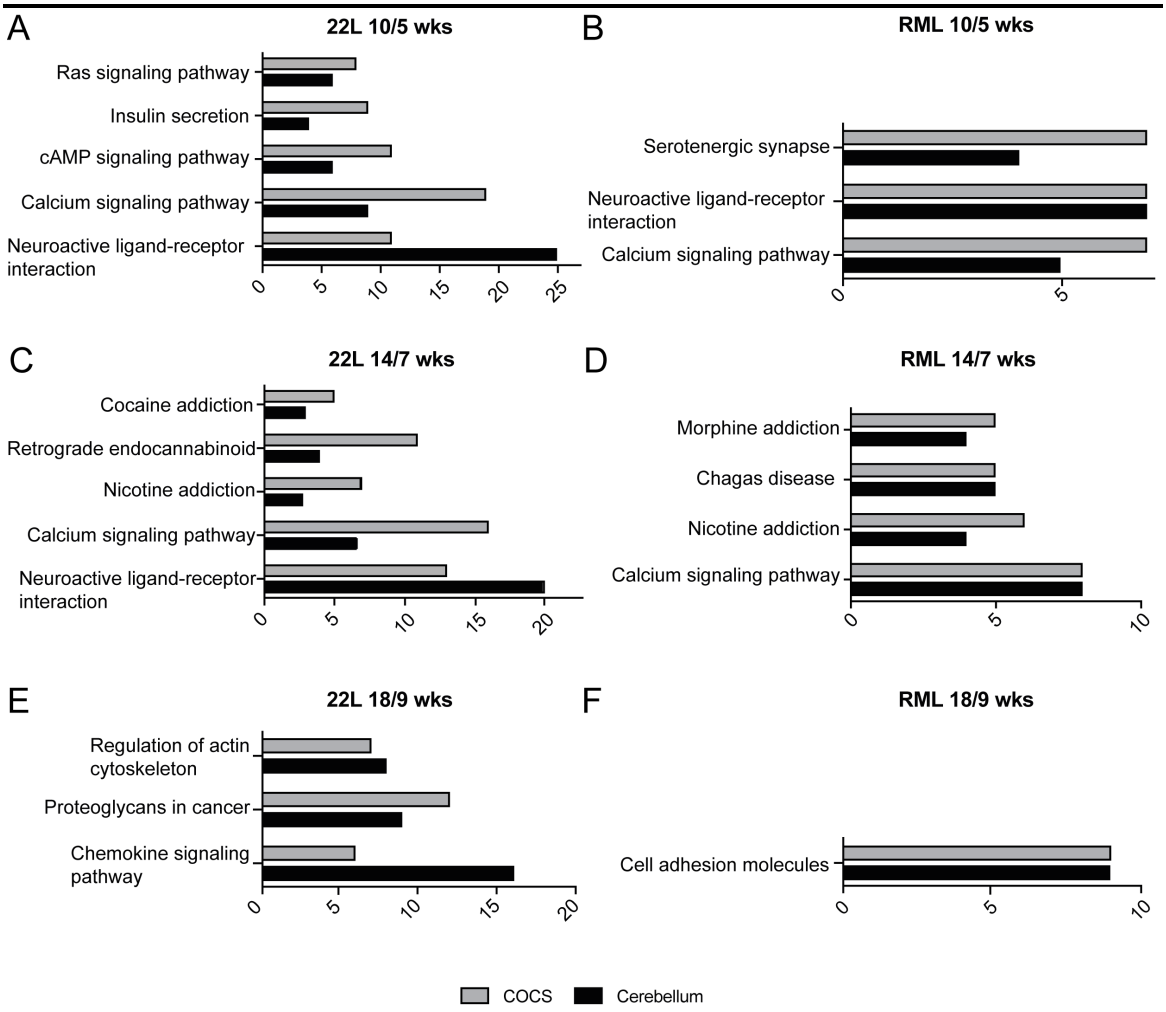

Figure 28. *In vivo* and *ex vivo* deregulated pathways in prion infection. (A – F) Pathway analysis was performed with DAVID 6.8 of the 250 most differentially expressed genes. Only pathways that are deregulated *in vivo* and *ex vivo* at a distinct time point are shown. wks = weeks.

Table 10. List of genes deregulated in an individual pathway either in the cerebellum or in COCS

Pathway	DEGs Cerebellum 22L 10 wks	DEGs COCS 22L 5 wks
Neuroactive ligand-receptor interaction	*OPRM1, GPR83, CGA, TACR3, GLRA1, DRD2, NPY2R, TACR1, GLRA3, HCRTR1, HTR1A, PRL, RXFP3, GABRA5, HTR4, NPY1R, NTSR1, NPY5R, GRM5, CRHR2, CHRM3, HTR7, MC4R, HTR2C, GH*	*GABRD, GRM4, GRIA2, GABRA3, GABRB2, GRIN2C, GABRA6, GRIN1, GRIN2A, GRM1, NTSR2*
Calcium signaling pathway	*GRM5, TACR3, CHRM3, TACR1, HTR7, HTR4, CACNA1H, NTSR1, HTR2C*	*ADCY1, SLC8A2, GRIN1, CACNA1I, GRIN2A, PRKCG, GRM1, ITPR1, CAMK4, GRIN2C, ATP2A3, CACNA1G, RYR2, CACNA1E, CAMK2B, NOS2, CACNA1C, CAMK2A, CACNA1B*
cAMP signaling pathway	*FXYD2, HTR1A, DRD2, HTR4, CREB3L3, NPY1R*	*ADCY1, GRIA2, CAMK4, TIAM1, GRIN2C, GRIN1, GRIN2A, RYR2, CAMK2B, CACNA1C, CAMK2A*
Insulin secretion	*FXYD2, STX1A, CHRM3, CREB3L3*	*KCNMA1, ADCY1, RYR2, PRKCG, CAMK2B, CACNA1C, SNAP25, CAMK2A, ABCC8*
Ras signaling pathway	*PAK6, FGF18, RASGRF2, HTR7, HGF, FGF3*	*KSR2, FGF9, TIAM1, FGF14, VEGFA, GRIN1, GRIN2A, PRKCG*
Pathway	**DEGs Cerebellum 22L 14 wks**	**DEGs COCS 22L 7 wks**
Neuroactive ligand-receptor interaction	*CALCR, GPR83, GLRA1, CCKBR, TACR3, DRD2, RXFP3, GLRA3, TACR1, TRHR, GABRA5, NPY1R, NPY5R, GRM5, HCRTR1, HTR1A, CHRM3, CHRNB3, GABRQ, HTR2A*	*CRHR1, GABRD, GRM4, HTR1B, SSTR3, GRM2, GABRB2, OPRL1, GRIN2C, GABRA6, GRIN1, GLRA2, GRIN2A*
Calcium signaling pathway	*GRM5, TACR3, CHRM3, CCKBR, TACR1, TRHR, HTR2A*	*ADCY1, SLC8A2, NOS1, GRIN1, CACNA1I, GRIN2A, PRKCG, ITPKA, ITPR1, CAMK4, ATP2A3, GRIN2C, RYR1, CACNA1E, CAMK2B, CAMK2A*
Nicotine addiction	*SLC17A6, GABRA5, GABRQ*	*SLC17A7, GABRD, GABRB2, GRIN2C, GABRA6, GRIN1, GRIN2A*
Retrograde endocannabinoid	*GRM5, SLC17A6, GABRA5, GABRQ*	*SLC17A7, GABRD, ADCY1, KCNJ9, GABRB2, MAPK13, GABRA6, GNG13, PRKCG, RIMS1, ITPR1*
Cocaine addiction	*DRD2, TH, PDYN*	*GRM2, GRIN2C, GRIN1, TH, GRIN2A*
Pathway	**DEGs Cerebellum 22L 18 wks**	**DEGs COCS 22L 9 wks**
Chemokine signaling pathway	*CCL3, CCL2, FGR, NCF1, CCL9, CXCL9, CCL5, CCL4, VAV1, CCL6, CXCL10, CCL12, DOCK2, RAC2, CXCL13, CXCL16*	*ADCY1, TIAM1, ROCK2, GNG13, PIK3R1, CCL6*
Proteoglycans in cancer	*PTPN6, TNF, HPSE, ITGA5, MET, TLR2, HGF, PLAU, PLAUR*	*ANK1, TIAM1, ANK3, ROCK2, CBL, MET, PRKCG, CAMK2B, FLNC, ARHGEF12, PIK3R1,*

		ITPR1
Regulation of actin cytoskeleton	*ITGAX, RAC2, ITGA5, IQGAP3, NCKAP1L, ITGB2, VAV1, CD14*	*TIAM1, ROCK2, ITGB4, IQGAP2, ARHGEF12, PIK3R1, APC*
Pathway	**DEGs Cerebellum RML 10 wks**	**DEGs COCS RML 5 wks**
Neuroactive ligand-receptor interaction	*CCKAR, CGA, ADORA3, GLRA1, TACR3, DRD2, GLRA3, TACR1, RXFP3, GABRA5, NPY1R, NPY5R, HCRTR1, CRHR2, HTR1A, PRL, HTR2C, CHRNE, GH*	*CRHR1, GABRD, GRM4, GRM2, GRM8, GRIN2C, GABRA6, GRIN1, GLRA2, GRIN2A, VIPR1, HTR5A*
Calcium signaling pathway	*CCKAR, TACR3, TNNC1, TACR1, HTR2C*	*ADCY1, SLC8A2, NOS1, GRIN1, CACNA1I, GRIN2A, ITPR1, CAMK4, ATP2A3, GRIN2C, CACNA1G, RYR1, CACNA1E, CAMK2B, NOS2, CAMK2A, HTR5A*
Serotonergic synapse	*HTR1A, SLC6A4, HTR2C, TPH2*	*KCND2, KCNJ6, KCNJ9, GNG13, GNG4, KCNJ3, HTR5A, ITPR1*
Pathway	**DEGs Cerebellum RML 14 wks**	**DEGs COCS RML 7 wks**
Calcium signaling pathway	*GRM5, TACR3, CCKBR, CHRM2, TACR1, HTR7, DRD5, TRHR*	*ATP2B2, ATP2B3, ADCY1, PLCB4, CAMK4, GRIN1, CAMK2B, ITPR1*
Nicotine addiction	*SLC17A6, GABRA5, CHRNA6, GABRQ*	*SLC17A7, GABRD, GRIA1*
Chagas disease	*CCL12, CCL3, CCL2, SERPINE1, CCL5*	*FOS, ACE, ADCY1, PLCB4, NFKBIA*
Morphine addiction	*OPRM1, GABRA5, PDE11A, GABRQ*	*GABRD, ADCY1, GABRA1, GABRA6, GNG13*
Pathway	**DEGs Cerebellum RML 18 wks**	**DEGs COCS RML 9 wks**
Cell adhesion molecules	*PTPRC, CD86, H2-OB, CLDN1, CLDN2, CD22, H2-DMB1, ITGB2, PDCD1*	*CLDN1, NTNG1, CLDN2, CNTNAP2, L1CAM, CDH1, CDH3*

Interestingly, the calcium signaling pathway and neuroactive ligand-receptor interaction were deregulated most frequently. At almost all conditions the calcium signaling pathway was changed compared to Mock (Figure 29). Only cerebella at the late time point showed no changes in this pathway. Also neuroactive ligand-receptor interactions were strongly deregulated in 22L and RML infected COCS and mice cerebella especially at early and intermediate time points. Only at late time point in RML infected COCS neuroactive ligand-receptor interactions were deregulated. Again the genes involved in the deregulated pathways were not necessarily the same (Table 11).

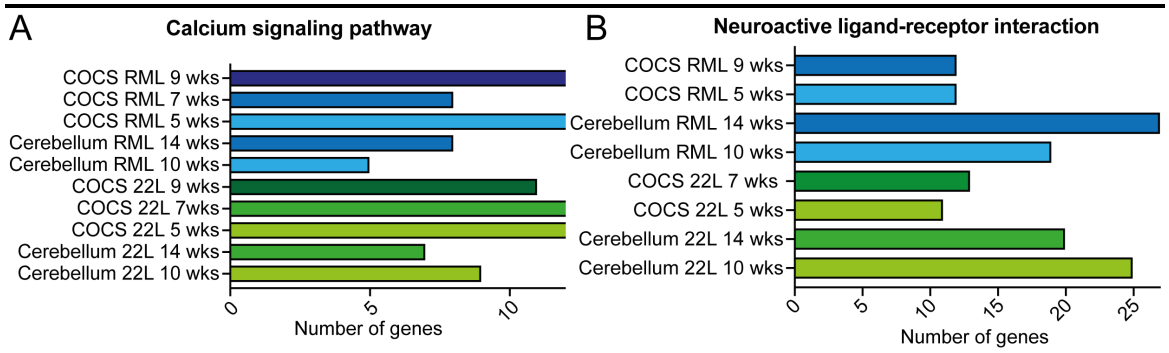

Figure 29. Calcium signaling pathway (A) and neuroactive ligand-interaction (B) were most frequently deregulated in 22L and RML infected *in vivo* and *ex vivo* experiments.

Table 11. Deregulated genes in calcium signaling pathway and neuroactive ligand-receptor interaction

	Genes involved in calcium signaling pathway	Genes involved in neuroactive ligand-receptor interaction
Cerebellum 22L 10 wks	*GRM5, TACR3, CHRM3, TACR1, HTR7, HTR4, CACNA1H, NTSR1, HTR2C*	*OPRM1, GPR83, CGA, TACR3, GLRA1, DRD2, NPY2R, TACR1, GLRA3, HCRTR1, HTR1A, PRL, RXFP3, GABRA5, HTR4, NPY1R, NTSR1, NPY5R, GRM5, CRHR2, CHRM3, HTR7, MC4R, HTR2C, GH*
Cerebellum 22L 14 wks	*GRM5, TACR3, CHRM3, CCKBR, TACR1, TRHR, HTR2A*	*CALCR, GPR83, GLRA1, CCKBR, TACR3, DRD2, RXFP3, GLRA3, TACR1, TRHR, GABRA5, NPY1R, NPY5R, GRM5, HCRTR1, HTR1A, CHRM3, CHRNB3, GABRQ, HTR2A*
COCS 22L 5 wks	*ADCY1, SLC8A2, GRIN1, CACNA1I, GRIN2A, PRKCG, GRM1, ITPR1, CAMK4, GRIN2C, ATP2A3, CACNA1G, RYR2, CACNA1E, CAMK2B, NOS2, CACNA1C, CAMK2A, CACNA1B*	*GABRD, GRM4, GRIA2, GABRA3, GABRB2, GRIN2C, GABRA6, GRIN1, GRIN2A, GRM1, NTSR2*
COCS 22L 7 wks	*ADCY1, SLC8A2, NOS1, GRIN1, CACNA1I, GRIN2A, PRKCG, ITPKA, ITPR1, CAMK4, ATP2A3, GRIN2C, RYR1, CACNA1E, CAMK2B, CAMK2A*	*CRHR1, GABRD, GRM4, HTR1B, SSTR3, GRM2, GABRB2, OPRL1, GRIN2C, GABRA6, GRIN1, GLRA2, GRIN2A*
COCS 22L 9 wks	*ATP2B3, ADCY1, SLC8A2, CAMK4, ATP2A3, CACNA1I, GRIN1, CACNA1G, PRKCG, CAMK2B, ITPR1*	
Cerebellum RML 10 wks	*CCKAR, TACR3, TNNC1, TACR1, HTR2C*	*CCKAR, CGA, ADORA3, GLRA1, TACR3, DRD2, GLRA3, TACR1, RXFP3, GABRA5, NPY1R, NPY5R, HCRTR1, CRHR2, HTR1A, PRL, HTR2C, CHRNE, GH*
Cerebellum RML 14 wks	*GRM5, TACR3, CCKBR, CHRM2, TACR1, HTR7, DRD5, TRHR*	*CALCR, OPRM1, GPR156, C3AR1, MCHR1, CCKBR, GLRA1, TACR3, DRD2, RXFP3, GLRA3, TACR1, DRD5,*

		GLRA2, TRHR, GABRA5, NPY1R, NPY5R, GRM5, HTR1A, CHRM2, HTR7, CHRNB3, CHRNA6, PRL, GABRQ, GH
COCS RML 5 wks	*ADCY1, SLC8A2, NOS1, GRIN1, CACNA1I, GRIN2A, ITPR1, CAMK4, ATP2A3, GRIN2C, CACNA1G, RYR1, CACNA1E, CAMK2B, NOS2, CAMK2A, HTR5A*	*CRHR1, GABRD, GRM4, GRM2, GRM8, GRIN2C, GABRA6, GRIN1, GLRA2, GRIN2A, VIPR1, HTR5A*
COCS RML 7 wks	*ATP2B2, ATP2B3, ADCY1, PLCB4, CAMK4, GRIN1, CAMK2B, ITPR1*	
COCS RML 9 wks	*ADCY1, SLC8A2, GRIN1, CACNA1I, GRIN2A, PRKCG, ITPKA, GRM1, ITPR1, ATP2B3, CAMK4, PDE1C, ATP2A3, GRIN2C, CACNA1G, CACNA1E, CAMK2B, HTR2C*	*CRHR1, GABRD, GRM4, GRM2, GRIN2C, GABRA6, CNR1, LEPR, GRIN1, GRIN2A, GRM1, HTR2C*

Nine genes were chosen for further analysis and validation of differentially expressed genes in COCS. The same COCS samples used for next generation sequencing analysis were transcribed to cDNA and real time PCR was performed. Three genes served as internal controls: *Gfap, Cxcl10* and *Snap25*. *GFAP* and *CXCL10* are known to be upregulated in prion disease (175) and *Snap25* is typically downregulated (176). The other chosen genes were either differentially expressed and/or were potential binding partners of DEGs (Figure 30).

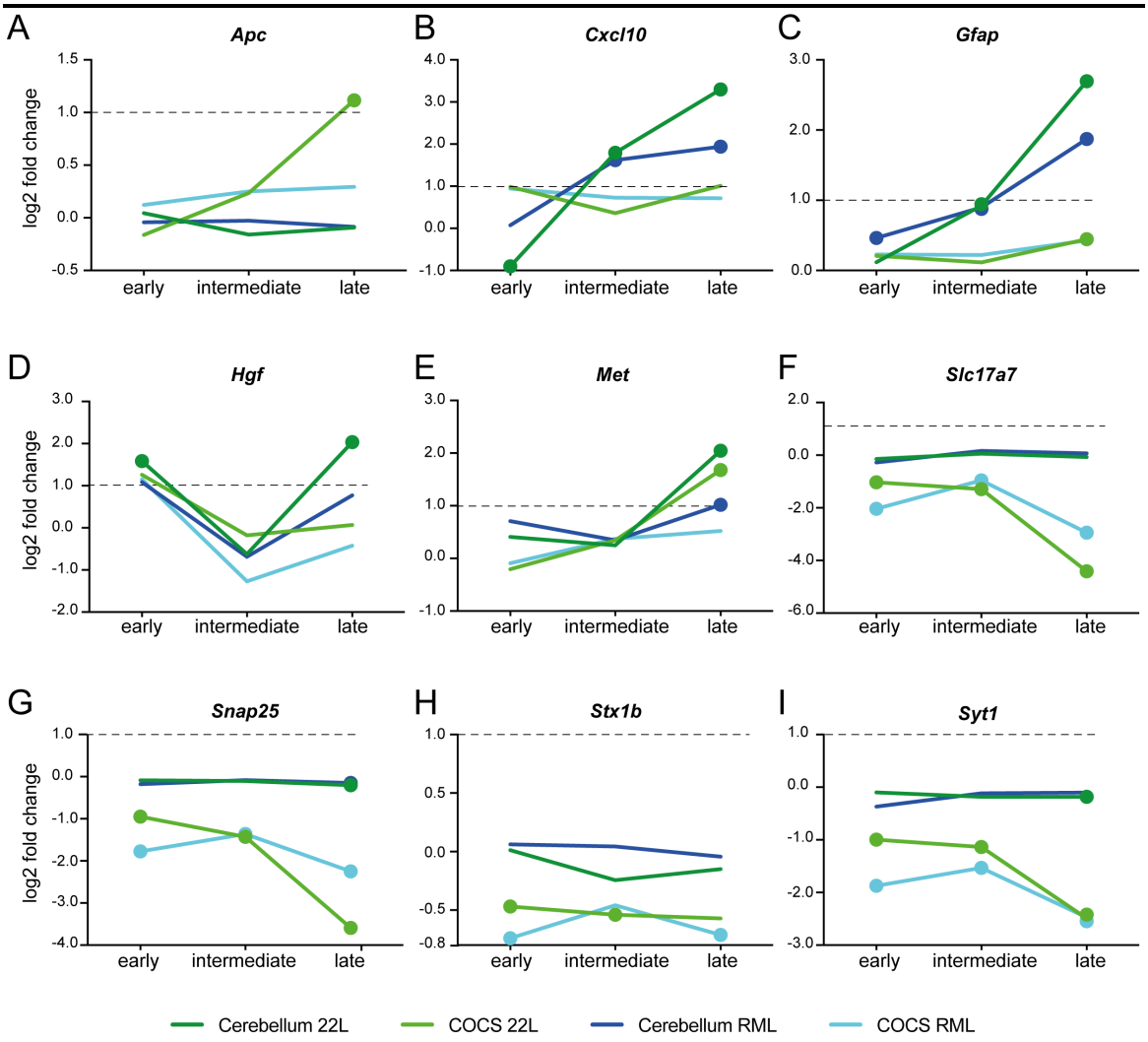

Figure 30 Sequencing results of DEGs chosen for qPCR validation. (A-I) Log2 fold change of different DEGs normalized to actin and relative to Mock samples. Genes above a log2 fold change of 1 are upregulated and beneath downregulated (dashed line). Unpaired t test was used to statistically analyze the data. Dots indicate a significant deregulation compared to Mock ($p \leq 0.05$).

Quantification of qPCR for COCS showed that *Cxcl10* was upregulated at all conditions but not necessarily significant, *Gfap* was significantly upregulated after nine weeks in 22L and RML infected COCS (Figure 31 B, C) and *Snap25* was downregulated from week five on, except for COCS infected for 7 weeks with RML prions were it showed no significant deregulation (Figure 31 H). *Snap25* data were comparable to sequencing data (Figure 30 G), in contrast to *Cxcl10*, which showed no significant changes in sequencing analysis for COCS (Figure 30 B). *Gfap* showed a not significant down-

regulation in both, sequencing analysis and qPCR analysis at week five and seven, but sequencing analysis showed no upregulation nine weeks post infection with 22L or RML. Sequencing analysis of *Hgf*, *Met* and *Slc17a7* could be validated by qPCR. In both, sequencing analysis and qPCR *Hgf* showed a not significant downregulation at all time points, *Met* a significant upregulation 9 weeks post 22L infection and *Slc17a7* was significantly downregulated at all time points except for qPCR analysis of COCS 5 weeks post 22L infection by (Figure 31 D-F, Figure 30 D-F). However, *Stx1b* displayed contrary results as it showed a significant upregulation by qPCR analysis and for most time points a significant downregulation in sequencing analysis (Figure 30 H, Figure 31 H). Also *Apc* showed different results in qPCR analysis and sequencing analysis. *Apc* was significantly downregulated five weeks post 22L infection significantly in qPCR analysis (Figure 31 A), but sequencing analysis revealed a significant upregulation 9 weeks post 22L infection (Figure 30 A). *Syt1* could not be detected by qPCR analysis, maybe because the amount of DNA was too low in the samples as it was strongly downregulated in sequencing analysis.

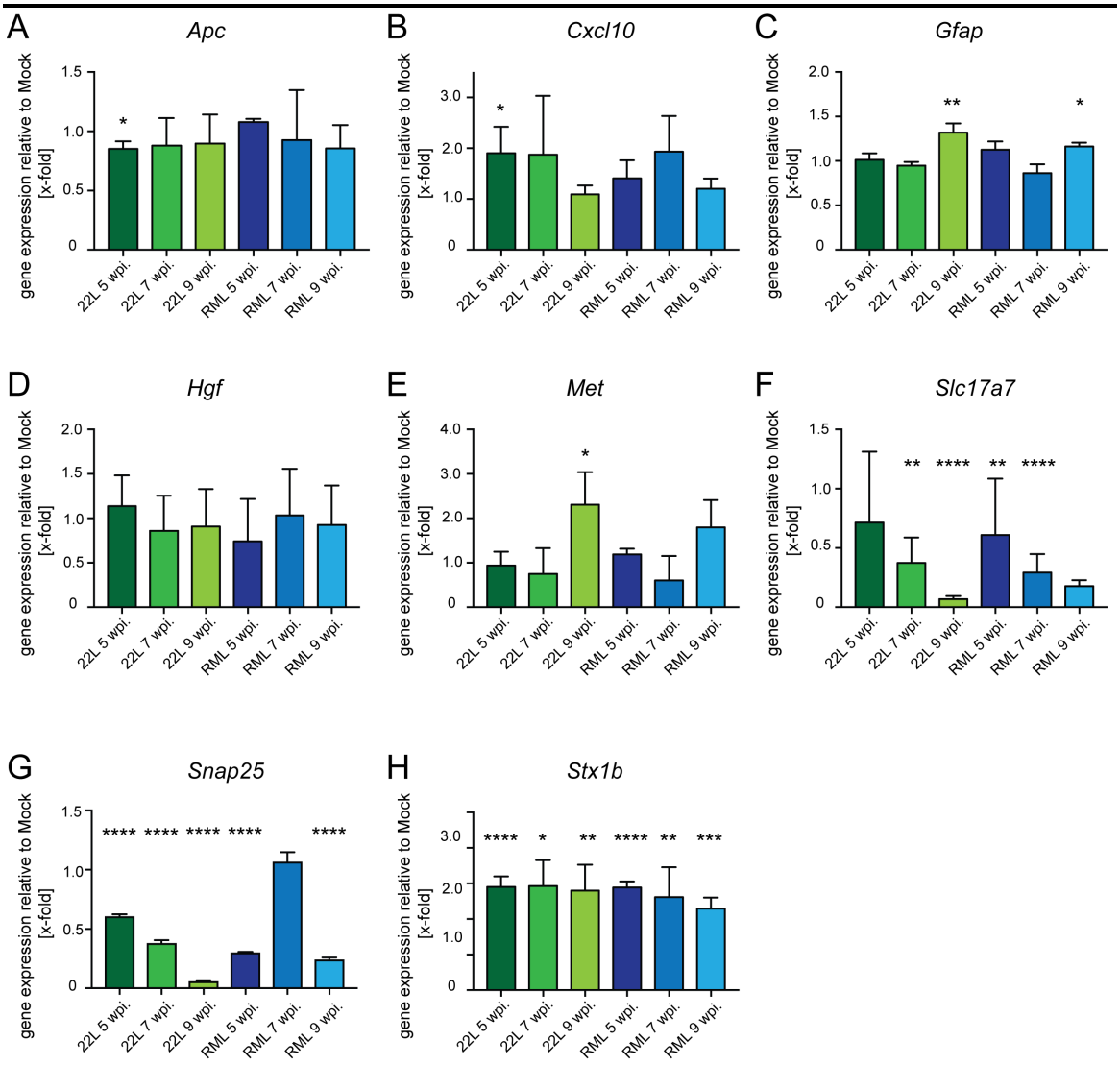

Figure 31. Quantitative qPCR to validate sequencing results for COCS. RNA of COCS samples that was sent in for next generation sequencing analysis were transcribed to cDNA. 200 ng of produced cDNA was mixed with probes of genes of interest **(A – H)** and actin was used to normalize. Gene expression is shown relative to Mock control, which was defined as 1. Experiments were done in triplicates. One-way ANOVA with Dunnett's multiple comparisons test was performed. Bars represent mean values ± SD. (*p ≤ 0.05, **p ≤ 0.01, ***p ≤ 0.001, ****p ≤ 0.0001, ns: not significant).

To summarize, changes in gene expression of mice and COCS were comparable for distinct pathways. Several pathways, but not necessarily the same genes, were deregulated in brain as well as in COCS. However, gene expression in general also revealed differences between *in vivo* and *ex vivo* experiments. Regarding the pathways

that might be influenced by prion disease, several pathways like calcium signaling pathways or neuroactive ligand-receptor interaction were deregulated in *in vivo* and *ex vivo* infected cerebella.

4 Discussion

Currently, there are no therapies for prion disease and these diseases are always invariably fatal. Therefore, it is of great importance to identify compounds with therapeutic or prophylactic activity against prion disease (146). The present available screening methods were not successful and sufficient to detect such a compound. Several compounds could be detected with *in vitro* efficacy, but *in vivo* these compounds showed no effect (148, 177). Therefore, there is an urgent need to screen more compounds to finally identify a compound with *in vivo* anti-prion activity.

In this study a screening method for the high-throughput analysis of compound libraries was developed based on N2a cells persistently infected with 22L prions. Several inhibitory compounds were detected and further analyzed, resulting in the identification of at least one compound, PHA665752 with an IC_{50} of 0.42 µM, that should be tested *in vivo*.

4.1 Successful establishment of a high-throughput screening method and its potential and problems

The established screening method is the first one based on immunofluorescence detection of PrP^{Sc} on a single cell level. The performed screen was conducted with 152 compounds from a preselected library on N2a cells persistently infected with prion strain 22L. 30 % of the compounds had an inhibitory effect on PrP^{Sc} accumulation, 37 % were considered to act as activators, 23 % had dual effects and 10 % of the compounds were toxic and were thus excluded from further analysis.

This screening method has the potential to be extended to different cells lines, as we showed e.g. for persistently prion infected L929 cells, and more prion strains. Beside this, another opportunity would be to test compounds on cells infected with different prion strains. Different prion strains exhibit specific biological and biochemical properties and target different strain-specific brain regions and cause a characteristic lesion profile. Prion strains differ in their cell tropism to different kinds of cells like astrocytes and neurons (178, 179). Identification of a compound with anti-prion activity on different strains in different cell types would present a perfect candidate for *in vivo* experiments. To screen for compounds that influence the establishment of an infection, uninfected cells could be infected on 96-well plates and during this infection compounds could be

added as well. Also a pre-treatment of cells with different compounds before prion infection would be realizable. Pre-treatment can be used to study e.g. the internalization process of PrP^{Sc} into the cell by blocking specific receptors or routes (178). In this way it is also possible to study cell biological processes in prion infected cells. Additionally, the transmission of PrP^{Sc} between cells could be studied with co-culture experiments, in the presence and absence of compounds. For evaluation of a compound effect, the percentage of infected cells was determined in this assay. However, beside this, it is possible to further characterize the effect on treated cells if the algorithm would be adapted. Size, form and amount of aggregates per cell, as well as the effect on size and form on the whole cell could be evaluated. Further characterization of cells and aggregates would provide more information about the effects of compounds on cells and possible mechanism of actions and efficacy, e.g. the reduction of aggregates per cell could be monitored.
These different applications make this screening method powerful to study compounds with beneficial effects on stabilization of native PrP^{C}, interruption of the conversion of PrP^{C} into PrP^{Sc} or the reduction of already existing PrP^{Sc}.

However, next to the broad range of advantages and novel applications, the developed high-throughput screen exhibits also some limitations. One problem is the lack of an antibody that can discriminate between PrP^{C} and PrP^{Sc}. In this assay, PrP^{Sc} was detected by immunofluorescence staining in fixed and permeabilized cells after antigen-retrieval by guanidine hydrochloride (GdnHCl) treatment. This treatment enables discrimination of the two PrP isoforms as it reduces PrP^{C} background staining, while it drastically increases the immunoreactivity of PrP^{Sc} (147, 180, 181). In this screen, PrP^{Sc} was detected by an algorithm. This algorithm for detection of PrP^{Sc} aggregates is based on measured local fluorescent signal peaks. If a compound drastically increases the level of PrP^{C}, possibly densely packed within vesicles, this antigen-retrieval might not be sufficient so that the algorithm could detect false positive cells due to its inability to discriminate between different origins of local signal peaks. An alternative detection of PrP^{Sc} in immunofluorescence staining could be implemented by a pre-treatment of cells with proteinase K (181, 182). However, this could not be established at least for the used cell type, as proteinase K treatment reduces the attachment of cells to the substrate, and even with different coating methods, prolonged fixation and gentle handling too many cells detached and subsequent analysis could not be continued. However, further

training and development of the algorithm might be useful for an even more reliable distinction between PrP^{C} and PrP^{Sc}.

At this moment the screening method also has a limitation concerning the amount of compounds that can be tested at once, as the 96-well plates had to be stained manually until the guanidine hydrochloride treatment due to biosafety regulations of the screening facility. However, this limitation could easily be avoided in a screening facility with S2 permission. Thereby, thousands of compounds could be tested at once with an automated staining procedure.

4.2 Several strong inhibitors on PrP^{Sc} accumulation are found in the screen but cannot necessarily be validated by western blot analysis

Of the 152 tested compounds 84 had an inhibitory effect on PrP^{Sc} accumulation in persistently infected $N2a^{22L}$ cells. Seven of the strongest inhibitors with no (survival of cells treated with 10 µM of a compound ≥ 75 %) or weak toxicity (survival of cells treated with 10 µM of a compound < 75 %) were chosen for further validation by western blot analysis (Figure 17 and Table 12). Before western blot analysis, two rounds of limited dilution cloning were performed to increase the percentage of 22L infected cells. Only concentrations of compounds that were not toxic in the screen were tested by western blot analysis with the same experimental setup as used for the screen. Three out of seven compounds showed significant reduction of PrP^{Sc} accumulation after compound treatment in western blot analysis (Table 12). Quinacrine dihydrochloride was identified by the screen as inhibitor and has previously been reported to have an anti-prion activity (183). In contrast to existing studies, we were not able to show a significant reduction of PrP^{Sc} accumulation in persistently prion-strain 22L infected N2a cells by western blot analysis. This might be due to experimental differences, like incubation time and concentration of the drug. We incubated the cells only for 44 h with 1 µM or 0.1 µM quinacrine dihydrochlorid. In the other studies, cells were incubated at least for 72 h and up to six days and medium supplemented with fresh compound was changed daily or every second day partly at higher concentration up to 5 µM (159, 168, 183, 184). However, beside Quinacrine dihydrochloride and AEE788, all compounds showed a reduction of PrP^{Sc} signal intensity, but due to variation between the three independent western blot results these changes are not significant.

Table 12. Summary of further validated compound identified by the screen

Compound	Reduction of PrP^{Sc} infected cells in %	Conformation by western blot analysis
Quinacrine dihydrochloride	64	No
Indatraline hydrochloride	70	No
Maprotiline hydrochloride	68	No
Methiothepin mesylate	53	Yes
AEE788	70	No
SB590885	90	Yes
PHA665752	71	Yes

The two different experimental setups were tried to be kept as similar as possible. However, the slightly different results may arise from some adaptation for western blot analysis. Firstly, western blot analysis was performed with a subclone of $N2a^{22L}$ cells. Subclones of cells can differ slightly from the bulk population, also a cell population develops heterogeneity even after biological cloning (185). It is e.g. known that prion susceptibility can differ between clones and also their ability to transmit PrP^{Sc} over several passages (124, 186). It was reported, that treatment with drugs in different cell clones could result in a slightly different response to the treatment (185, 187). Secondly, within the two experiments (screen vs. western blot analysis) cells were treated with compounds from different batches or even different producers. For the screen compounds available in screening libraries from Tocris, Selleckchem and Lopac were used. For western blot analysis compounds were ordered, if individually available, from Selleckchem and Sigma. Slight differences in cellular response to compound treatment might result from the different batch or producer (188, 189). Finally, the biggest difference between the two experiments, which cannot be avoided, is the detection methods for PrP^{Sc}. As described earlier PrP^{Sc} in the screen was detected by immunofluorescence staining after antigen-retrieval by guanidine hydrochloride treatment to reduce PrP^{C} background staining and increase the immunoreactivity of PrP^{Sc}. For western blot analysis, cell lysates were treated with proteinase K and only PK resistant PrP^{Sc} was detected. This may also have led to different results for the independent experiments.

4.3 Identified inhibitors of PrP^S accumulation may interfere with the autophagy pathway

The three compounds Methiothepin mesylate, SB590885 and PHA665752, had comparably strong inhibitory effects on PrP^{Sc} accumulation in the screen as well as in western blot analysis. Treatment of $N2a^{22L}$ cells with Methiothepin mesylate decreases PrP^{Sc} accumulation levels at 10 µM to 60 %, whereas 1 µM of SB590885 led to a decrease of PrP^{Sc} accumulation of 89 % and 1 µM PHA665752 of 85 %. PHA665752 was also the only compound that showed a significant reduction of PrP^{Sc} accumulation at 0.25 µM of 23 % (Figure 19). To determine the half maximal inhibitory concentration a dose response curve of these three compounds was produced. Surprisingly, this time the reduction of PrP^{Sc} accumulation levels was slightly lower than in the experiment before. This is likely due to the fact that for both experiments the same stock compound was used. Thus, compounds used for the dose response experiment were stored for around 5 weeks, compared to one day in the first experiment, and were additionally frozen and thawed one more time. Storage of compounds in DMSO, as well as thaw and freeze cycles can lead to significant compound degradation and reduces the activity of a compound (190). To understand the underlying mechanism that leads to the reduction of PrP^{Sc} levels in cells, the sites of action of compounds need to be elucidated. Methiothepin mesylate is a 5-$HT_{2\beta}$ receptor antagonist (191) and is used in several *in vitro* and *in vivo* experiments to study the role of serotonin in different pathways (192-194). The 5-$HT_{2\beta}$ receptor is a G-protein coupled receptor for 5-hydroxytryptamine (serotonin) (195), but also binds various alkaloid derivatives and psychoactive substances (196). Binding of a ligand results in conformational changes that trigger signaling via guanine nucleotide-binding proteins (G proteins) and modulate the activity of down-stream pathways (195). These affect, amongst others, neural activity, perception of pain, and regulation of behavior, including impulsive behavior (197). Several studies of the 5-$HT_{2\beta}$ receptor showed that it might be a potential target in cardiovascular diseases (198, 199), as it has functions in heart development, the adaptation of pulmonary arteries to chronic hypoxia and protects cardiomyocytes against apoptosis (195, 200).

SB590885 is a small molecule kinase inhibitor of the triarylimidazole class. This novel, low molecular weight compound inhibits potently and selectively B-Raf kinase activity, as SB-590885 occupies the ATP-binding pocket B-Raf and binds to an active conformation of B-Raf (201). It also binds with a lower selectivity to Erk (201). B-Raf is a member of

the Raf kinase family of growth signal transduction protein kinases and amongst others it plays a role in regulating the MAP kinase and ERKs signaling pathway by which it affects cell division, differentiation, and secretion (202). B-raf is composed of three conserved domains, a conserved region 1 (CR1), a Ras-GTP-binding self-regulatory domain (CR2) and a serine-rich hinge region, and conserved region 3 (CR3) (203). B-Raf is associated with several types of cancers, such as colorectal cancer, papillary thyroid cancer, melanoma, and ovarian cancer (204-207). *In vivo* administration of SB590885 potently decreases tumorigenesis in murine xenografts established from mutant B-Raf-expressing A375P melanoma cells, and modestly inhibits tumor growth (201).

PHA665752 is a small molecule inhibitor of c-met kinase. PHA665752 has a high specificity for c-Met, as it is 50 times more selective for c-Met than for other tyrosine/serine-threonine kinases (208). The receptor tyrosine kinase c-Met is encoded by the MET proto-oncogene. Hepatocyte growth factor (HGF) is the only known ligand for the c-MET receptor. Binding of HGF to c-Met leads to dimerization and autophosphorylation. This creates an active docking site for proteins that mediate downstream signaling pathways (209). Via the c-Met signal transduction pathway PHA665752 was shown to inhibit cell growth, induce cell-cycle arrest or apoptosis and affect cell motility (208). *In vivo*, administration of PHA-665752 induces a dose-dependent tumor growth inhibition (210, 211). PHA665752 also significantly inhibits angiogenesis, due to decreasing the production of vascular endothelial growth factor and increasing the production of the angiogenesis inhibitor thrombospondin-1 (212).

The mechanisms of action of these compounds on PrP^{Sc} accumulation were not further analyzed within this work. However, several mechanisms are conceivable like inhibition of PrP^{Sc} formation, degradation or stabilization of PrP^{C}. All three compounds target receptors or molecules, which are involved in many different pathways that regulate various intracellular processes. However, we focus on one common process that is likely to play a role in PrP^{Sc} degradation and is affected by the three compounds, namely autophagy.

Autophagy is a highly conserved catabolic process that degrades cytosolic macromolecules, damaged organelles, aggregated proteins and pathogens (213). Autophagy is required for the removal of proteins and plays a role in neurodegenerative diseases, cancer and inflammatory disorders (54, 214, 215). Autophagy functions in

maintaining neuronal homeostasis and plays a particularly important role in postmitotic neurons, as the level of altered proteins and damaged organelles cannot be diluted by means of cell division. Dysfunction in autophagy is denoted as a secondary pathologic mechanism for various neurodegenerative diseases, such as Alzheimer's disease, Parkinson's disease, Huntington's disease and amyotrophic lateral sclerosis (213).

There are three processes of autophagy described, including macroautophagy, which is most common and hereafter referred to as autophagy, microautophagy and chaperon-mediated autophagy. Under physiological conditions autophagy is generally active at low levels in most tissues to maintain protein and organelle quality by the elimination of damaged material. In response to stress and starvation, but also during inhibition of the mTOR pathway autophagy can be upregluated. Autophagy is controlled by products of the autophagy-related genes, the *Atg* (214, 216).

Here, a possible mechanism of PrP^{Sc} degradation in response to Methiothepin mesylate, SB590885 and PHA665752 treatment is suggested. Treatment with Methiothepin mesylate inhibits the 5-HT receptor, which amongst others leads to reduced activation of mTOR via the PI3K/AKT pathway (Figure 32 A) (217). If cells are treated with PHA665752, it inhibits the c-Met receptor, which in turn can inhibit mTOR via two different pathways. Less activation of GABA leads on one hand also to inhibition of the PI3K/AKT pathway and on the other to reduced mTOR activity via inhibition of Ras, which inhibits Raf resulting in reduced levels of MEK and Erk activation. It was shown that SB590885 is a novel triarylimidazole that selectively inhibits Raf kinases (201, 218) and thereby inhibits mTOR (Figure 32 A). Inhibition of mTOR leads to activation of autophagy, as it negatively regulates autophagy (217).

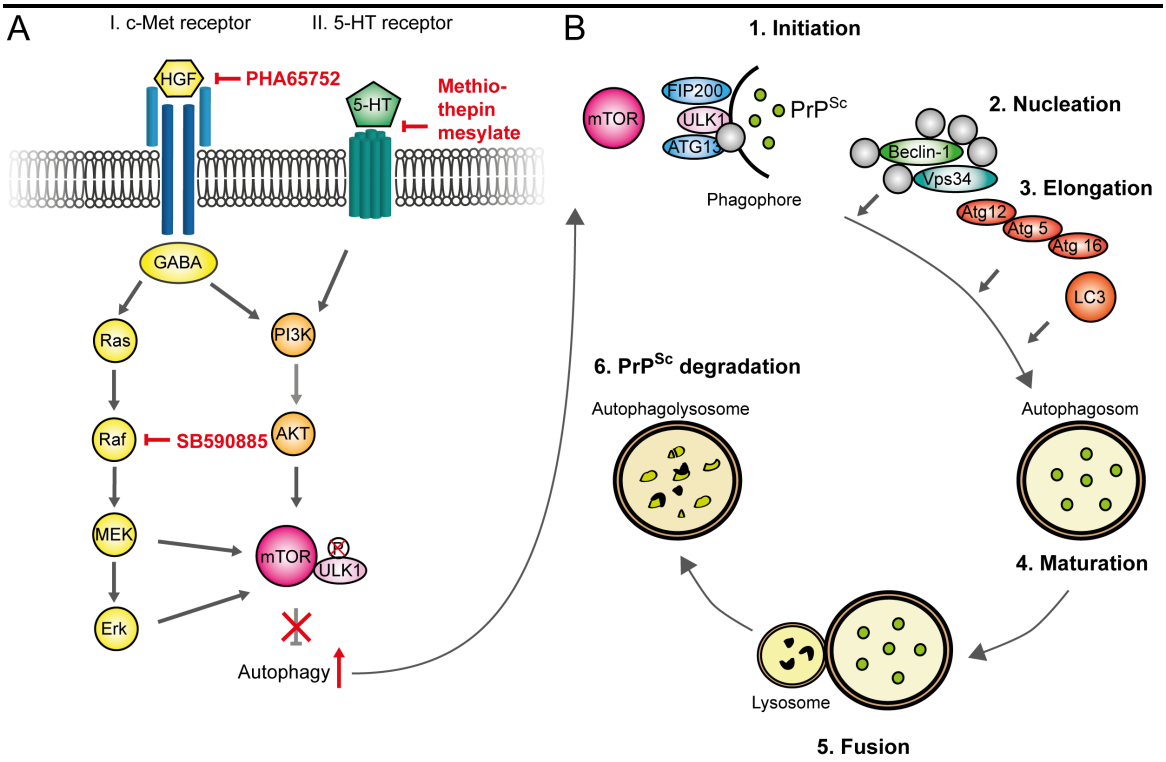

Figure 32. Proposed mechanism of Methiothepin mesylate, SB590885 and PHA665752 on PrP^{Sc} accumulation. (A) Compound treatment could inhibit mTOR signaling as shown in other cell models (170, 191, 201). Methiothepin mesylate inhibits the 5-HT receptor resulting in mTOR inhibition via the PI3K/AKT pathway. PHA665752 inhibits binding of HGF to c-Met receptor, resulting in less mTOR activation via PI3K/AKT and Ras/Raf, whereas SB590885 has an inhibitory effect via Raf. **(B)** PrP^{Sc} degradation by autophagy. Inhibition of mTOR results in activation of autophagy. In the initiation phase a phagophore assembles around PrP^{Sc} and is accomplished by formation of the UKL1/Atg1-Atg13-FIP200/Atg17 complex. The nucleation of the membrane starts with the formation of the Beclin-1/PI3KC3 complex elongated by formation of the Atg12-Atg5-Atg16L homology tetramer complex and LC3 is lipidated by binding to phosphatidylethanolamine. The formed autophagosome fuses with lysosomes resulting in autophagolysosome formation, which could degrade PrP^{Sc} .

Inhibition of mTOR leads to activation of ULK1 by dephosphorylation, which in turn forms the UKL1/Atg1-Atg13-FIP200/Atg17 complex (Figure 32 B). Once this complex is formed, autophagy is initiated. It begins with the formation of an isolation membrane or phagophore around the material, in this case PrP^{Sc} that should be engulfed (54). The phagophore is characterized as a small crescent-shaped structure. Formation of the autophagosome is classified in two steps: the nucleation and the elongation. The

nucleation of the membrane is initiated by the formation of Beclin-1/PI3KC3 complex composed of Beclin-1, UVRAG, Bif-1, ambra1, Vps15, and Vps3. To elongate the vesicle membrane, other Atg proteins are required. There are two ubiquitin-like protein systems involved in extension and expansion, the Atg12-Atg5-Atg16L homology tetramer complex, which leads to formation of vesicle curvature and LC3 (Atg8). LC3 is lipidated by binding to phosphatidylethanolamine (PE) located on the surface of the autophagic membrane (214). The formed autophagosome fuses with lysosomes and forms the autophagolysosome, where PrP^{Sc} degradation could take place (215).

In prion disease autophagy could function as a conserved host defense response to prion infection and could play a protective role by degrading aggregate-prone proteins accumulated within endosomal/lysosomal vesicles (54, 215). Recently, first studies showed that induction of autophagy can result in PrP^{Sc} degradation. It was shown that pharmacological inhibition of autophagy or siRNA gene-silencing of essential members of the autophagic machinery leads to impaired PrP^{Sc} degradation (54). Lithium for example, enhances clearance of PrP^{Sc} *in vitro* by inducing autophagy in an mTOR-independent manner (219), whereas Rapamycin reduces PrP^{Sc} levels in an mTOR-dependent manner (214). In contrast, treatment of prion-infected cells with a potent inhibitor of autophagy, like 3-methyladenine, counteracted the anti-prion effect of lithium (219).

Taken together there is clear evidence that induction of autophagy mediates degradation of PrP^{Sc}, which supports the proposed mechanism of action of Methiothepin mesylate, SB590885 and PHA665752 in persistently prion infected cells. Western blot pattern and reduction of PrP^{Sc} accumulation depended on concentrations were highly comparable for SB590885 and PHA665752. This might be due to the fact, that they inhibit the same signal transduction pathway. Additionally, PHA665752 showed the strongest inhibitory effect on PrP^{Sc} accumulation, which might result from mTOR dependent autophagy inhibition by two different signal transduction pathways. However, these two hypothesis needs to be validated by experiments concerning the autophagy pathway.

As PHA665752 showed such a strong inhibitory effect on PrP^{Sc} accumulation and is an approved drug candidate (220), it was chosen for *ex vivo* analysis, as it seems to be a promising candidate for a potential therapeutic in prion disease. However, it is unknown if PHA665752 is capable to cross the blood brain barrier. Due to the small size and its lipophilicity it might be possible that it can pass the blood brain barrier (221).

Therefore, 22L prion infected cerebellar organotypic slices (COCS) were treated with 1 µM PHA665752 for five weeks, as this concentration showed no toxicity at all. Western blot analysis revealed a decrease in PrP^{Sc} accumulation upon PHA665752 treatment. However, this decrease was statistically not significant. There might be several explanations why this decrease is statistically not significant and some possible options to increase the compound effect in future experiments. A higher number of the samples might already be sufficient to monitor a significant reduction of PrP^{Sc} accumulation. Beside significance a stronger reduction of PrP^{Sc} accumulation would be desirable. This could be accomplished by treatment with a higher concentration of PHA665752. In cell culture experiments 10 µM of PHA665752 was toxic, but 5 µM showed no toxicity. It would be also possible to increase the incubation time of COCS with PHA665752 to e.g. seven or nine weeks. Furthermore already thawed and frozen drugs were used which can reduce the activity of a drug as described earlier (190). Additionally the drug in DMSO was thawed, diluted in culture medium, containing amongst others horse serum, aliquoted and frozen. Before medium exchange one of this aliquot was thawed again. PHA665752 may have interacted with media components, which can result in a decreased half-life and activity of the compound (222, 223).

An improved experimental setup could already be sufficient to increase the reduction of PrP^{Sc} accumulation in COCS, but also higher concentrations and longer incubation can be considered.

4.4 *Ex vivo* experiments on prion infected COCS revealed that FeTMPyP and PIM-B31 appear to be no promising targets for PrP^{Sc} inhibition

Furthermore, two other compounds with potential anti-prion activities were tested on COCS, FeTMPyP and PIM-B31, in cooperation with Emiliano Biasini (University of Trento, Italy) who did the *in vitro* pretesting.

5,10,15,20-tetrakis(*N*-methyl-4´-pyridyl)porphyrinato iron(III) (FeTMPyP) is a peroxynitrite decomposition catalyst (PDC), which has been shown to protect against cytokine-induced cytotoxicity in hippocampal culture (224) and methamphetamine-induced neurotoxicity in rats (225). PDCs isomerize peroxynitrites to nitrate anions and hence decrease their decomposition to highly reactive intermediates such as nitrogen dioxide and hydroxyl radicals (224). In addition to the peroxynitrite decomposition effect,

these compounds do have moderate superoxide dismutase activity resulting in a neuroprotective effect. Oxidative stress has been shown to play a role in several neurodegenerative disorders (226). Peroxynitrite (PN) is a marker for oxidative stress. The formation of the powerful oxidant peroxynitrite by the reaction of superoxide anion with nitric oxide has been shown to be a kinetically favored reaction and contributes to cellular injury and death at sites of tissue inflammation (224). PN has been shown to cause lipid peroxidation (227), chemical cleavage of DNA (228), inactivation of key metabolic enzymes (229), and reduction in cellular antioxidant defenses (230). PN can also nitrate protein tyrosine residues (nitrotyrosine), leading to the disruption of key cytoskeletal components that may contribute to the pathogenesis of diseases such as amyotrophic lateral sclerosis (231) or ALS. Nitrotyrosine has been detected in tissues from Alzheimer's (232), multiple sclerosis (233), ALS (231), and rheumatoid arthritis (234) patients. In scrapie-infected mouse brains, high level of nitrotyrosine were found, suggesting damage by free radicals (226). Therefore antioxidants like FeTMPyP, are a potential therapy for these disorders. Additionally, recent force spectroscopy analysis on single molecule level revealed that FeTMPyP binds to PrP and inhibits misfolding by stabilizing the native state while suppressing interactions driving aggregation (235).

However, in the conducted experiment, already a treatment with 1 µM FeTMPyP had such toxic effects that COCS completely dissolved and analysis could not be conducted. Further experiments with concentrations below the analyzed molarity range would be necessary for FeTMPyP to provide sufficient evidence for anti-prion effects. Nevertheless, it is disputable if it makes sense to continue experiments with a compound with such a high toxicity at 1 µM.

The second tested compound was PIM-B31, a self-synthetized compound from Emiliano Biasini. In contrast to FeTMPyP, PIM-B31 showed no toxicity on COCS. Treatment with the first batch of compound led to a slight increase of PrP^{Sc} accumulation in 22L infected slices at a concentration of 10 µM. However, treatment with a higher concentration decreased PrP^{Sc} accumulation strongly. Both concentrations reduced PrP^{Sc} accumulation in RML infected COCS, but the variation between the two experiments was high. For those reasons, experiments were repeated with more cerebellar slices (n = 5) and a new synthesized batch of PIM-B31. Treatment of 22L infected COCS with 10 µM of PIM-B31 led again to a slight but significant increase of PrP^{Sc} accumulation. Strikingly, treatment with 50 µM on 22L infected COCS and both concentrations on RML infected COCS had no effect on PrP^{Sc} accumulation. To exclude that the newly

synthesized has a lower activity than the old batch, cells were treated with 50 µM of the old and new batch. Here, both compounds reduced PrP^{Sc} accumulation (- 45 % vs. - 32 %) but the old batch appeared to be more potent though the differences between the two batches were not significant. To summarize, PIM-B31 appears to have a dual effect in COCS (inhibitor and activator, depending on concentration and strain). It is a known phenomenon that different compounds result in concentration dependent dual effects (236-239). Inconsistencies in experiments with new and old batches may in part be explained by biological activity of PIM-B31, the old batch appears to be more potent. PIM-B31 has a dual effect on PrP^{Sc} accumulation in COCS. The results of treatment on RML infected COCS are hard to interpret due to the inconsistency of the results. Differences among experiments may potentially result from the batch-to-batch variation. No precipitation of the compound was observed that could explain lack of activity at high concentrations.

4.5 Several comparable pathways are deregulated *in vivo* and *ex vivo* although differential expressed gene are not that similar

A comparative study of the host response between *ex vivo* and *in vivo* was performed to evaluate the comparability between the two systems. To demonstrate this, COCS were prepared from pubs of C57BL/6JRj mice, infected with 22L and RML prions and RNA was isolated at three different time points post infection. In parallel, C57BL/6JRj mice were injected with the same 22L and RML prions and RNA was isolated from the cerebella at comparable time points concerning disease progression. RNA sequencing analysis was performed and analyzed. The 250 most significant differentially expressed genes at each condition were compared to each other. DEGs from COCS (*ex vivo*) infected with one prion strain at a distinct time point were compared to DEGs from mouse cerebella infected with the same strain and at a comparable time point (*in vivo*). Between two to nineteen comparable genes were identified at a specific condition.

Comparison of 22L infected COCS and cerebella revealed that only three genes were similarly deregulated between *in vivo* and *ex vivo*. *Myo5B* and *Met* were upregulated at early respectively at late time point, whereas *Dlk1* was down regulated at the intermediate time point. A possible influence of *Met* on prion disease was proposed earlier in this work. *Dlk1* codes for delta like non-canonical Notch ligand 1 which contains multiple epidermal growth factor repeats. These growth factor repeats function as

regulator for cell growth. Mutation of this gene is associated with obesity and is not related to neurodegenerative diseases until now (240). In contrast, *Myo5b* encodes for myosin Vb which is suggested to play a role in Alzheimer's disease where it might interfere the balance of beta-amyloid production and clearance (241).

Comparison of RML infected COCS and cerebella led to the identification of two similar regulated genes, again *Dlk1* and *Serpina3n*. Both genes were downregulated at the late time point. *Serpina3n* encodes for serpin family A member 3 and functions as plasma protease inhibitor and serine protease inhibitor. Variation of this protein's sequence have been implicated in Alzheimer's disease (242), Parkinson disease (243) and chronic obstructive pulmonary disease (244) and deficiency of this protein has been associated with liver disease. However, in a recent publication, *Serpina3n* was shown to be upregulated in human prion disease (245). The frontal cortex from patients suffering from vCJD, iCJD, sCJD, FFI and GSS were analyzed by qPCR and showed a strong up-regulation of *Serpina3n* (245). There also an upregulation of *Serpina3n* in mice infected with prion strain RML could be detected. However, in contrast to our experiments, the isolated RNA of the frontal cortex of the human brain or one hemisphere of CD1 mouse whole brain tissue was analyzed, instead of analyzing the isolated RNA of the cerebellum, as presented here.

DAVID 6.8 pathway analysis of the 250 most significant differentially expressed genes revealed that several pathways (Table 10) were similarly affected by prion infection of COCS and cerebella. The two most influenced pathways were the calcium signaling pathways and the neuroactive ligand-receptor pathway. It is known, that prion infection leads to changes in the calcium signaling pathways as PrP^{Sc} accumulation leads to extensive ER stress, resulting in the rapid release of calcium to the cytoplasm and the activation of the UPR (246). Also the neuroactive ligand-receptor pathway is known to be deregulated during *in vivo* and *ex vivo* (247) prion infection. The neuroactive ligand-receptor pathway is involved in the communication of several neurotransmitters like serotonin, dopamine and glutamate (247). Both pathways can be altered by activation or inhibition of the N-Methyl-D-aspartate (NMDA) (246-248). The NMDA receptor is one of the major classes of ionotropic glutamate receptors in the mammalian brain that interacts with PrP^{C} (249). NMDA receptors are heterotetrameric channels. The assembly of two GluN1 and two GluN2/GluN3 subunits forms the receptor. Glycine binds to GluN1 and GluN3 subunit, while the GluN2 subunit contains the binding site for glutamate. The NMDA receptor can be localized synaptic, perisynaptic, extrasynaptic, or presynaptic.

The localization of the receptor is coupled to specific cellular events (250). In general, activation of synaptic localized NMDA receptors leads to activation of pro-survival signaling. In contrast, activation of extrasynaptic localized NMDA receptors leads to activation of pro-death signaling (251). In general, NMDA receptor activation by glutamate results in the opening of non-selective cation channels and calcium and sodium ion influx into the cytosol. At the synapse, glutamate is released by the presynaptic terminals, diffuses across the synaptic cleft and activates NMDA receptors at the post-synaptic membrane. This activation leads to depolarization of the post-synaptic membrane and induces an excitatory postsynaptic potential (EPSP) (248). Beside the physiological role of NMDA receptors in learning and memory, an altered expression is likely to play a role in the pathophysiology of a wide variety of CNS disorders like neurodegenerative diseases (248). Mice inoculated with variant CJD prions showed increased NMDA receptor excitation (252). In vitro cultured neurons were incubated with PrP^{Sc}-like PrP106-126 peptide and treatment with NMDA receptor antagonists blocked the resulting neurotoxicity (253). However, down regulation of NMDA receptor activity may lead to a loss of the physiological PrP^{C} function, which may also contribute to the pathogenic process (254). Genetic PrP^{C} depletion leads to an increased hippocampal NMDA receptor-mediated excitation and glutamate excitotoxicity (255) . Furthermore, PrP knockout mice showed to be more susceptible to seizures induced by kainic acid than wild-type controls (256), likely due to facilitated NMDA receptor-mediated excitation in the hippocampus (257). However, although the exact physiological function of PrP^{C} on the NMDA receptor is not fully understood, it is becoming clear that loss of PrP^{C} regulation of NMDA receptor can result in toxicity in a variety of pathological conditions (258). There is a need to investigate the physiological interaction between PrP^{C} and NMDA receptors and how this activity impacts signal transduction in both healthy and diseased organisms.

4.6 Outlook

The developed high-throughput screen represents a powerful tool to identify potential compounds to treat prion disease. In the future the presented screen can be extended to several different cell lines, but also different strains. Further improvement of the algorithms that detect prion aggregates in the screen could reveal more information of the effect of a single compound with regard to e.g. amount and size of PrP^{Sc} aggregates in a single cell.

Beside *in vitro* experiments, it would be necessary to test more compounds e.g. Methiothepin mesylate and SB590885 on prion infected cerebellar slices. Here it would be also interesting, if the identified compounds are capable of inhibiting PrP^{Sc} accumulation, if slices were infected with different strains. Genetic manipulation of slices e.g. by viral transduction is also a possible method to gain more information on the mode of action of different compounds.

Identified compounds capable of inhibiting PrP^{Sc} accumulation *in vitro* and *ex vivo* without any toxicity should be tested *in vivo* in mouse experiments. In the case of PHA665752, we will test it again on 22L infected COCS with a newly ordered compound, solved in DMSO, aliquoted and solved in slices culture medium right before use. If treatment results in a significant reduction of PrP^{Sc} accumulation, PHA665752 will be tested in prion infected mice and might be tested further in a prion therapeutic clinical trial.

RNA sequencing analysis led, amongst others, to the identification of *Dlk1*, which was downregulated at every time point, in cerebella and cerebellar slices infected with 22L and RML prions. Further analysis of *Dlk1* and associate proteins could reveal cytopathological pathways and hands additional insights in prion disease pathology.

Further investigation of the interaction between NMDA receptors and PrP^{C} and better understanding of the underlying molecular mechanism might lead to the possibility of targeted modulation of this interaction in neurodegenerative diseases, such as prion disease.

Bibliography

1. Requena JR, Kristensson K, Korth C, Zurzolo C, Simmons M, Aguilar-Calvo P, et al. The Priority position paper: Protecting Europe's food chain from prions. Prion. 2016;10(3):165-81.

2. Schneider K, Fangerau H, Michaelsen B, Raab WH. The early history of the transmissible spongiform encephalopathies exemplified by scrapie. Brain Res Bull. 2008;77(6):343-55.

3. Fast C, and Groschup, M. H. 'Classical and atypical scrapie in sheep and goats,'' in Prions and Diseases: Animals, Humans and the Environment. New York: Springer; 2013.

4. B S. A chronic encephalitis of sheep- with general remarks on infections which develop slowly and some of their special characteristics. BrVetJ. 1954;66:341-54.

5. Alper T, Cramp WA, Haig DA, Clarke MC. Does the agent of scrapie replicate without nucleic acid? Nature. 1967;214(5090):764-6.

6. Alper T, Haig DA, Clarke MC. The exceptionally small size of the scrapie agent. Biochem Biophys Res Commun. 1966;22(3):278-84.

7. Griffith JS. Self-replication and scrapie. Nature. 1967;215(5105):1043-4.

8. Bolton DC, McKinley MP, Prusiner SB. Identification of a protein that purifies with the scrapie prion. Science. 1982;218(4579):1309-11.

9. Aguzzi A, Heikenwalder M. Pathogenesis of prion diseases: current status and future outlook. Nat Rev Microbiol. 2006;4(10):765-75.

10. Sparkes RS, Simon M, Cohn VH, Fournier RE, Lem J, Klisak I, et al. Assignment of the human and mouse prion protein genes to homologous chromosomes. Proc Natl Acad Sci U S A. 1986;83(19):7358-62.

11. Basler K, Oesch B, Scott M, Westaway D, Walchli M, Groth DF, et al. Scrapie and cellular PrP isoforms are encoded by the same chromosomal gene. Cell. 1986;46(3):417-28.

12. Westaway D, Cooper C, Turner S, Da Costa M, Carlson GA, Prusiner SB. Structure and polymorphism of the mouse prion protein gene. Proc Natl Acad Sci U S A. 1994;91(14):6418-22.

13. Brockes JP. Topics in prion cell biology. Curr Opin Neurobiol. 1999;9(5):571-7.

14. White AR, Enever P, Tayebi M, Mushens R, Linehan J, Brandner S, et al. Monoclonal antibodies inhibit prion replication and delay the development of prion disease. Nature. 2003;422(6927):80-3.

15. Zahn R, Liu A, Luhrs T, Riek R, von Schroetter C, Lopez Garcia F, et al. NMR solution structure of the human prion protein. Proc Natl Acad Sci U S A. 2000;97(1):145-50.

16. Oesch B, Westaway D, Walchli M, McKinley MP, Kent SB, Aebersold R, et al. A cellular gene encodes scrapie PrP 27-30 protein. Cell. 1985;40(4):735-46.

17. Haraguchi T, Fisher S, Olofsson S, Endo T, Groth D, Tarentino A, et al. Asparagine-linked glycosylation of the scrapie and cellular prion proteins. Arch Biochem Biophys. 1989;274(1):1-13.

18. Turk E, Teplow DB, Hood LE, Prusiner SB. Purification and properties of the cellular and scrapie hamster prion proteins. Eur J Biochem. 1988;176(1):21-30.

19. Stahl N, Baldwin MA, Hecker R, Pan KM, Burlingame AL, Prusiner SB. Glycosylinositol phospholipid anchors of the scrapie and cellular prion proteins contain sialic acid. Biochemistry. 1992;31(21):5043-53.

20. Vazquez-Fernandez E, Vos MR, Afanasyev P, Cebey L, Sevillano AM, Vidal E, et al. The Structural Architecture of an Infectious Mammalian Prion Using Electron Cryomicroscopy. PLoS Pathog. 2016;12(9):e1005835.

21. Grassmann A, Wolf H, Hofmann J, Graham J, Vorberg I. Cellular aspects of prion replication in vitro. Viruses. 2013;5(1):374-405.

22. Walmsley AR, Watt NT, Taylor DR, Perera WS, Hooper NM. alpha-cleavage of the prion protein occurs in a late compartment of the secretory pathway and is independent of lipid rafts. Mol Cell Neurosci. 2009;40(2):242-8.

23. Campana V, Caputo A, Sarnataro D, Paladino S, Tivodar S, Zurzolo C. Characterization of the properties and trafficking of an anchorless form of the prion protein. J Biol Chem. 2007;282(31):22747-56.

24. Alfa Cisse M, Sunyach C, Slack BE, Fisher A, Vincent B, Checler F. M1 and M3 muscarinic receptors control physiological processing of cellular prion by modulating ADAM17 phosphorylation and activity. J Neurosci. 2007;27(15):4083-92.

25. Alais S, Simoes S, Baas D, Lehmann S, Raposo G, Darlix JL, et al. Mouse neuroblastoma cells release prion infectivity associated with exosomal vesicles. Biol Cell. 2008;100(10):603-15.

26. Starke R, Harrison P, Drummond O, Macgregor I, Mackie I, Machin S. The majority of cellular prion protein released from endothelial cells is soluble. Transfusion. 2003;43(5):677-8; author reply 8.

27. Mironov A, Jr., Latawiec D, Wille H, Bouzamondo-Bernstein E, Legname G, Williamson RA, et al. Cytosolic prion protein in neurons. J Neurosci. 2003;23(18):7183-93.

28. Rane NS, Yonkovich JL, Hegde RS. Protection from cytosolic prion protein toxicity by modulation of protein translocation. EMBO J. 2004;23(23):4550-9.

29. Crozet C, Vezilier J, Delfieu V, Nishimura T, Onodera T, Casanova D, et al. The truncated 23-230 form of the prion protein localizes to the nuclei of inducible cell lines independently of its nuclear localization signals and is not cytotoxic. Mol Cell Neurosci. 2006;32(4):315-23.

30. Marina-Garcia N, Franchi L, Kim YG, Hu Y, Smith DE, Boons GJ, et al. Clathrin- and dynamin-dependent endocytic pathway regulates muramyl dipeptide internalization and NOD2 activation. J Immunol. 2009;182(7):4321-7.

31. Capurro MI, Shi W, Filmus J. LRP1 mediates Hedgehog-induced endocytosis of the GPC3-Hedgehog complex. J Cell Sci. 2012;125(Pt 14):3380-9.

32. Yin S, Pham N, Yu S, Li C, Wong P, Chang B, et al. Human prion proteins with pathogenic mutations share common conformational changes resulting in enhanced binding to glycosaminoglycans. Proc Natl Acad Sci U S A. 2007;104(18):7546-51.

33. Kang YS, Zhao X, Lovaas J, Eisenberg E, Greene LE. Clathrin-independent internalization of normal cellular prion protein in neuroblastoma cells is associated with the Arf6 pathway. J Cell Sci. 2009;122(Pt 22):4062-9.

34. Taylor DR, Watt NT, Perera WS, Hooper NM. Assigning functions to distinct regions of the N-terminus of the prion protein that are involved in its copper-stimulated, clathrin-dependent endocytosis. J Cell Sci. 2005;118(Pt 21):5141-53.

35. Magalhaes AC, Silva JA, Lee KS, Martins VR, Prado VF, Ferguson SS, et al. Endocytic intermediates involved with the intracellular trafficking of a fluorescent cellular prion protein. J Biol Chem. 2002;277(36):33311-8.

36. Bueler H, Aguzzi A, Sailer A, Greiner RA, Autenried P, Aguet M, et al. Mice devoid of PrP are resistant to scrapie. Cell. 1993;73(7):1339-47.

37. Tobler I, Gaus SE, Deboer T, Achermann P, Fischer M, Rulicke T, et al. Altered circadian activity rhythms and sleep in mice devoid of prion protein. Nature. 1996;380(6575):639-42.

38. Criado JR, Sanchez-Alavez M, Conti B, Giacchino JL, Wills DN, Henriksen SJ, et al. Mice devoid of prion protein have cognitive deficits that are rescued by reconstitution of PrP in neurons. Neurobiol Dis. 2005;19(1-2):255-65.

39. Brown DR, Nicholas RS, Canevari L. Lack of prion protein expression results in a neuronal phenotype sensitive to stress. J Neurosci Res. 2002;67(2):211-24.

40. Singh A, Qing L, Kong Q, Singh N. Change in the characteristics of ferritin induces iron imbalance in prion disease affected brains. Neurobiol Dis. 2012;45(3):930-8.

41. Aguzzi A, Polymenidou M. Mammalian prion biology: one century of evolving concepts. Cell. 2004;116(2):313-27.

42. Solforosi L, Criado JR, McGavern DB, Wirz S, Sanchez-Alavez M, Sugama S, et al. Cross-linking cellular prion protein triggers neuronal apoptosis in vivo. Science. 2004;303(5663):1514-6.

43. Eghiaian F, Grosclaude J, Lesceu S, Debey P, Doublet B, Treguer E, et al. Insight into the PrPC-->PrPSc conversion from the structures of antibody-bound ovine prion scrapie-susceptibility variants. Proc Natl Acad Sci U S A. 2004;101(28):10254-9.

44. Acevedo-Morantes CY, Wille H. The structure of human prions: from biology to structural models-considerations and pitfalls. Viruses. 2014;6(10):3875-92.

45. Pan KM, Baldwin M, Nguyen J, Gasset M, Serban A, Groth D, et al. Conversion of alpha-helices into beta-sheets features in the formation of the scrapie prion proteins. Proc Natl Acad Sci U S A. 1993;90(23):10962-6.

46. Prusiner SB, Groth DF, Bolton DC, Kent SB, Hood LE. Purification and structural studies of a major scrapie prion protein. Cell. 1984;38(1):127-34.

47. Caughey B, Kocisko DA, Raymond GJ, Lansbury PT, Jr. Aggregates of scrapie-associated prion protein induce the cell-free conversion of protease-sensitive prion protein to the protease-resistant state. Chem Biol. 1995;2(12):807-17.

48. Jarrett JT, Lansbury PT, Jr. Seeding "one-dimensional crystallization" of amyloid: a pathogenic mechanism in Alzheimer's disease and scrapie? Cell. 1993;73(6):1055-8.

49. Come JH, Fraser PE, Lansbury PT, Jr. A kinetic model for amyloid formation in the prion diseases: importance of seeding. Proc Natl Acad Sci U S A. 1993;90(13):5959-63.

50. Knowles TP, Waudby CA, Devlin GL, Cohen SI, Aguzzi A, Vendruscolo M, et al. An analytical solution to the kinetics of breakable filament assembly. Science. 2009;326(5959):1533-7.

51. Orgel LE. Prion replication and secondary nucleation. Chem Biol. 1996;3(6):413-4.

52. Stefani M, Dobson CM. Protein aggregation and aggregate toxicity: new insights into protein folding, misfolding diseases and biological evolution. J Mol Med (Berl). 2003;81(11):678-99.

53. Wickner RB, Shewmaker F, Kryndushkin D, Edskes HK. Protein inheritance (prions) based on parallel in-register beta-sheet amyloid structures. Bioessays. 2008;30(10):955-64.

54. Heiseke A, Aguib Y, Schatzl HM. Autophagy, prion infection and their mutual interactions. Curr Issues Mol Biol. 2010;12(2):87-97.

55. Silveira JR, Raymond GJ, Hughson AG, Race RE, Sim VL, Hayes SF, et al. The most infectious prion protein particles. Nature. 2005;437(7056):257-61.

56. Budka H. Neuropathology of prion diseases. Br Med Bull. 2003;66:121-30.

57. Wadsworth JD, Collinge J. Molecular pathology of human prion disease. Acta Neuropathol. 2011;121(1):69-77.

58. Budka H, Aguzzi A, Brown P, Brucher JM, Bugiani O, Gullotta F, et al. Neuropathological diagnostic criteria for Creutzfeldt-Jakob disease (CJD) and other human spongiform encephalopathies (prion diseases). Brain Pathol. 1995;5(4):459-66.

59. Fiorini M, Bongianni M, Monaco S, Zanusso G. Biochemical Characterization of Prions. Prog Mol Biol Transl Sci. 2017;150:389-407.

60. Pattison IH, Millson GC. Scrapie produced experimentally in goats with special reference to the clinical syndrome. J Comp Pathol. 1961;71:101-9.

61. Bessen RA, Marsh RF. Identification of two biologically distinct strains of transmissible mink encephalopathy in hamsters. J Gen Virol. 1992;73 (Pt 2):329-34.

62. McKintosh E, Tabrizi SJ, Collinge J. Prion diseases. J Neurovirol. 2003;9(2):183-93.

63. Fraser H. The pathology of a natural and experimental scrapie. Front Biol. 1976;44:267-305.

64. Hecker R, Taraboulos A, Scott M, Pan KM, Yang SL, Torchia M, et al. Replication of distinct scrapie prion isolates is region specific in brains of transgenic mice and hamsters. Genes Dev. 1992;6(7):1213-28.

65. Bruce ME, McConnell I, Fraser H, Dickinson AG. The disease characteristics of different strains of scrapie in Sinc congenic mouse lines: implications for the nature of the agent and host control of pathogenesis. J Gen Virol. 1991;72 (Pt 3):595-603.

66. Cali I, Castellani R, Alshekhlee A, Cohen Y, Blevins J, Yuan J, et al. Co-existence of scrapie prion protein types 1 and 2 in sporadic Creutzfeldt-Jakob disease: its effect on the phenotype and prion-type characteristics. Brain. 2009;132(Pt 10):2643-58.

67. Parchi P, Strammiello R, Notari S, Giese A, Langeveld JP, Ladogana A, et al. Incidence and spectrum of sporadic Creutzfeldt-Jakob disease variants with mixed phenotype and co-occurrence of PrPSc types: an updated classification. Acta Neuropathol. 2009;118(5):659-71.

68. Spassov S, Beekes M, Naumann D. Structural differences between TSEs strains investigated by FT-IR spectroscopy. Biochim Biophys Acta. 2006;1760(7):1138-49.

69. Colby DW, Giles K, Legname G, Wille H, Baskakov IV, DeArmond SJ, et al. Design and construction of diverse mammalian prion strains. Proc Natl Acad Sci U S A. 2009;106(48):20417-22.

70. Bessen RA, Kocisko DA, Raymond GJ, Nandan S, Lansbury PT, Caughey B. Non-genetic propagation of strain-specific properties of scrapie prion protein. Nature. 1995;375(6533):698-700.

71. Castilla J, Morales R, Saa P, Barria M, Gambetti P, Soto C. Cell-free propagation of prion strains. EMBO J. 2008;27(19):2557-66.

72. Barria MA, Gonzalez-Romero D, Soto C. Cyclic amplification of prion protein misfolding. Methods Mol Biol. 2012;849:199-212.

73. Weissmann C. Birth of a prion: spontaneous generation revisited. Cell. 2005;122(2):165-8.

74. Collinge J, Clarke AR. A general model of prion strains and their pathogenicity. Science. 2007;318(5852):930-6.

75. Karapetyan YE, Saa P, Mahal SP, Sferrazza GF, Sherman A, Sales N, et al. Prion strain discrimination based on rapid in vivo amplification and analysis by the cell panel assay. PLoS One. 2009;4(5):e5730.

76. Weissmann C. A 'unified theory' of prion propagation. Nature. 1991;352(6337):679-83.

77. Weissmann C. Thoughts on mammalian prion strains. Folia Neuropathol. 2009;47(2):104-13.

78. Moore RA, Vorberg I, Priola SA. Species barriers in prion diseases--brief review. Arch Virol Suppl. 2005(19):187-202.

79. Sweeting B, Khan MQ, Chakrabartty A, Pai EF. Structural factors underlying the species barrier and susceptibility to infection in prion disease. Biochem Cell Biol. 2010;88(2):195-202.

80. Priola SA, Chabry J, Chan K. Efficient conversion of normal prion protein (PrP) by abnormal hamster PrP is determined by homology at amino acid residue 155. J Virol. 2001;75(10):4673-80.

81. Lloyd SE, Mead S, Collinge J. Genetics of prion diseases. Curr Opin Genet Dev. 2013;23(3):345-51.

82. Prusiner SB. Prions. Proc Natl Acad Sci U S A. 1998;95(23):13363-83.

83. Collinge J. Molecular neurology of prion disease. J Neurol Neurosurg Psychiatry. 2005;76(7):906-19.

84. Collinge J. Prion diseases of humans and animals: their causes and molecular basis. Annu Rev Neurosci. 2001;24:519-50.

85. Brown P, Cathala F, Raubertas RF, Gajdusek DC, Castaigne P. The epidemiology of Creutzfeldt-Jakob disease: conclusion of a 15-year investigation in France and review of the world literature. Neurology. 1987;37(6):895-904.

86. Kovacs GG, Trabattoni G, Hainfellner JA, Ironside JW, Knight RS, Budka H. Mutations of the prion protein gene phenotypic spectrum. J Neurol. 2002;249(11):1567-82.

87. Mead S. Prion disease genetics. Eur J Hum Genet. 2006;14(3):273-81.

88. Alpers MP. Review. The epidemiology of kuru: monitoring the epidemic from its peak to its end. Philos Trans R Soc Lond B Biol Sci. 2008;363(1510):3707-13.

89. Will RG, Ironside JW, Zeidler M, Cousens SN, Estibeiro K, Alperovitch A, et al. A new variant of Creutzfeldt-Jakob disease in the UK. Lancet. 1996;347(9006):921-5.

90. Wilesmith JW. Bovine spongiform encephalopathy. Vet Rec. 1988;122(25):614.

91. Smith PG, Bradley R. Bovine spongiform encephalopathy (BSE) and its epidemiology. Br Med Bull. 2003;66:185-98.

92. Corona C, Costassa EV, Iulini B, Caramelli M, Bozzetta E, Mazza M, et al. Phenotypical Variability in Bovine Spongiform Encephalopathy: Epidemiology, Pathogenesis, and Diagnosis of Classical and Atypical Forms. Prog Mol Biol Transl Sci. 2017;150:241-65.

93. Dickinson AG, Stamp JT, Renwick CC. Maternal and lateral transmission of scrapie in sheep. J Comp Pathol. 1974;84(1):19-25.

94. Sohn HJ, Kim JH, Choi KS, Nah JJ, Joo YS, Jean YH, et al. A case of chronic wasting disease in an elk imported to Korea from Canada. J Vet Med Sci. 2002;64(9):855-8.

95. Kahn S, Dube C, Bates L, Balachandran A. Chronic wasting disease in Canada: Part 1. Can Vet J. 2004;45(5):397-404.

96. Kim TY, Shon HJ, Joo YS, Mun UK, Kang KS, Lee YS. Additional cases of Chronic Wasting Disease in imported deer in Korea. J Vet Med Sci. 2005;67(8):753-9.

97. Benestad SL, Mitchell G, Simmons M, Ytrehus B, Vikoren T. First case of chronic wasting disease in Europe in a Norwegian free-ranging reindeer. Vet Res. 2016;47(1):88.

98. Mathiason CK, Powers JG, Dahmes SJ, Osborn DA, Miller KV, Warren RJ, et al. Infectious prions in the saliva and blood of deer with chronic wasting disease. Science. 2006;314(5796):133-6.

99. Soto C. Diagnosing prion diseases: needs, challenges and hopes. Nat Rev Microbiol. 2004;2(10):809-19.

100. Clarke MC, Haig DA. Evidence for the multiplication of scrapie agent in cell culture. Nature. 1970;225(5227):100-1.

101. Nishida N, Harris DA, Vilette D, Laude H, Frobert Y, Grassi J, et al. Successful transmission of three mouse-adapted scrapie strains to murine neuroblastoma cell lines overexpressing wild-type mouse prion protein. J Virol. 2000;74(1):320-5.

102. Rubenstein R, Carp RI, Callahan SM. In vitro replication of scrapie agent in a neuronal model: infection of PC12 cells. J Gen Virol. 1984;65 (Pt 12):2191-8.

103. Rubenstein R, Deng H, Race RE, Ju W, Scalici CL, Papini MC, et al. Demonstration of scrapie strain diversity in infected PC12 cells. J Gen Virol. 1992;73 (Pt 11):3027-31.

104. Rubenstein R, Deng H, Scalici CL, Papini MC. Alterations in neurotransmitter-related enzyme activity in scrapie-infected PC12 cells. J Gen Virol. 1991;72 (Pt 6):1279-85.

105. Arjona A, Simarro L, Islinger F, Nishida N, Manuelidis L. Two Creutzfeldt-Jakob disease agents reproduce prion protein-independent identities in cell cultures. Proc Natl Acad Sci U S A. 2004;101(23):8768-73.

106. Miyazawa K, Emmerling K, Manuelidis L. High CJD infectivity remains after prion protein is destroyed. J Cell Biochem. 2011;112(12):3630-7.

107. Vella LJ, Sharples RA, Lawson VA, Masters CL, Cappai R, Hill AF. Packaging of prions into exosomes is associated with a novel pathway of PrP processing. J Pathol. 2007;211(5):582-90.

108. Courageot MP, Daude N, Nonno R, Paquet S, Di Bari MA, Le Dur A, et al. A cell line infectible by prion strains from different species. J Gen Virol. 2008;89(Pt 1):341-7.

109. Vorberg I, Raines A, Story B, Priola SA. Susceptibility of common fibroblast cell lines to transmissible spongiform encephalopathy agents. J Infect Dis. 2004;189(3):431-9.

110. Lawson VA. Quantitative bioassay of surface-bound prion infectivity. Methods Mol Biol. 2008;459:265-73.

111. Akimov S, Vasilyeva I, Yakovleva O, McKenzie C, Cervenakova L. Murine bone marrow stromal cell culture with features of mesenchymal stem cells susceptible to mouse-adapted human TSE agent, Fukuoka-1. Folia Neuropathol. 2009;47(2):205-14.

112. Cervenakova L, Akimov S, Vasilyeva I, Yakovleva O, McKenzie C, Cervenak J, et al. Fukuoka-1 strain of transmissible spongiform encephalopathy agent infects murine bone marrow-derived cells with features of mesenchymal stem cells. Transfusion. 2011;51(8):1755-68.

113. Giri RK, Young R, Pitstick R, DeArmond SJ, Prusiner SB, Carlson GA. Prion infection of mouse neurospheres. Proc Natl Acad Sci U S A. 2006;103(10):3875-80.

114. Milhavet O, Casanova D, Chevallier N, McKay RD, Lehmann S. Neural stem cell model for prion propagation. Stem Cells. 2006;24(10):2284-91.

115. Herva ME, Relano-Gines A, Villa A, Torres JM. Prion infection of differentiated neurospheres. J Neurosci Methods. 2010;188(2):270-5.

116. Cronier S, Laude H, Peyrin JM. Prions can infect primary cultured neurons and astrocytes and promote neuronal cell death. Proc Natl Acad Sci U S A. 2004;101(33):12271-6.

117. Kocisko DA, Caughey B. Searching for anti-prion compounds: cell-based high-throughput in vitro assays and animal testing strategies. Methods Enzymol. 2006;412:223-34.

118. Klohn PC, Stoltze L, Flechsig E, Enari M, Weissmann C. A quantitative, highly sensitive cell-based infectivity assay for mouse scrapie prions. Proc Natl Acad Sci U S A. 2003;100(20):11666-71.

119. Chasseigneaux S, Pastore M, Britton-Davidian J, Manie E, Stern MH, Callebert J, et al. Genetic heterogeneity versus molecular analysis of prion susceptibility in neuroblasma N2a sublines. Arch Virol. 2008;153(9):1693-702.

120. Bosque PJ. Bovine spongiform encephalopathy, chronic wasting disease, scrapie, and the threat to humans from prion disease epizootics. Curr Neurol Neurosci Rep. 2002;2(6):488-95.

121. McNally KL, Ward AE, Priola SA. Cells expressing anchorless prion protein are resistant to scrapie infection. J Virol. 2009;83(9):4469-75.

122. Maas E, Geissen M, Groschup MH, Rost R, Onodera T, Schatzl H, et al. Scrapie infection of prion protein-deficient cell line upon ectopic expression of mutant prion proteins. J Biol Chem. 2007;282(26):18702-10.

123. Butler DA, Scott MR, Bockman JM, Borchelt DR, Taraboulos A, Hsiao KK, et al. Scrapie-infected murine neuroblastoma cells produce protease-resistant prion proteins. J Virol. 1988;62(5):1558-64.

124. Bosque PJ, Prusiner SB. Cultured cell sublines highly susceptible to prion infection. J Virol. 2000;74(9):4377-86.

125. Raymond GJ, Olsen EA, Lee KS, Raymond LD, Bryant PK, 3rd, Baron GS, et al. Inhibition of protease-resistant prion protein formation in a transformed deer cell line infected with chronic wasting disease. J Virol. 2006;80(2):596-604.

126. Vanni S. Omics of Prion Diseases. Prog Mol Biol Transl Sci. 2017;150:409-31.

127. Dandoy-Dron F, Guillo F, Benboudjema L, Deslys JP, Lasmezas C, Dormont D, et al. Gene expression in scrapie. Cloning of a new scrapie-responsive gene and the identification of increased levels of seven other mRNA transcripts. J Biol Chem. 1998;273(13):7691-7.

128. Campbell IL, Eddleston M, Kemper P, Oldstone MB, Hobbs MV. Activation of cerebral cytokine gene expression and its correlation with onset of reactive astrocyte and acute-phase response gene expression in scrapie. J Virol. 1994;68(4):2383-7.

129. Diedrich JF, Minnigan H, Carp RI, Whitaker JN, Race R, Frey W, 2nd, et al. Neuropathological changes in scrapie and Alzheimer's disease are associated with increased expression of apolipoprotein E and cathepsin D in astrocytes. J Virol. 1991;65(9):4759-68.

130. Riemer C, Neidhold S, Burwinkel M, Schwarz A, Schultz J, Kratzschmar J, et al. Gene expression profiling of scrapie-infected brain tissue. Biochem Biophys Res Commun. 2004;323(2):556-64.

131. Carroll JA, Striebel JF, Race B, Phillips K, Chesebro B. Prion infection of mouse brain reveals multiple new upregulated genes involved in neuroinflammation or signal transduction. J Virol. 2015;89(4):2388-404.

132. Majer A, Medina SJ, Niu Y, Abrenica B, Manguiat KJ, Frost KL, et al. Early mechanisms of pathobiology are revealed by transcriptional temporal dynamics in hippocampal CA1 neurons of prion infected mice. PLoS Pathog. 2012;8(11):e1003002.

133. Hwang D, Lee IY, Yoo H, Gehlenborg N, Cho JH, Petritis B, et al. A systems approach to prion disease. Mol Syst Biol. 2009;5:252.

134. Gahwiler BH, Capogna M, Debanne D, McKinney RA, Thompson SM. Organotypic slice cultures: a technique has come of age. Trends Neurosci. 1997;20(10):471-7.

135. Falsig J, Aguzzi A. The prion organotypic slice culture assay--POSCA. Nat Protoc. 2008;3(4):555-62.

136. Stoppini L, Buchs PA, Muller D. A simple method for organotypic cultures of nervous tissue. J Neurosci Methods. 1991;37(2):173-82.

137. Falsig J, Sonati T, Herrmann US, Saban D, Li B, Arroyo K, et al. Prion pathogenesis is faithfully reproduced in cerebellar organotypic slice cultures. PLoS Pathog. 2012;8(11):e1002985.

138. Falsig J, Julius C, Margalith I, Schwarz P, Heppner FL, Aguzzi A. A versatile prion replication assay in organotypic brain slices. Nat Neurosci. 2008;11(1):109-17.

139. Campeau JL, Wu G, Bell JR, Rasmussen J, Sim VL. Early increase and late decrease of purkinje cell dendritic spine density in prion-infected organotypic mouse cerebellar cultures. PLoS One. 2013;8(12):e81776.

140. Herrmann US, Sonati T, Falsig J, Reimann RR, Dametto P, O'Connor T. Correction: Prion infections and anti-PrP antibodies trigger converging neurotoxic pathways. PLoS Pathog. 2015;11(4):e1004808.

141. Doh-ura K, Ishikawa K, Murakami-Kubo I, Sasaki K, Mohri S, Race R, et al. Treatment of transmissible spongiform encephalopathy by intraventricular drug infusion in animal models. J Virol. 2004;78(10):4999-5006.

142. Caughey B, Raymond GJ. Sulfated polyanion inhibition of scrapie-associated PrP accumulation in cultured cells. J Virol. 1993;67(2):643-50.

143. Adjou KT, Demaimay R, Lasmezas C, Deslys JP, Seman M, Dormont D. MS-8209, a new amphotericin B derivative, provides enhanced efficacy in delaying hamster scrapie. Antimicrob Agents Chemother. 1995;39(12):2810-2.

144. Caughey WS, Raymond LD, Horiuchi M, Caughey B. Inhibition of protease-resistant prion protein formation by porphyrins and phthalocyanines. Proc Natl Acad Sci U S A. 1998;95(21):12117-22.

145. Horiuchi M, Priola SA, Chabry J, Caughey B. Interactions between heterologous forms of prion protein: binding, inhibition of conversion, and species barriers. Proc Natl Acad Sci U S A. 2000;97(11):5836-41.

146. Kocisko DA, Baron GS, Rubenstein R, Chen J, Kuizon S, Caughey B. New inhibitors of scrapie-associated prion protein formation in a library of 2000 drugs and natural products. J Virol. 2003;77(19):10288-94.

147. Wolf H, Hossinger A, Fehlinger A, Buttner S, Sim V, McKenzie D, et al. Deposition pattern and subcellular distribution of disease-associated prion protein in cerebellar organotypic slice cultures infected with scrapie. Front Neurosci. 2015;9:410.

148. McMahon HE. Cell Culture Methods for Screening of Prion Therapeutics. Methods Mol Biol. 2017;1658:295-304.

149. Caughey B, Ernst D, Race RE. Congo red inhibition of scrapie agent replication. J Virol. 1993;67(10):6270-2.

150. Molloy B, McMahon HE. A cell-biased effect of estrogen in prion infection. J Virol. 2014;88(2):1342-53.

151. Prior M, Lehmann S, Sy MS, Molloy B, McMahon HE. Cyclodextrins inhibit replication of scrapie prion protein in cell culture. J Virol. 2007;81(20):11195-207.

152. Mange A, Nishida N, Milhavet O, McMahon HE, Casanova D, Lehmann S. Amphotericin B inhibits the generation of the scrapie isoform of the prion protein in infected cultures. J Virol. 2000;74(7):3135-40.

153. Tsuboi Y, Doh-Ura K, Yamada T. Continuous intraventricular infusion of pentosan polysulfate: clinical trial against prion diseases. Neuropathology. 2009;29(5):632-6.

154. Geschwind MD, Kuo AL, Wong KS, Haman A, Devereux G, Raudabaugh BJ, et al. Quinacrine treatment trial for sporadic Creutzfeldt-Jakob disease. Neurology. 2013;81(23):2015-23.

155. Ertmer A, Gilch S, Yun SW, Flechsig E, Klebl B, Stein-Gerlach M, et al. The tyrosine kinase inhibitor STI571 induces cellular clearance of PrPSc in prion-infected cells. J Biol Chem. 2004;279(40):41918-27.

156. Robert M. Haralick KS, I. Dinstein. Textural Features for Image Classification. IEEE Tranactions on Systems, Man, and Cybernetics. 1973;3:610-21.

157. Pfaffl MW. A new mathematical model for relative quantification in real-time RT-PCR. Nucleic Acids Res. 2001;29(9):e45.

158. Kupfer L, Hinrichs W, Groschup MH. Prion protein misfolding. Curr Mol Med. 2009;9(7):826-35.

159. Barret A, Tagliavini F, Forloni G, Bate C, Salmona M, Colombo L, et al. Evaluation of quinacrine treatment for prion diseases. J Virol. 2003;77(15):8462-9.

160. Stincardini C, Massignan T, Biggi S, Elezgarai SR, Sangiovanni V, Vanni I, et al. An antipsychotic drug exerts anti-prion effects by altering the localization of the cellular prion protein. PLoS One. 2017;12(8):e0182589.

161. Massignan T, Cimini S, Stincardini C, Cerovic M, Vanni I, Elezgarai SR, et al. A cationic tetrapyrrole inhibits toxic activities of the cellular prion protein. Sci Rep. 2016;6:23180.

162. Gahwiler BH. Organotypic cultures of neural tissue. Trends Neurosci. 1988;11(11):484-9.

163. Tremblay RG, Sikorska M, Sandhu JK, Lanthier P, Ribecco-Lutkiewicz M, Bani-Yaghoub M. Differentiation of mouse Neuro 2A cells into dopamine neurons. J Neurosci Methods. 2010;186(1):60-7.

164. Provost P. Interpretation and applicability of microRNA data to the context of Alzheimer's and age-related diseases. Aging (Albany NY). 2010;2(3):166-9.

165. Race RE, Fadness LH, Chesebro B. Characterization of scrapie infection in mouse neuroblastoma cells. J Gen Virol. 1987;68 (Pt 5):1391-9.

166. Bach S, Talarek N, Andrieu T, Vierfond JM, Mettey Y, Galons H, et al. Isolation of drugs active against mammalian prions using a yeast-based screening assay. Nat Biotechnol. 2003;21(9):1075-81.

167. Hofmann JP, Denner P, Nussbaum-Krammer C, Kuhn PH, Suhre MH, Scheibel T, et al. Cell-to-cell propagation of infectious cytosolic protein aggregates. Proc Natl Acad Sci U S A. 2013;110(15):5951-6.

168. Korth C, May BC, Cohen FE, Prusiner SB. Acridine and phenothiazine derivatives as pharmacotherapeutics for prion disease. Proc Natl Acad Sci U S A. 2001;98(17):9836-41.

169. Ghaemmaghami S, Ahn M, Lessard P, Giles K, Legname G, DeArmond SJ, et al. Continuous quinacrine treatment results in the formation of drug-resistant prions. PLoS Pathog. 2009;5(11):e1000673.

170. McDermott U, Pusapati RV, Christensen JG, Gray NS, Settleman J. Acquired resistance of non-small cell lung cancer cells to MET kinase inhibition is mediated by a switch to epidermal growth factor receptor dependency. Cancer Res. 2010;70(4):1625-34.

171. Arsac JN, Andreoletti O, Bilheude JM, Lacroux C, Benestad SL, Baron T. Similar biochemical signatures and prion protein genotypes in atypical scrapie and Nor98 cases, France and Norway. Emerg Infect Dis. 2007;13(1):58-65.

172. Altmeppen HC, Puig B, Dohler F, Thurm DK, Falker C, Krasemann S, et al. Proteolytic processing of the prion protein in health and disease. Am J Neurodegener Dis. 2012;1(1):15-31.

173. Kranich J, Krautler NJ, Falsig J, Ballmer B, Li S, Hutter G, et al. Engulfment of cerebral apoptotic bodies controls the course of prion disease in a mouse strain-dependent manner. J Exp Med. 2010;207(10):2271-81.

174. Sandberg MK, Al-Doujaily H, Sharps B, De Oliveira MW, Schmidt C, Richard-Londt A, et al. Prion neuropathology follows the accumulation of alternate prion protein isoforms after infective titre has peaked. Nat Commun. 2014;5:4347.

175. Lazarini F, Boussin F, Deslys JP, Tardy M, Dormont D. Astrocyte gene expression in experimental mouse scrapie. J Comp Pathol. 1994;111(1):87-98.

176. Saba R, Goodman CD, Huzarewich RL, Robertson C, Booth SA. A miRNA signature of prion induced neurodegeneration. PLoS One. 2008;3(11):e3652.

177. Barreca ML, Iraci N, Biggi S, Cecchetti V, Biasini E. Pharmacological Agents Targeting the Cellular Prion Protein. Pathogens. 2018;7(1).

178. Fehlinger A, Wolf H, Hossinger A, Duernberger Y, Pleschka C, Riemschoss K, et al. Prion strains depend on different endocytic routes for productive infection. Sci Rep. 2017;7(1):6923.

179. Gonzalez L, Martin S, Jeffrey M. Distinct profiles of PrP(d) immunoreactivity in the brain of scrapie- and BSE-infected sheep: implications for differential cell targeting and PrP processing. J Gen Virol. 2003;84(Pt 5):1339-50.

180. McKinley MP, Taraboulos A, Kenaga L, Serban D, Stieber A, DeArmond SJ, et al. Ultrastructural localization of scrapie prion proteins in cytoplasmic vesicles of infected cultured cells. Lab Invest. 1991;65(6):622-30.

181. Taraboulos A, Serban D, Prusiner SB. Scrapie prion proteins accumulate in the cytoplasm of persistently infected cultured cells. J Cell Biol. 1990;110(6):2117-32.

182. Veith NM, Plattner H, Stuermer CA, Schulz-Schaeffer WJ, Burkle A. Immunolocalisation of PrPSc in scrapie-infected N2a mouse neuroblastoma cells by light and electron microscopy. Eur J Cell Biol. 2009;88(1):45-63.

183. Chung E, Prelli F, Dealler S, Lee WS, Chang YT, Wisniewski T. Styryl-based and tricyclic compounds as potential anti-prion agents. PLoS One. 2011;6(9):e24844.

184. Ishibashi D, Nakagaki T, Ishikawa T, Atarashi R, Watanabe K, Cruz FA, et al. Structure-Based Drug Discovery for Prion Disease Using a Novel Binding Simulation. EBioMedicine. 2016;9:238-49.

185. Oelschlegel AM, Weissmann C. Acquisition of drug resistance and dependence by prions. PLoS Pathog. 2013;9(2):e1003158.

186. Uryu M, Karino A, Kamihara Y, Horiuchi M. Characterization of prion susceptibility in Neuro2a mouse neuroblastoma cell subclones. Microbiol Immunol. 2007;51(7):661-9.

187. Wang R, Jin C, Hu X. Evidence of drug-response heterogeneity rapidly generated from a single cancer cell. Oncotarget. 2017;8(25):41113-24.

188. McNerny DQ, Leroueil PR, Baker JR. Understanding specific and nonspecific toxicities: a requirement for the development of dendrimer-based pharmaceuticals. Wiley Interdiscip Rev Nanomed Nanobiotechnol. 2010;2(3):249-59.

189. Bouhaddou M, DiStefano MS, Riesel EA, Carrasco E, Holzapfel HY, Jones DC, et al. Drug response consistency in CCLE and CGP. Nature. 2016;540(7631):E9-E10.

190. Kozikowski BA, Burt TM, Tirey DA, Williams LE, Kuzmak BR, Stanton DT, et al. The effect of freeze/thaw cycles on the stability of compounds in DMSO. J Biomol Screen. 2003;8(2):210-5.

191. Mainou BA, Ashbrook AW, Smith EC, Dorset DC, Denison MR, Dermody TS. Serotonin Receptor Agonist 5-Nonyloxytryptamine Alters the Kinetics of Reovirus Cell Entry. J Virol. 2015;89(17):8701-12.

192. Gharbawie OA, Whishaw IQ. Cholinergic and serotonergic neocortical projection lesions given singly or in combination cause only mild impairments on tests of skilled movement in rats: evaluation of a model of dementia. Brain Res. 2003;970(1-2):97-109.

193. Zhang Y, Benton JL, Beltz BS. 5-HT receptors mediate lineage-dependent effects of serotonin on adult neurogenesis in Procambarus clarkii. Neural Dev. 2011;6:2.

194. Pappert EJ, Goetz CG, Stebbins GT, Belden M, Carvey PM. 5-Hydroxytryptophan-induced myoclonus in guinea pigs: mediation through 5-HT1/2 receptor subtypes. Eur J Pharmacol. 1998;347(1):51-6.

195. Schmuck K, Ullmer C, Engels P, Lubbert H. Cloning and functional characterization of the human 5-HT2B serotonin receptor. FEBS Lett. 1994;342(1):85-90.

196. Wacker D, Wang C, Katritch V, Han GW, Huang XP, Vardy E, et al. Structural features for functional selectivity at serotonin receptors. Science. 2013;340(6132):615-9.

197. Bevilacqua L, Doly S, Kaprio J, Yuan Q, Tikkanen R, Paunio T, et al. A population-specific HTR2B stop codon predisposes to severe impulsivity. Nature. 2010;468(7327):1061-6.

198. Poissonnet G, Parmentier JG, Boutin JA, Goldstein S. The emergence of selective 5-HT 2B antagonists structures, activities and potential therapeutic applications. Mini Rev Med Chem. 2004;4(3):325-30.

199. Shyu KG. Serotonin 5-HT2B receptor in cardiac fibroblast contributes to cardiac hypertrophy: a new therapeutic target for heart failure? Circ Res. 2009;104(1):1-3.

200. Ullmer C, Boddeke HG, Schmuck K, Lubbert H. 5-HT2B receptor-mediated calcium release from ryanodine-sensitive intracellular stores in human pulmonary artery endothelial cells. Br J Pharmacol. 1996;117(6):1081-8.

201. King AJ, Patrick DR, Batorsky RS, Ho ML, Do HT, Zhang SY, et al. Demonstration of a genetic therapeutic index for tumors expressing oncogenic BRAF by the kinase inhibitor SB-590885. Cancer Res. 2006;66(23):11100-5.

202. Matallanas D, Birtwistle M, Romano D, Zebisch A, Rauch J, von Kriegsheim A, et al. Raf family kinases: old dogs have learned new tricks. Genes Cancer. 2011;2(3):232-60.

203. Cutler RE, Jr., Stephens RM, Saracino MR, Morrison DK. Autoregulation of the Raf-1 serine/threonine kinase. Proc Natl Acad Sci U S A. 1998;95(16):9214-9.

204. Weisenberger DJ, Siegmund KD, Campan M, Young J, Long TI, Faasse MA, et al. CpG island methylator phenotype underlies sporadic microsatellite instability and is tightly associated with BRAF mutation in colorectal cancer. Nat Genet. 2006;38(7):787-93.

205. Tufano RP, Teixeira GV, Bishop J, Carson KA, Xing M. BRAF mutation in papillary thyroid cancer and its value in tailoring initial treatment: a systematic review and meta-analysis. Medicine (Baltimore). 2012;91(5):274-86.

206. Lee JH, Choi JW, Kim YS. Frequencies of BRAF and NRAS mutations are different in histological types and sites of origin of cutaneous melanoma: a meta-analysis. Br J Dermatol. 2011;164(4):776-84.

207. Nakayama N, Nakayama K, Yeasmin S, Ishibashi M, Katagiri A, Iida K, et al. KRAS or BRAF mutation status is a useful predictor of sensitivity to MEK inhibition in ovarian cancer. Br J Cancer. 2008;99(12):2020-8.

208. Chattopadhyay C, El-Naggar AK, Williams MD, Clayman GL. Small molecule c-MET inhibitor PHA665752: effect on cell growth and motility in papillary thyroid carcinoma. Head Neck. 2008;30(8):991-1000.

209. Sierra JR, Tsao MS. c-MET as a potential therapeutic target and biomarker in cancer. Ther Adv Med Oncol. 2011;3(1 Suppl):S21-35.

210. Christensen JG, Schreck R, Burrows J, Kuruganti P, Chan E, Le P, et al. A selective small molecule inhibitor of c-Met kinase inhibits c-Met-dependent phenotypes in vitro and exhibits cytoreductive antitumor activity in vivo. Cancer Res. 2003;63(21):7345-55.

211. Ma PC, Schaefer E, Christensen JG, Salgia R. A selective small molecule c-MET Inhibitor, PHA665752, cooperates with rapamycin. Clin Cancer Res. 2005;11(6):2312-9.

212. Puri N, Khramtsov A, Ahmed S, Nallasura V, Hetzel JT, Jagadeeswaran R, et al. A selective small molecule inhibitor of c-Met, PHA665752, inhibits tumorigenicity and angiogenesis in mouse lung cancer xenografts. Cancer Res. 2007;67(8):3529-34.

213. Tan CC, Yu JT, Tan MS, Jiang T, Zhu XC, Tan L. Autophagy in aging and neurodegenerative diseases: implications for pathogenesis and therapy. Neurobiol Aging. 2014;35(5):941-57.

214. Yao H, Zhao D, Khan SH, Yang L. Role of autophagy in prion protein-induced neurodegenerative diseases. Acta Biochim Biophys Sin (Shanghai). 2013;45(6):494-502.

215. Goold R, McKinnon C, Tabrizi SJ. Prion degradation pathways: Potential for therapeutic intervention. Mol Cell Neurosci. 2015;66(Pt A):12-20.

216. Strohecker AM, White E. Targeting mitochondrial metabolism by inhibiting autophagy in BRAF-driven cancers. Cancer Discov. 2014;4(7):766-72.

217. Jung CH, Ro SH, Cao J, Otto NM, Kim DH. mTOR regulation of autophagy. FEBS Lett. 2010;584(7):1287-95.

218. Takle AK, Brown MJ, Davies S, Dean DK, Francis G, Gaiba A, et al. The identification of potent and selective imidazole-based inhibitors of B-Raf kinase. Bioorg Med Chem Lett. 2006;16(2):378-81.

219. Heiseke A, Aguib Y, Riemer C, Baier M, Schatzl HM. Lithium induces clearance of protease resistant prion protein in prion-infected cells by induction of autophagy. J Neurochem. 2009;109(1):25-34.

220. Sigma. 2018 [Available from: https://www.sigmaaldrich.com/catalog/product/sigma/pz0147?lang=de&region=DE.

221. Carpenter TS, Kirshner DA, Lau EY, Wong SE, Nilmeier JP, Lightstone FC. A method to predict blood-brain barrier permeability of drug-like compounds using molecular dynamics simulations. Biophys J. 2014;107(3):630-41.

222. Jensen EM, LaPolla RJ, Kirby PE, Haworth SR. In vitro studies of chemical mutagens and carcinogens. I. Stability studies in cell culture medium. J Natl Cancer Inst. 1977;59(3):941-4.

223. Kern M, Fridrich D, Reichert J, Skrbek S, Nussher A, Hofem S, et al. Limited stability in cell culture medium and hydrogen peroxide formation affect the growth inhibitory properties of delphinidin and its degradation product gallic acid. Mol Nutr Food Res. 2007;51(9):1163-72.

224. Misko TP, Highkin MK, Veenhuizen AW, Manning PT, Stern MK, Currie MG, et al. Characterization of the cytoprotective action of peroxynitrite decomposition catalysts. J Biol Chem. 1998;273(25):15646-53.

225. Imam SZ, Newport GD, Itzhak Y, Cadet JL, Islam F, Slikker W, Jr., et al. Peroxynitrite plays a role in methamphetamine-induced dopaminergic neurotoxicity: evidence from mice lacking neuronal nitric oxide synthase gene or overexpressing copper-zinc superoxide dismutase. J Neurochem. 2001;76(3):745-9.

226. Guentchev M, Voigtlander T, Haberler C, Groschup MH, Budka H. Evidence for oxidative stress in experimental prion disease. Neurobiol Dis. 2000;7(4):270-3.

227. Radi R, Beckman JS, Bush KM, Freeman BA. Peroxynitrite-induced membrane lipid peroxidation: the cytotoxic potential of superoxide and nitric oxide. Arch Biochem Biophys. 1991;288(2):481-7.

228. Douki T, Cadet J, Ames BN. An adduct between peroxynitrite and 2'-deoxyguanosine: 4,5-dihydro-5-hydroxy-4-(nitrosooxy)-2'-deoxyguanosine. Chem Res Toxicol. 1996;9(1):3-7.

229. Radi R, Rodriguez M, Castro L, Telleri R. Inhibition of mitochondrial electron transport by peroxynitrite. Arch Biochem Biophys. 1994;308(1):89-95.

230. Salgo MG, Bermudez E, Squadrito GL, Pryor WA. Peroxynitrite causes DNA damage and oxidation of thiols in rat thymocytes [corrected]. Arch Biochem Biophys. 1995;322(2):500-5.

231. Beckman JS, Carson M, Smith CD, Koppenol WH. ALS, SOD and peroxynitrite. Nature. 1993;364(6438):584.

232. Good PF, Werner P, Hsu A, Olanow CW, Perl DP. Evidence of neuronal oxidative damage in Alzheimer's disease. Am J Pathol. 1996;149(1):21-8.

233. Bagasra O, Michaels FH, Zheng YM, Bobroski LE, Spitsin SV, Fu ZF, et al. Activation of the inducible form of nitric oxide synthase in the brains of patients with multiple sclerosis. Proc Natl Acad Sci U S A. 1995;92(26):12041-5.

234. Kaur H, Halliwell B. Evidence for nitric oxide-mediated oxidative damage in chronic inflammation. Nitrotyrosine in serum and synovial fluid from rheumatoid patients. FEBS Lett. 1994;350(1):9-12.

235. Gupta AN, Neupane K, Rezajooei N, Cortez LM, Sim VL, Woodside MT. Pharmacological chaperone reshapes the energy landscape for folding and aggregation of the prion protein. Nat Commun. 2016;7:12058.

236. Zhou M, Xu SL, Chen B. [Dual effects of different concentrations of alpha-synuclein on the neurotoxicity of 6-hydroxydopamine in SH-SY5Y cells]. Sheng Li Xue Bao. 2009;61(4):324-30.

237. Chueh SC, Guh JH, Chen J, Lai MK, Teng CM. Dual effects of ouabain on the regulation of proliferation and apoptosis in human prostatic smooth muscle cells. J Urol. 2001;166(1):347-53.

238. Iwakami S, Misu H, Takeda T, Sugimori M, Matsugo S, Kaneko S, et al. Concentration-dependent dual effects of hydrogen peroxide on insulin signal transduction in H4IIEC hepatocytes. PLoS One. 2011;6(11):e27401.

239. Calik P, Bilir E, Ozcelik IS, Calik G, Ozdamar TH. Inorganic compounds have dual effect on recombinant protein production: influence of anions and cations on serine alkaline protease production. J Appl Microbiol. 2004;96(1):194-200.

240. Charalambous M, Da Rocha ST, Radford EJ, Medina-Gomez G, Curran S, Pinnock SB, et al. DLK1/PREF1 regulates nutrient metabolism and protects from steatosis. Proc Natl Acad Sci U S A. 2014;111(45):16088-93.

241. Oliveira LT, Matos PA, Provance DW, Jr., de Mello FG, Andrade LR, Sorenson MM, et al. beta-Amyloid peptide is internalized into chick retinal neurons and alters the distribution of myosin Vb. Cytoskeleton (Hoboken). 2012;69(3):166-78.

242. Kamboh MI, Minster RL, Kenney M, Ozturk A, Desai PP, Kammerer CM, et al. Alpha-1-antichymotrypsin (ACT or SERPINA3) polymorphism may affect age-at-onset and disease duration of Alzheimer's disease. Neurobiol Aging. 2006;27(10):1435-9.

243. Lannan EA, Galliher-Beckley AJ, Scoltock AB, Cidlowski JA. Proinflammatory actions of glucocorticoids: glucocorticoids and TNFalpha coregulate gene expression in vitro and in vivo. Endocrinology. 2012;153(8):3701-12.

244. Wood AM, Stockley RA. The genetics of chronic obstructive pulmonary disease. Respir Res. 2006;7:130.

245. Vanni S, Moda F, Zattoni M, Bistaffa E, De Cecco E, Rossi M, et al. Differential overexpression of SERPINA3 in human prion diseases. Sci Rep. 2017;7(1):15637.

246. Soto C, Satani N. The intricate mechanisms of neurodegeneration in prion diseases. Trends Mol Med. 2011;17(1):14-24.

247. Syed M, Nourizadeh-Lillabadi R, Press CM, Alestrom P. Prion protein function and the disturbance of early embryonic development in zebrafish. Prion. 2011;5(2):88-92.

248. Stys PK, You H, Zamponi GW. Copper-dependent regulation of NMDA receptors by cellular prion protein: implications for neurodegenerative disorders. J Physiol. 2012;590(6):1357-68.

249. McBain CJ, Mayer ML. N-methyl-D-aspartic acid receptor structure and function. Physiol Rev. 1994;74(3):723-60.

250. Paoletti P, Bellone C, Zhou Q. NMDA receptor subunit diversity: impact on receptor properties, synaptic plasticity and disease. Nat Rev Neurosci. 2013;14(6):383-400.

251. Hardingham GE, Bading H. Synaptic versus extrasynaptic NMDA receptor signalling: implications for neurodegenerative disorders. Nat Rev Neurosci. 2010;11(10):682-96.

252. Ratte S, Vreugdenhil M, Boult JK, Patel A, Asante EA, Collinge J, et al. Threshold for epileptiform activity is elevated in prion knockout mice. Neuroscience. 2011;179:56-61.

253. Muller WE, Ushijima H, Schroder HC, Forrest JM, Schatton WF, Rytik PG, et al. Cytoprotective effect of NMDA receptor antagonists on prion protein (PrionSc)-induced toxicity in rat cortical cell cultures. Eur J Pharmacol. 1993;246(3):261-7.

254. Biasini E, Turnbaugh JA, Unterberger U, Harris DA. Prion protein at the crossroads of physiology and disease. Trends Neurosci. 2012;35(2):92-103.

255. Khosravani H, Zhang Y, Tsutsui S, Hameed S, Altier C, Hamid J, et al. Prion protein attenuates excitotoxicity by inhibiting NMDA receptors. J Gen Physiol. 2008;131(6):i5.

256. Rangel A, Burgaya F, Gavin R, Soriano E, Aguzzi A, Del Rio JA. Enhanced susceptibility of Prnp-deficient mice to kainate-induced seizures, neuronal apoptosis, and death: Role of AMPA/kainate receptors. J Neurosci Res. 2007;85(12):2741-55.

257. Maglio LE, Perez MF, Martins VR, Brentani RR, Ramirez OA. Hippocampal synaptic plasticity in mice devoid of cellular prion protein. Brain Res Mol Brain Res. 2004;131(1-2):58-64.

258. Black SA, Stys PK, Zamponi GW, Tsutsui S. Cellular prion protein and NMDA receptor modulation: protecting against excitotoxicity. Front Cell Dev Biol. 2014;2:45.

Abbreviations

µ	micro (10^{-6})
µl	microliter
AD	Alzheimer's disease
BH	brain homogenate
bp	base pare
BSA	bovine serum albumin
BSE	bovine spongiform encephalopathy
c	concentration
°C	degree Celsius
cDNA	complementary deoxyribonucleic acid
CJD	Creutzfeldt-Jakob disease
CNS	central nervous system
COCS	cerebellar organotypic cultures
C-terminal	carboxy terminal
Cu	copper
CWD	chronic wasting disease
d	day
DEG	differential expressed genes
dest.	destilled
DMEM	Dulbecco´s modified Eagle Medium
DMSO	dimethyl sulfoxide
DNA	deoxyribonucleic acid
DNase	desoxyribonuclease
DOC	sodium deoxycholate
dsDNA	double strand DNA
e.g.	for example ("*exempla gratia"*)
E. coli	*Escherichia coli*
EDTA	ethylenediaminetetraacetic acid disodium salt
ER	endoplasmatic reticulum
et al.	and others ("*et alii*")
fCJD	familiar Creutzfeldt-Jakob disease
FFI	fatale familial insomnia

g	gram; acceleration of gravity
GdnHCl	guanidine hydrochloride
GFP	green fluorescent protein
GPI	glycosyl-phosphatidyl-inositol
GSS	Gerstmann-Sträußler-Scheinker syndrome
h	hour(s)
HEPES	4-(2-Hydroxyethyl)piperazine-1-ethanesulfonic acid
HGF	Hepatocyte growth factor
$H_2O_{dest.}$	destilled water
HRP	horseradish peroxidase
IC_{50}	half maximal inhibitory concentration
iCJD	iatrogenic Creutzfeldt-Jakob disease
IF	immunofluorescence
IgG	immunoglobulin G
kb	kilo base pairs
kDa	kilodalton
l	liter
m	milli
M	molar
mAb	monoclonal antibody
min	minute
ml	milliliter
MOPS	3-(N-morpholino)propanesulfonic acid
mRNA	messenger RNA
n	nano
NaCl	sodium chloride
NaN_3	sodium azide
NaOH	sodium hydroxide
N-terminal	amino terminal
ORF	open reading frame
PAGE	polyacrylamide gel electrophoresis
pAb	polyclonal antibody
PBS	phosphate buffered saline
PFA	paraformaldehyde

p.i.	post infection
PMCA	protein misfolding cyclic amplification
PK	proteinase K
POSCA	prion organotypic slice culture assay
PrP	prion protein
Prnp$^{-/-}$	PrP knock-out
PrP^{C}	cellular non-pathogenic form of the prion protein
PrP^{Sc}	pathogenic isoform of the prion protein
PVDF	polyvinylidene difluoride
RNA	ribonucleic acid
RNase	ribonuclease
RT	room temperature
sCJD	sporadic Creutzfeldt-Jakob disease
SDS	sodium dodecyl sulfate
sec	second
SD	standard deviation
SOD1	superoxide dismutase1
t	time
Tris	tris-(hydroxymethyl-)aminomethan
TME	transmissible mink encephalopathy
TSE	transmissible spongiform encephalopathy
U	unit
UTR	untranslated region
UV	ultraviolet
V	Volt
vCJD	variant Creutzfeldt-Jakob disease
W	Watt
WB	western blot
WT	wild type
% (w/v)	weight/volume percentage
% (v/v)	volume/volume percentage

Publications and congress contributions

PUBLIKATIONEN

Alexander Zielinski, Catharina Pleschka, Bernd Hoffmann, Ronald Springer, Rudolf Merkel: Reorientation dynamics and structural interdependencies of actin, microtubules and intermediate filaments upon cyclic stretch application.

Ronald Springer, Alexander Zielinski, Catharina Pleschka, Bernd Hoffmann, Rudolf Merkel: Unbiased pattern analysis reveals highly diverse responses of cytoskeletal systems to cyclic straining. (Submitted)

Andrea Fehlinger, Hanna Wolf, André Hossinger, Yvonne Dürnberger, Catharina Pleschka, Katrin Riemschoss, Shu Liu, Romina Bester, Lydia Paulsen, Suzette Priola, Martin Groschup, Hermann Schätzl, and Ina Vorberg: Prion strains depend on different endocytic routes for productive infection.

Rishibha Sachdev, Karin Kappes-Horn, Lydia Paulsen, Yvonne Duernberger, Catharina Pleschka, Philip Denner, Bishwajit Kundu, Jens Reimannand Ina Vorberg: Endoplasmatic reticulum stress induces myostatin high molecular weight aggregates and impairs mature myostatin secretion.

Llorens F, Thüne K, Tahir W, Kanata E, Diaz-Lucena D, Xanthopoulos K, Kovatsi E, Pleschka C, Garcia-Esparcia P, Schmitz M, Ozbay D, Correia S, Correia Â, Milosevic I, Andréoletti O, Fernández-Borges N, Vorberg IM, Glatzel M, Sklaviadis T, Torres JM, Krasemann S, Sánchez-Valle R, Ferrer I, Zerr I: YKL-40 in the brain and cerebrospinal fluid of neurodegenerative dementia.

POSTER PRESENTATION

11/2016	DZNE PhD Retreat, Bonn, Deutschland
08/2016	Propagation in Neurodegenerative Disease, Dublin, Irland
09/2015	DZNE Retreat, Nürburg, Deutschland
05/2015	Prion2015, Fort Collins, Colorado, USA
10/2013	Cell Mechanics Meeting , Obergurgel

TALKS

05/2015	HAI-NDR Conference, Banff, Alberta, Kanada

Appendix

Table 13. 22L vs. Mock: 250 significant DEGs sorted by log2 fold change in COCS

5 wks			7 wks			9 wks		
Gene name	**log2Fold Change**	**P value**	**Gene name**	**log2Fold Change**	**P value**	**Gene name**	**log2Fold Change**	**P value**
Nos2	-4.99	5.17E-03	Xist	4.76	4.30E-04	Th	-5.38	4.88E-11
Ddn	-3.99	1.98E-04	Sln	-2.97	3.84E-04	Mast1	-4.68	6.53E-03
Il22	-3.52	1.32E-02	Srrm4	-2.88	2.95E-02	Slc8a2	-4.45	1.55E-02
Car9	-3.38	8.82E-08	Gm26917	2.83	7.43E-03	Slc17a7	-4.41	1.64E-16
Ndufa4l2	-2.57	4.34E-05	Mapk13	-2.69	2.81E-02	Tmem178	-4.39	1.92E-02
Fam163b	-2.54	2.67E-02	A330094K24Rik	-2.62	1.15E-02	Synpr	-4.25	1.10E-03
Sln	-1.95	4.98E-03	Otx2os1	-2.43	4.06E-02	Ecel1	-4.25	2.94E-02
Gm15169	-1.95	5.07E-02	Ecel1	-2.41	3.29E-03	Cntnap5b	-4.18	3.64E-02
Samd3	-1.94	4.23E-02	Bcl2l15	-2.13	1.58E-04	Calb2	-4.14	2.19E-14
Pcdh8	-1.92	1.49E-02	Vgf	-2.12	3.90E-03	Vsnl1	-4.13	1.37E-04
Ankrd37	-1.89	5.14E-02	Mybpc3	-2.03	1.50E-04	Mybpc3	-4.02	3.70E-03
Xist	-1.89	5.14E-02	Glra2	-1.92	4.71E-02	Pcp2	-4.00	1.49E-17
Lars2	1.88	7.51E-37	Slc5a1	-1.85	8.33E-04	Grm4	-3.93	5.53E-03
Klc3	1.87	4.06E-02	Doc2g	-1.85	4.07E-02	Fat2	-3.84	2.54E-06
Fndc1	-1.79	1.70E-02	4833427G06Rik	-1.83	2.97E-02	Slco1c1	-3.74	1.68E-03
Dlk1	1.77	1.10E-09	Grm2	-1.81	1.80E-02	Aqp1	-3.67	2.46E-03
Xkr7	-1.73	4.79E-02	Car4	-1.80	2.53E-04	Slc1a6	-3.61	1.46E-12
Abcc8	-1.73	7.08E-03	Caly	-1.78	1.08E-02	Snap25	-3.59	7.11E-25
Prss35	-1.72	5.74E-05	Nrn1	-1.77	3.81E-06	Sycp1	-3.47	6.29E-03
Fam19a2	-1.64	1.88E-02	Serinc2	-1.75	4.87E-04	Ppp1r17	-3.45	1.00E-04
Car4	-1.62	1.30E-04	Slc16a11	-1.73	1.65E-02	Dlk1	-3.45	9.59E-10
Eomes	-1.61	1.11E-03	Nell1	-1.73	1.31E-04	Rasgef1a	-3.44	4.26E-04
Colq	-1.60	4.74E-02	Krt8	-1.73	2.14E-03	Stmn2	-3.40	4.03E-07
Miat	-1.60	4.74E-02	Gm10800	1.72	1.02E-03	Dpp10	-3.39	4.50E-06
Snhg11	-1.59	4.15E-04	Snca	-1.71	3.33E-09	St6galnac2	-3.39	2.29E-03
Trhde	-1.57	1.34E-02	Sstr3	-1.71	2.92E-02	Asb10	-3.39	3.92E-02
Cntnap5b	-1.50	5.54E-03	Kcnk10	-1.69	4.33E-02	Nrn1	-3.39	3.92E-02
Trank1	-1.50	3.81E-05	Grin2c	-1.69	1.53E-06	Pld5	-3.39	3.92E-02
Camk2a	-1.50	7.37E-07	AI118078	-1.65	9.36E-05	Gabra6	-3.36	6.22E-06
Wdr86	1.50	3.10E-02	Sowahb	-1.64	1.94E-02	Serinc2	-3.30	1.32E-02
Nuak2	1.48	2.45E-02	Sv2c	-1.61	8.29E-05	Rbfox3	-3.29	4.36E-06
Moxd1	1.46	5.04E-03	Pcp2	-1.60	1.36E-10	Cbln1	-3.25	4.68E-03
Elfn2	-1.45	4.85E-02	Hes3	-1.60	6.41E-03	Ttr	-3.24	2.26E-44
Saa3	1.44	3.40E-02	Mast1	-1.59	1.73E-02	Clstn3	-3.24	2.45E-10
Stra6	1.44	1.01E-03	Kcnk3	-1.58	1.50E-04	Gabrd	-3.21	2.19E-04
Prr32	1.44	5.68E-03	Sidt1	-1.58	4.47E-02	Gng13	-3.20	2.56E-08
Sycp1	-1.39	6.35E-03	Th	-1.58	8.40E-05	Car12	-3.20	4.85E-06
Th	-1.39	3.17E-03	Vsnl1	-1.58	4.14E-11	Nptx1	-3.14	7.94E-03
Myo5b	1.36	4.16E-02	Mir124a-1hg	-1.57	4.16E-04	Clec2l	-3.13	1.09E-03
Sfrp4	1.35	3.99E-02	Barhl2	-1.56	6.41E-03	Rph3a	-3.11	1.22E-05
Pnmal1	-1.33	1.36E-03	Nhlh2	-1.56	3.81E-02	Sv2b	-3.10	3.43E-03
Neb	-1.29	4.05E-02	Tmem51	-1.55	6.19E-03	D11Wsu47e	-3.10	2.72E-02
Plcxd2	-1.28	1.39E-02	Tll1	-1.54	2.31E-02	Car8	-3.09	5.00E-20
Vegfa	-1.27	7.23E-09	Kcnip4	-1.54	1.66E-02	Prkcg	-3.09	2.95E-07
Meg3	-1.26	8.81E-05	Abcc8	-1.54	1.49E-02	Camk2b	-3.05	1.13E-10
Dgkg	-1.26	2.14E-04	Cbln3	-1.53	2.55E-17	Folr1	-3.00	3.90E-06
Cntn6	-1.26	1.68E-02	Atp2a3	-1.53	5.23E-07	Pcp4	-2.95	9.78E-07
A330050F15Rik	-1.25	6.98E-03	Crhr1	-1.52	4.55E-03	Dnm1	-2.94	1.09E-13
Exph5	-1.25	9.99E-04	Neb	-1.52	2.22E-02	Sncb	-2.93	1.29E-06
Necab1	-1.23	2.17E-03	Meg3	-1.52	1.29E-07	Tmem63c	-2.93	4.64E-02
Cacna1e	-1.23	7.66E-05	Itpka	-1.51	1.07E-03	Mfrp	-2.90	3.17E-08
Kcnip4	-1.23	5.19E-02	Rps6kl1	-1.50	1.64E-02	L1cam	-2.90	4.10E-03
Vsnl1	-1.21	4.34E-09	Diras2	-1.48	1.82E-12	Npr3	-2.88	2.24E-02
Gm13111	1.20	3.45E-02	Npas4	-1.48	8.57E-03	Sphkap	-2.84	5.67E-03
Kif2c	1.20	5.42E-02	Clec2l	-1.47	2.67E-06	Sptbn4	-2.84	2.65E-02
Slc6a5	-1.19	7.16E-03	Kcnj9	-1.47	4.03E-06	Mpp3	-2.83	7.17E-04
Rims1	-1.18	1.97E-05	Arhgdig	-1.47	3.68E-02	Sptbn2	-2.80	9.44E-15
Cdk1	1.18	1.11E-03	Gabra6	-1.45	5.84E-12	Grin1	-2.79	3.91E-05
Itpr1	-1.18	4.66E-16	Dpp10	-1.45	1.91E-07	Atp1a3	-2.79	2.14E-20
Cabp7	-1.17	3.64E-05	Syt13	-1.45	1.08E-06	Dlgap3	-2.78	1.55E-02

Rasgef1a	-1.17	5.61E-04	Cntn6	-1.45	1.16E-02	Clic6	-2.77	8.88E-06
Gabra6	-1.16	7.41E-10	Snhg11	-1.43	3.78E-04	Rap1gap2	-2.77	7.82E-03
Gabra3	-1.16	4.27E-02	Sycp1	-1.43	3.49E-03	Slc12a5	-2.74	1.56E-07
Ntsr2	-1.15	5.05E-05	Fhad1	-1.43	1.02E-04	Snca	-2.74	3.90E-04
AI118078	-1.14	4.41E-03	Snap25	-1.43	1.21E-17	Cpne9	-2.71	1.53E-03
Camk4	-1.13	2.83E-10	Ramp3	-1.42	5.16E-03	Cacna1i	-2.68	4.38E-02
Barhl2	-1.12	1.73E-02	Sptbn4	-1.42	7.33E-04	Galnt9	-2.65	2.52E-02
Ralyl	-1.12	1.73E-02	Rltpr	-1.41	5.29E-03	Slc4a10	-2.65	5.18E-10
Mfrp	1.12	1.30E-02	Ppp1r17	-1.41	4.33E-10	Frmpd4	-2.63	5.16E-02
Kl	1.12	6.83E-07	Fxyd6	-1.39	2.29E-07	Slc29a4	-2.59	3.24E-03
Gpc5	-1.11	4.35E-02	Ryr1	-1.39	3.93E-02	Ckmt1	-2.58	1.25E-03
Fhad1	1.11	2.06E-02	Cntnap4	-1.38	1.62E-04	Camk4	-2.55	2.01E-02
Krt18	1.10	2.39E-03	Atp10b	1.37	4.77E-02	Strip2	-2.55	2.58E-05
Col8a1	1.10	1.44E-06	Rgs8	-1.36	8.68E-11	Gabra1	-2.54	1.66E-03
Car12	1.10	2.63E-06	Kif26b	-1.36	1.35E-03	Atp2a3	-2.51	8.31E-03
Folr1	1.09	2.12E-04	Pnck	-1.36	4.49E-02	Otx2	-2.51	4.05E-02
Scn2a1	-1.09	4.25E-07	Rec8	-1.35	2.66E-02	Syt1	-2.49	3.57E-03
Snhg14	-1.09	2.08E-03	Crtam	-1.35	1.22E-04	Oca2	-2.48	1.61E-02
Ttr	1.08	3.25E-15	Slc35f3	-1.34	3.47E-02	Dgkg	-2.48	1.00E-03
Kcnk3	-1.08	2.76E-03	Olfm3	-1.34	2.37E-06	Nell1	-2.47	2.74E-02
Col8a2	1.08	1.31E-04	Kcnj12	-1.32	1.21E-03	Eps8l2	-2.46	6.74E-03
Grin1	-1.08	1.81E-04	Calb2	-1.32	5.82E-09	Spint2	-2.43	1.88E-04
Loxl1	1.08	2.34E-02	Plch2	-1.32	5.59E-04	Sez6l	-2.43	6.08E-04
Serpinb1b	1.07	4.01E-02	Neurl1a	-1.32	7.66E-04	Cacna1g	-2.42	6.93E-05
Cbln3	-1.07	5.28E-12	Oprl1	-1.32	5.46E-02	Celf4	-2.40	9.00E-03
Nptx1	-1.07	2.77E-09	Stmn2	-1.31	8.57E-11	Shf	-2.39	2.76E-03
Adcy1	-1.07	7.20E-12	Cplx1	-1.31	2.65E-09	Rims1	-2.39	3.71E-02
Trpv4	1.06	2.22E-02	Nefh	-1.30	4.12E-03	Itpr1	-2.36	1.56E-20
Cldn2	1.05	3.94E-04	Slc17a7	-1.29	3.80E-10	Napb	-2.35	1.63E-03
Ank1	-1.05	5.23E-06	Cadps2	-1.29	9.08E-08	Krt18	-2.34	2.59E-03
Myt1	-1.05	1.20E-03	Kcnip1	-1.29	1.13E-03	Prmt8	-2.31	2.13E-03
Nell1	-1.04	1.81E-02	Grm4	-1.28	1.30E-05	Adcy1	-2.29	1.75E-03
Grin2a	-1.04	1.56E-02	Tmem200b	-1.28	5.00E-02	Cyb561	-2.28	1.59E-02
Wscd2	-1.04	4.36E-05	Pifo	-1.28	1.37E-02	Trpc3	-2.25	1.82E-02
Rtn4r	-1.04	2.25E-02	Rasgef1a	-1.28	1.93E-04	Kcnip1	-2.25	2.65E-02
Tiam1	-1.03	2.29E-05	Fgf14	-1.28	3.46E-03	Kl	-2.25	2.65E-02
Slc17a7	-1.03	1.41E-08	Cbln1	-1.27	2.96E-10	Kalrn	-2.22	2.10E-02
Galnt13	-1.03	1.56E-03	Pxylp1	-1.27	3.80E-03	Rian	-2.19	4.65E-03
Celsr3	-1.02	5.06E-03	Trank1	-1.27	8.35E-05	Slc6a15	-2.18	3.51E-02
Grin2c	-1.02	1.06E-03	Cgn	-1.27	4.11E-02	Pde5a	-2.17	5.19E-02
Olfm3	-1.02	1.94E-05	Tmem130	-1.26	1.17E-03	Plekhd1	-2.17	5.19E-02
Car8	-1.02	3.12E-11	Rtn4r	-1.26	3.19E-02	Tacc2	-2.15	4.29E-03
Fgf14	-1.02	1.11E-02	Shf	-1.26	9.71E-06	Slc4a5	-2.13	8.69E-05
Calb2	-1.02	7.37E-08	Ank1	-1.26	2.35E-07	Baiap2l1	-2.06	5.31E-02
Cfap54	-1.02	2.36E-02	Cacna1e	-1.25	2.06E-05	Ace	-2.06	3.38E-11
Dpp10	-1.01	8.97E-05	Susd4	-1.25	2.51E-04	Car7	-2.05	4.14E-02
Caly	-1.01	4.63E-02	Kcne2	-1.25	2.81E-05	Gad1	-2.04	4.36E-07
Ppfia2	-1.01	3.86E-04	Scn4b	-1.25	3.49E-03	Pcsk2	-2.02	2.81E-03
Cacna1g	-1.01	1.26E-05	Spint2	-1.24	1.39E-05	Dync1i1	-2.01	6.05E-05
Slitrk4	-1.01	1.04E-02	Ttr	-1.24	3.83E-15	Rgs7	-2.00	8.23E-03
Gsg1l	-1.01	4.34E-02	Wscd2	-1.23	3.18E-05	Calb1	-1.97	2.92E-11
Car7	-1.00	3.72E-03	Sostdc1	-1.23	1.18E-04	Emb	-1.93	1.85E-02
Pxylp1	-1.00	1.03E-02	Cxcl1	1.23	2.91E-02	Gm2694	-1.93	3.74E-02
Il16	-1.00	3.49E-03	Emb	-1.23	1.54E-04	Pvalb	-1.93	1.71E-07
Gm2694	-1.00	1.45E-02	Slc8a2	-1.23	1.18E-04	Calml4	-1.91	1.66E-02
Cdh7	-1.00	6.28E-03	Nptx1	-1.22	1.72E-09	Tiam1	-1.89	5.43E-02
Syt1	-1.00	1.44E-08	Gabrd	-1.22	1.26E-05	Atp2b3	-1.85	1.61E-03
Stxbp5l	-0.99	1.05E-02	Hpca	-1.22	3.68E-03	Cadps2	-1.84	1.78E-03
Zfp385b	-0.99	2.98E-03	Sema5b	-1.22	4.46E-02	Cplx1	-1.82	2.99E-02
Cpne9	-0.99	1.54E-02	Lgi2	-1.22	1.71E-05	Fxyd6	-1.81	3.78E-02
L1cam	-0.99	2.20E-03	Camk2b	-1.22	1.61E-09	Dpp6	-1.80	1.05E-04
Slco1c1	0.98	2.91E-02	Dgkg	-1.22	9.42E-05	Igfbp2	-1.76	1.04E-04
Sptbn2	-0.98	2.26E-08	Gprin3	-1.20	5.28E-02	Rab3a	-1.74	1.69E-04
Kcne2	0.98	3.07E-03	Sncb	-1.20	1.76E-05	Abca4	-1.72	6.64E-03
Firre	-0.97	8.87E-03	Slc6a17	-1.19	2.78E-07	Ank1	-1.70	3.70E-03
Inadl	-0.97	1.83E-05	Pcp4	-1.19	6.35E-08	Met	1.68	2.33E-02
Atp2a3	-0.97	4.87E-04	1110017D15Rik	-1.19	4.12E-02	Chgb	-1.66	4.51E-03
St6galnac2	0.96	2.78E-02	Htr1b	-1.19	2.92E-02	Dner	-1.65	1.68E-05
Fgf9	-0.96	2.66E-02	Rian	-1.17	6.75E-07	Sptb	-1.62	1.10E-02
Lcn2	-0.96	4.63E-04	Sv2b	-1.17	1.37E-07	Mical2	-1.54	3.96E-02

Scn1a	-0.96	2.30E-04	Cdh7	-1.17	4.24E-03	Stxbp1	-1.54	4.48E-06
Snap25	-0.95	5.72E-11	Ckmt1	-1.17	6.31E-05	Arhgef33	-1.54	3.14E-02
Arhgef33	-0.95	3.19E-04	Npr3	-1.17	1.84E-05	Hsd11b1	-1.53	2.50E-02
Ryr2	-0.95	7.09E-04	Cdr1	1.16	9.94E-04	Slc13a4	-1.51	8.57E-03
Sptb	-0.95	2.14E-06	Pde5a	-1.16	2.57E-04	Tmem132a	-1.50	1.57E-02
Ebf1	-0.94	1.11E-03	Cyb561	-1.16	8.31E-06	Pik3c2b	1.47	1.86E-02
Sv2b	-0.94	1.31E-06	Epn3	-1.15	5.96E-03	Eno2	-1.47	1.75E-05
Caln1	-0.94	3.79E-07	Kcnt1	-1.14	1.36E-04	Gabbr2	-1.47	6.77E-03
Kcnt1	-0.93	1.98E-03	Syt1	-1.14	1.42E-08	Snap91	-1.46	8.43E-04
Megf11	-0.93	5.04E-06	Actl6b	-1.13	1.84E-02	Flnc	1.46	3.13E-05
Snca	-0.93	4.02E-04	Dnm1	-1.13	3.04E-09	Zmym6	1.44	5.23E-02
Unc13c	-0.92	5.24E-04	Itpr1	-1.13	3.24E-12	Olfm1	-1.43	2.46E-04
Fat2	-0.92	2.05E-07	L1cam	-1.12	1.76E-03	Gpx3	-1.40	2.99E-08
Cntnap2	-0.91	6.13E-03	Pcsk2	-1.12	9.21E-05	Cds1	-1.40	3.90E-02
Iqsec3	-0.91	1.03E-02	St6galnac2	-1.12	2.62E-03	Pfkp	-1.39	2.92E-05
Cacnb2	-0.91	3.49E-02	Tc2n	-1.12	6.53E-03	Rnf112	-1.38	4.28E-02
Diras2	-0.91	4.04E-07	Jph4	-1.12	5.43E-05	Sh3gl2	-1.36	5.86E-03
Cnksr2	-0.91	1.29E-03	Mfrp	-1.12	4.27E-03	Enpp2	-1.36	2.69E-10
Cbln1	-0.90	1.37E-07	Eps8l2	-1.12	1.87E-02	Elmod1	-1.35	1.45E-02
Tmem178	-0.90	1.86E-04	Tenm1	-1.11	2.81E-04	Nfat5	1.35	1.34E-02
Susd4	-0.90	2.76E-03	Nos1	-1.11	1.01E-06	Nrep	-1.34	3.87E-03
Slc16a3	-0.90	1.43E-02	Atp1a3	-1.11	6.10E-10	Ndrg4	-1.32	8.81E-06
Kcnj12	-0.89	1.36E-02	Kcnd2	-1.11	3.72E-06	Cadm3	-1.32	9.60E-04
Tenm1	-0.89	5.90E-03	Caln1	-1.11	6.32E-08	Podxl2	-1.29	7.25E-03
Stac2	-0.89	2.04E-02	Cntnap2	-1.11	1.66E-03	Lbp	-1.28	1.10E-02
Tmem72	0.89	1.46E-03	Unc13c	-1.10	1.83E-04	Rap1gap	-1.28	4.52E-02
Rbfox1	-0.89	2.41E-04	Capsl	-1.10	1.59E-02	Tbc1d9	-1.27	1.18E-03
Tmem63c	-0.89	2.05E-02	Igfbp2	-1.10	1.43E-07	Cbl	1.26	9.47E-03
Tenm2	-0.89	3.46E-02	Sptbn2	-1.10	4.76E-09	Nbeal1	1.26	1.09E-02
Pdzd2	0.89	1.31E-02	Folr1	-1.10	8.35E-05	Kmt2a	1.22	1.29E-02
Rap1gap2	-0.88	1.90E-04	Rims1	-1.10	3.90E-04	Pde9a	-1.22	1.72E-02
Pld5	-0.88	7.28E-03	Synpr	-1.09	1.13E-05	Crmp1	-1.21	2.46E-02
Sacs	-0.88	1.12E-03	Col8a2	-1.09	2.40E-05	Glb1l2	-1.19	5.21E-02
Cacna2d1	-0.88	5.57E-03	Rbfox3	-1.09	7.42E-06	Syp	-1.18	6.49E-03
Dnm1	-0.88	9.27E-08	Tmem63c	-1.09	1.01E-02	Stmn3	-1.16	2.21E-03
Perp	0.88	2.10E-02	Dpp6	-1.09	3.87E-07	Inadl	-1.14	1.61E-02
Tmem132c	-0.88	4.80E-02	Gng13	-1.09	2.18E-04	Fbln1	-1.12	2.59E-02
Msx1	0.87	5.29E-02	Grin1	-1.09	9.03E-04	Apc	1.12	2.89E-03
Camk2b	-0.87	6.45E-07	Cacna1i	-1.09	9.62E-04	Igfbp4	-1.10	1.57E-02
Shank1	-0.86	6.19E-03	Tmem132c	-1.09	2.61E-02	Micu3	-1.10	4.94E-02
Ckap2	0.86	3.12E-03	Penk	-1.08	2.92E-03	Klc2	-1.08	2.44E-02
Clic6	0.86	6.59E-06	Rab3c	-1.08	7.27E-06	Lrp8	1.07	3.10E-02
Sphkap	-0.86	6.19E-07	Kcnh1	-1.08	2.63E-02	Abi3bp	1.06	1.88E-02
Chgb	-0.86	4.82E-07	Epha8	-1.07	2.11E-02	Slc24a2	1.06	1.94E-02
Ablim3	-0.86	1.04E-02	Ptpru	-1.07	2.64E-02	Sema3b	-1.06	4.48E-03
Gabrd	-0.85	7.54E-04	Oca2	-1.07	5.08E-02	Enpp6	1.04	4.50E-02
Slc8a2	-0.85	2.71E-03	Grin2a	-1.07	1.27E-02	Rbp1	-1.03	3.35E-03
Pcnxl2	-0.85	5.40E-02	Prkcg	-1.07	2.84E-05	Plec	1.03	4.24E-03
D430041D05Rik	-0.84	3.56E-04	Car8	-1.06	4.22E-10	Tnrc6b	1.01	5.35E-02
Nrn1	-0.84	1.69E-02	Ccdc153	-1.06	6.06E-03	Prkar1b	-1.00	4.43E-02
Gprin1	-0.84	1.71E-03	Rims4	-1.06	1.56E-04	Postn	-0.99	4.87E-03
Rims3	-0.84	1.04E-04	Napb	-1.06	4.12E-08	Chn2	-0.97	4.72E-03
Slc6a15	-0.84	1.78E-03	Krt18	-1.06	6.49E-04	Dst_1	0.96	4.98E-05
Slc12a5	-0.84	1.31E-06	Tmem145	-1.05	3.50E-02	Mast4	0.96	3.40E-02
Kif26b	-0.84	2.57E-02	Pdzd2	-1.05	7.43E-04	Ptgds	-0.96	1.65E-05
Slc4a5	0.84	1.27E-03	Mpp3	-1.04	1.17E-04	Fam63b	0.95	1.37E-02
Rgs6	-0.84	2.00E-02	Scn1a	-1.04	1.56E-04	Heg1	0.95	2.44E-02
Neurl1a	-0.84	1.44E-02	Nefm	-1.04	1.93E-03	Zranb1	-0.94	3.53E-02
Grm4	-0.83	1.00E-03	Sphkap	-1.04	5.00E-08	Nsg1	-0.93	1.07E-02
Cnnm1	-0.83	3.02E-03	Exph5	-1.03	9.17E-03	Vat1l	-0.93	4.86E-02
Trpc3	-0.83	5.48E-03	Slc6a5	-1.03	4.06E-02	Arhgap32	0.93	3.09E-02
Dpf1	-0.82	3.41E-02	Gap43	-1.03	5.92E-05	Reln	-0.92	3.40E-02
Kcnma1	-0.82	7.60E-03	Abca4	-1.03	3.34E-03	Taok1	0.92	1.77E-02
Pgm2l1	-0.82	1.42E-04	Tub	-1.03	4.32E-04	Epb4.1l3	-0.91	4.18E-02
Gabrb2	-0.82	3.88E-04	Srrm3	-1.03	4.06E-02	Sox6	0.91	4.03E-02
Reln	-0.81	1.36E-04	Dusp5	-1.02	3.73E-03	Dennd4c	0.90	3.71E-02
Kcnj9	-0.81	4.13E-03	Syt7	-1.02	4.13E-06	Eef1a2	-0.90	6.22E-03
Syt2	-0.81	4.39E-05	Car12	-1.02	3.45E-06	Fam120c	0.90	3.55E-02
Gria2	-0.81	1.78E-05	Trpv4	-1.02	7.98E-03	Abca1	0.90	5.03E-04
Panx2	-0.81	3.49E-02	Tiam1	-1.02	2.64E-04	Ccl6	-0.89	1.46E-02

Mybpc3	-0.80	4.97E-02	Dnah6	-1.02	7.14E-03	Got1	-0.89	1.81E-02
Grm1	-0.80	1.55E-04	Aqp1	-1.02	1.87E-05	Arsg	-0.88	4.94E-02
Galnt9	-0.80	2.00E-02	Slc9a5	-1.02	3.55E-02	Ralgps1	0.88	5.42E-02
Kcnd2	-0.79	1.31E-04	Camk2a	-1.02	3.77E-03	Itih3	-0.87	3.91E-03
Abca4	0.79	5.25E-02	Slc29a4	-1.01	3.19E-03	Ptpn4	0.87	2.42E-02
Syt7	-0.79	1.58E-04	Sptb	-1.01	5.92E-06	Tgfbi	0.87	1.73E-02
Lgi2	-0.79	1.40E-03	Ifitm10	-1.01	3.56E-02	Gdf10	-0.86	8.10E-03
Cacna1b	-0.79	2.12E-02	Slitrk4	-1.01	1.51E-02	Tnks	0.86	8.72E-03
Mpp3	-0.79	8.42E-04	Sez6l	-1.01	4.61E-05	Snrpn	-0.85	1.69E-03
Cacna1i	-0.79	7.25E-03	Iqsec3	-1.01	4.23E-03	Dip2b	0.84	3.42E-03
St8sia5	-0.79	5.10E-03	Celf3	-1.00	4.09E-02	Nkain4	-0.84	1.95E-02
Bzrap1	-0.79	7.98E-03	Rbfox1	-1.00	2.63E-04	Tacc1	0.82	1.83E-02
Cadm3	-0.79	6.96E-07	Mtus2	-1.00	8.85E-04	Acap2	0.82	5.66E-03
Cacna1c	-0.79	1.18E-02	Fbxl12	-1.00	3.26E-02	Pitpnm1	-0.81	2.60E-02
Crtam	-0.78	8.55E-03	Galnt9	-0.99	1.11E-02	Nf1	0.81	5.86E-03
Cntnap1	-0.78	6.67E-04	Wdr86	-0.99	5.44E-02	Iqgap2	0.81	2.33E-02
Dab1	-0.78	7.08E-03	Tuft1	-0.99	1.31E-02	Kat6a	0.81	2.12E-02
Doc2b	-0.78	1.54E-02	Slc4a10	-0.98	1.58E-07	Chd6	0.80	4.81E-02
Golga7b	-0.78	2.04E-02	Adcy1	-0.98	1.39E-08	Vps13d	0.79	7.65E-03
Ksr2	-0.78	1.87E-02	Gabrb2	-0.98	9.52E-05	Adgrg6	0.79	1.51E-02
Dpp6	-0.77	2.20E-05	Golga7b	-0.98	7.45E-03	Sned1	0.78	3.17E-03
Cdh18	-0.77	2.71E-02	Prr32	-0.98	2.32E-02	Ildr2	0.78	5.40E-02
Sez6l	-0.77	7.90E-04	Cnnm1	-0.98	1.52E-03	Macf1	0.78	1.31E-03
Kcnab2	-0.77	3.10E-03	Otx2	-0.97	2.07E-04	Sep_05	-0.78	1.18E-02
Fry	-0.77	7.85E-04	Scd3	-0.97	3.75E-02	Bptf	0.78	3.38E-02
Chn2	-0.77	1.27E-04	Rapgef4	-0.97	7.61E-05	Atp5g1	-0.77	5.25E-02
Sptbn4	-0.76	4.72E-02	Dlk1	-0.97	4.89E-05	Hipk2	0.76	5.15E-02
Slc1a6	-0.76	1.68E-04	Scrt1	-0.97	1.22E-02	Utrn	0.76	5.79E-03
Gxylt2	0.76	4.40E-02	Clstn3	-0.97	2.35E-06	Birc6	0.74	1.64E-02
Cntn4	-0.76	3.55E-02	Elmod1	-0.97	5.53E-06	S100a6	0.71	1.44E-02
Syne1	-0.76	3.34E-04	Camk4	-0.97	9.88E-07	Pamr1	0.71	2.95E-02
Plekhd1	-0.76	1.90E-02	Trpc3	-0.97	1.50E-03	Pik3r1	0.71	8.03E-03
Napb	-0.76	8.67E-06	Stxbp1	-0.96	9.78E-08	Ank3	0.71	4.08E-02
Syt13	-0.75	1.74E-03	Slitrk1	-0.96	8.43E-03	Tmem59l	-0.70	4.54E-02
Cadps2	-0.75	6.03E-04	Rap1gap	-0.96	1.07E-03	Rock2	0.70	2.12E-02
Syp	-0.75	8.09E-05	Fam110b	-0.96	1.23E-02	Wdfy3	0.70	1.74E-02
Arfgef3	-0.74	1.26E-02	Rap1gap2	-0.95	2.76E-04	Hprt	-0.69	3.19E-02
Mctp1	-0.74	1.71E-02	Dpysl4	-0.95	1.62E-02	Gucy1a3	0.69	2.50E-02
Chga	-0.74	1.86E-02	Mmp24	-0.95	1.10E-04	Cab39l	-0.68	4.35E-02
AI593442	-0.74	3.06E-02	Slc1a6	-0.95	1.91E-05	Prex2	0.66	4.93E-03
Ppp1r17	-0.73	4.00E-04	Map3k9	-0.94	6.22E-03	Notch1	0.66	4.96E-02
Brinp2	-0.73	1.24E-02	Inadl	-0.94	6.14E-05	Serinc5	0.66	2.43E-02
Pde10a	-0.73	4.35E-02	Kcnq2	-0.94	2.18E-03	Usp53	0.65	2.06E-02
Rgs8	-0.73	5.40E-05	Galnt13	-0.94	6.24E-03	Erbb2ip	0.64	5.46E-03
Eml5	-0.73	5.07E-03	Frmpd4	-0.94	1.73E-04	Arhgef12	0.63	8.03E-03
Kcnc1	-0.72	9.86E-05	Cldn2	-0.94	4.41E-04	Mfge8	-0.63	5.20E-02
Bsn	-0.72	2.46E-03	Clic6	-0.94	1.19E-06	Itgb4	0.63	4.34E-02
Nrk	-0.72	4.79E-02	6030419C18Rik	-0.94	2.56E-03	Kif5a	-0.62	5.08E-02
Rgs7	-0.72	1.01E-02	Zfp385b	-0.93	1.69E-02	Tmod2	0.62	1.63E-02
Prkcg	-0.72	7.47E-04	Phyhip	-0.93	2.85E-06	Scn1b	-0.62	3.12E-02

Table 14. RML vs. Mock: 250 significant DEGs sorted by log2 fold change in COCS

5 weeks			7 weeks			9 weeks		
Gene name	**log2 fold change**	**p-value**	**Gene name**	**log2 fold change**	**p-value**	**Gene name**	**log2 fold change**	**p-value**
B230312C02Rik	5.81	3.11E-05	Gm14005	-4.81	1.31E-02	Scand1	4.76	1.06E-14
Gm10800	4.58	1.25E-02	Lrrc71	-4.37	4.54E-02	1810049J17Rik	4.40	2.27E-02
Nrgn	4.13	4.60E-04	Sv2b	4.17	2.70E-04	Gm26917	4.12	2.35E-04
Ddn	3.93	4.45E-07	S100a3	-4.15	9.28E-03	Gm1673	4.06	1.06E-12
Fam163b	3.83	1.20E-02	Xist	-4.04	8.96E-04	Gm14236	3.59	2.62E-02
Nrtn	3.74	7.39E-07	Fbxl15	-3.78	8.35E-03	Nrtn	3.51	2.70E-07
mt-Nd3	3.73	4.21E-13	Snhg18	-3.71	3.60E-02	Gm11681	3.45	3.92E-02
Bpifb6	-3.69	2.47E-02	Tcerg1l	3.68	1.15E-02	Th	3.34	6.10E-06
Iltifb	3.64	5.16E-03	Calca	-3.64	1.35E-02	Ccdc85b	3.19	7.60E-13
Scand1	3.35	1.15E-04	Marc1	-3.61	4.75E-02	Pcsk1n	3.13	7.66E-25
A530053G22Rik	3.26	8.10E-03	Nudt6	-3.36	1.39E-04	Sumo2	3.11	4.61E-03

Tmem200b	3.03	9.05E-03	Tha1	-3.32	3.62E-02	Itpka	3.06	5.84E-03
C1qtnf4	2.96	2.40E-02	Fcna	-3.30	1.78E-02	Nme3	3.02	1.68E-02
Htr1b	2.95	3.72E-03	1700007G11Rik	-3.23	2.24E-02	Cox8b	3.00	4.50E-02
1700026J14Rik	2.86	9.79E-03	Etohi1	-3.23	4.65E-02	Prr7	2.94	3.46E-05
Gpx4	2.86	3.32E-09	Scand1	-3.23	4.65E-02	Fam181b	2.81	2.07E-04
Ppp1r17	2.85	1.08E-07	Th	3.18	1.71E-02	Yjefn3	2.69	8.12E-03
BC089491	2.83	6.56E-03	1810032O08Rik	-3.18	8.19E-03	Vkorc1	2.64	3.78E-08
Stra13	2.78	1.26E-08	Gabrd	3.16	3.81E-03	Gadd45gip1	2.59	4.67E-09
Gadd45gip1	2.78	2.64E-07	Gm14326	-3.15	2.80E-02	Pcp2	2.48	1.26E-05
Sycp1	2.78	8.24E-03	Lmo1	-3.15	2.80E-02	Rnaseh2c	2.44	3.42E-13
Wfdc3	2.72	4.35E-03	BC051226	-2.99	7.15E-03	Rps16	2.39	3.61E-10
Tmem256	2.70	2.08E-08	Chst2	-2.83	1.21E-03	Zfp771	2.36	8.04E-10
BC051226	2.69	1.61E-06	Klk8	-2.83	1.70E-05	Erdr1	2.36	3.19E-02
Batf	2.69	1.16E-02	Slc17a7	2.82	3.11E-04	Tpgs1	2.27	7.64E-13
Cntnap5a	2.69	5.41E-02	Alkbh2	-2.80	2.09E-02	Bola1	2.26	8.50E-08
Pigyl	2.67	5.29E-08	Ifi27l2a	-2.77	2.26E-05	Hist1h4h	2.24	2.64E-03
Fbll1	2.65	2.99E-03	Klc3	-2.77	3.73E-03	1110008P14Rik	2.21	1.06E-07
Dctpp1	2.65	8.77E-08	Tro	2.71	3.50E-02	Drd1	-2.17	4.05E-02
Adcyap1	2.64	3.67E-02	Gpx4	-2.67	2.24E-05	Fadd	2.16	1.03E-02
Mrpl12	2.62	6.43E-08	Pigyl	-2.64	1.68E-03	Gng13	2.14	3.81E-03
Rpl22l1	2.60	8.57E-08	Ppp1r35	-2.64	1.68E-03	Cpne9	2.14	3.60E-02
AW047730	2.59	8.48E-04	2810002D19Rik	-2.64	4.75E-02	Tecrl	-2.12	2.05E-02
Camk2a	2.57	9.29E-06	Siva1	-2.62	9.59E-04	Shisa8	2.12	2.05E-03
Cpne6	2.57	2.89E-02	Ccdc115	-2.62	3.84E-03	Crlf2	2.10	5.09E-08
Vstm2l	2.57	2.89E-02	1500026H17Rik	-2.60	9.40E-03	Slc1a6	2.04	5.06E-05
Nr2f6	2.56	4.76E-06	Grm4	2.58	4.93E-02	Junb	1.98	4.69E-11
Gm26917	2.55	4.72E-02	Nudt11	-2.54	2.69E-02	H2afj	1.96	7.03E-09
Efcab10	2.54	6.83E-05	Sft2d1	-2.53	1.63E-04	Acox2	1.95	4.26E-02
Sft2d1	2.53	3.90E-07	Samd1	-2.52	1.94E-04	Ppp1r17	1.84	1.18E-04
Ly6h	2.51	3.88E-06	1810044D09Rik	-2.49	3.18E-02	1810043H04Rik	1.84	3.88E-06
Tppp3	2.45	2.86E-07	Lin7b	-2.49	5.29E-02	Scrt1	1.82	4.19E-03
Fbxl15	2.42	4.29E-05	Calb2	2.49	5.42E-04	AI849053	1.82	4.46E-02
Gm14322	2.42	1.60E-04	Vps37d	-2.46	1.16E-02	Grm4	1.80	5.65E-03
Ifi27l2a	2.42	7.43E-07	Mrpl12	-2.44	1.33E-04	Bbc3	1.79	1.02E-04
Polr2k	2.41	7.57E-07	Dctpp1	-2.43	3.26E-04	Gm13889	1.79	9.10E-03
1810044D09Rik	2.40	1.63E-05	Fam92b	-2.43	4.84E-02	Nkx6-2	1.77	3.26E-10
1810022K09Rik	2.37	3.37E-06	Fat2	2.42	6.51E-03	Klf2	1.77	2.72E-02
Nkx6-2	2.37	9.91E-07	Csrp2	-2.41	2.37E-03	Rsph10b	1.76	3.92E-02
Gm14005	2.36	1.14E-03	Polr2k	-2.39	1.91E-04	Grcc10	1.74	1.10E-04
Rnaseh2c	2.34	3.44E-06	Crlf2	-2.37	1.48E-03	Rbfox3	1.72	4.17E-04
2410006H16Rik	2.33	2.06E-06	Gadd45gip1	-2.37	1.16E-03	Kcnk3	1.71	4.12E-02
Pet100	2.33	1.32E-06	Ahnak	-2.36	1.04E-03	Cacna1g	1.67	1.94E-03
Vcpkmt	2.33	1.68E-05	Stra13	-2.36	2.14E-04	Flywch2	1.67	1.60E-02
2410015M20Rik	2.29	1.51E-06	1810026B05Rik_1	-2.35	6.37E-04	Jund	1.66	2.21E-10
Nme2	2.27	6.60E-06	Tmem256	-2.33	1.98E-04	Cacna1i	1.64	1.84E-02
Angptl6	2.27	1.34E-05	Syt1	2.33	1.62E-02	Sptbn2	1.63	2.24E-06
Snhg3	2.26	2.27E-04	Prkcg	2.32	2.09E-02	Chadl	1.62	3.04E-03
Plin5	2.26	6.48E-03	Trappc6a	-2.31	4.69E-04	Car8	1.61	1.33E-07
Rps16	2.25	2.85E-05	Gm10687	-2.31	2.34E-02	Ank1	1.61	1.28E-03
Smc2os	2.24	4.22E-03	Cgref1	-2.30	1.57E-03	Calb2	1.59	1.78E-04
AA465934	2.22	4.54E-03	Tppp3	-2.30	2.50E-04	Romo1	1.58	2.12E-08
Gm26534	2.22	4.42E-02	Gm12092	-2.28	3.52E-02	Snhg20	1.58	5.23E-02
Arf5	2.21	4.82E-06	Nkx6-2	-2.27	6.65E-04	Rims4	1.57	2.23E-03
Mrps28	2.21	6.87E-06	Fam120aos	-2.26	1.69E-02	Gpr4	1.56	1.95E-02
3930402G23Rik	2.19	2.10E-03	2610316D01Rik	-2.25	4.42E-02	Ppp1r35	1.55	3.13E-05
Snhg11	2.19	4.50E-04	Cdc34	-2.22	4.95E-04	Gabrd	1.55	9.35E-03
Meg3	2.18	1.75E-04	3930402G23Rik	-2.20	5.15E-02	Dlgap3	1.55	1.57E-02
A330069E16Rik	2.17	1.66E-02	Nme2	-2.20	5.88E-04	Pcp4	1.54	5.57E-04
Mpc1	2.17	8.22E-06	1810022K09Rik	-2.19	4.92E-03	Fbxl15	1.54	4.57E-04
Ppp1r14a	2.17	5.46E-06	Rpl22l1	-2.19	4.93E-04	Enkd1	1.53	4.30E-03
Metrn	2.17	4.50E-06	Isoc2b	-2.19	2.79E-03	Vps37d	1.52	2.65E-03
Ppp1r35	2.16	4.53E-05	2810410L24Rik	-2.19	1.66E-02	Col9a2	1.51	3.80E-02
Hist1h4h	2.15	4.37E-03	Zfp945	-2.18	7.41E-03	Ier5l	1.47	5.73E-05
Ndufb4	2.14	3.51E-05	Gm1673	-2.18	1.14E-02	Golga7b	1.47	4.20E-02
Cdc34	2.14	7.36E-06	Vwc2	-2.18	2.04E-02	Nr2f6	1.46	3.75E-04
Mrpl27	2.13	8.81E-06	Procr	-2.18	4.73E-02	Galnt9	1.45	4.05E-02
Vash2	-2.12	2.18E-02	Saa3	-2.17	3.07E-03	Grin2c	1.44	3.53E-02
Yjefn3	2.12	4.74E-02	Nat14	-2.16	3.24E-03	Uqcrq	1.44	4.74E-09
Adprhl2	2.11	1.01E-05	Serpinb6b	-2.15	2.28E-02	Endog	1.43	3.43E-03

Junb	2.11	2.00E-05	Enho	-2.15	1.01E-02	Ppp2r3d	1.43	5.09E-04
Gm14325	2.11	3.88E-05	Gm14322	-2.14	5.93E-03	Rhpn1	1.43	3.05E-03
Drap1	2.10	7.74E-06	2410006H16Rik	-2.13	8.28E-04	Ssbp4	1.43	4.93E-08
Fam120aos	2.10	1.44E-04	Smim5	-2.13	5.48E-02	Nkx3-2	1.42	2.97E-02
Ppp1r14b	2.10	1.21E-05	Ppp1r14a	-2.12	7.42E-04	Ppp1r1b	1.42	1.11E-07
Nat14	2.10	1.53E-05	Ptpn18	-2.12	3.45E-03	Ccdc124	1.41	1.03E-07
A930006K02Rik	2.08	2.98E-03	Rnaseh2c	-2.12	1.99E-03	Sdsl	1.40	1.04E-03
Ormdl2	2.07	1.60E-05	Rph3a	2.10	7.28E-03	Cdkn1c	1.39	1.28E-02
Mrap	2.07	1.76E-02	Comtd1	-2.10	4.01E-03	Irx1	1.39	3.94E-06
Ubtd1	2.07	1.76E-05	Adprhl2	-2.10	1.35E-03	Unc5a	1.39	2.59E-02
Glrx3	2.07	1.26E-05	Efcab10	-2.09	2.87E-02	Cebpd	1.38	5.66E-06
Car8	2.06	1.90E-05	Nme4	-2.08	8.60E-03	Eps8l1	1.37	1.73E-03
Zeb2os	2.06	9.64E-05	Rps27a	-2.07	4.66E-03	Slc39a4	1.37	3.33E-02
Gm1673	2.05	1.45E-03	Car8	2.06	6.88E-03	Ier2	1.35	2.55E-03
Atp6v0e	2.05	1.30E-05	Dmkn	-2.06	5.42E-03	Chil1	1.35	2.32E-04
Rnf139	2.04	9.30E-04	Tmsb15b1	-2.04	4.49E-02	Cbln1	1.34	7.51E-05
Arl5c	2.04	2.16E-04	Snhg3	-2.04	5.93E-03	Timm23	1.34	3.76E-02
Gm15860	2.04	2.83E-02	Hmga1	-2.03	1.12E-02	Irs4	-1.34	7.05E-03
Ttc9b	2.03	1.90E-03	Rbfox3	2.03	1.64E-02	Abhd8	1.34	8.54E-07
Clec2l	2.03	2.64E-04	Bcl7c	-2.03	1.75E-03	Mblac1	1.33	3.17E-02
Grin2b	2.03	5.80E-03	Miip	-2.03	1.03E-02	Mrpl52	1.33	4.78E-06
Emc8	2.03	3.23E-05	Tagln	-2.02	4.49E-03	Zfp865	1.32	1.68E-04
Iigp1	2.01	1.24E-03	Tspo	-2.02	1.79E-03	Gpx3	1.31	1.12E-08
Hyi	2.00	5.55E-05	Ubtd1	-2.01	5.80E-03	Toporsos	1.31	1.18E-02
Ssbp4	2.00	2.75E-05	Mrpl27	-2.01	2.14E-03	Map1s	1.30	5.48E-05
Fam195a	2.00	2.33E-03	Xlr	-2.01	3.35E-03	Ly6h	1.29	2.42E-03
BC051019	2.00	1.54E-02	Rnf180	-1.99	7.40E-03	Mpc1	1.29	2.13E-06
Lin7b	1.99	8.09E-03	Nos1	1.98	3.75E-02	Sssca1	1.28	3.36E-02
Cd164l2	1.98	3.64E-03	Tnfrsf12a	-1.98	3.13E-03	Rplp2	1.27	4.34E-07
Snrpd2	1.98	2.76E-05	Mxd3	-1.98	3.79E-02	Slc17a7	1.27	8.04E-04
Plekhj1	1.97	4.14E-05	Pmp2	-1.96	2.66E-02	Hic1	1.26	4.48E-02
Flywch2	1.95	1.29E-03	Pop5	-1.96	2.64E-03	Mrpl57	1.26	2.38E-04
Swi5	1.95	3.27E-05	Susd3	-1.95	4.56E-03	Rpl27	1.26	2.30E-02
E530001K10Rik	1.94	1.25E-02	Synpo2	1.95	4.16E-02	2810428I15Rik	1.25	9.96E-06
Stxbp5l	1.94	4.04E-02	Arf5	-1.95	1.82E-03	Dpm3	1.25	8.82E-05
Serpinb2	1.93	1.60E-02	Cenpw	-1.94	4.55E-02	Llgl2	1.25	3.83E-02
3830403N18Rik	1.93	7.91E-03	Zeb2os	-1.94	3.24E-03	Nfkbil1	1.24	8.79E-03
Tspo	1.93	5.40E-05	Gm14325	-1.94	4.93E-03	Crocc	1.24	6.26E-03
Gm19412	1.93	1.46E-02	Pet100	-1.94	1.90E-03	Fam179a	1.24	2.90E-02
Ccdc115	1.92	6.68E-05	Zfp593	-1.93	2.92E-02	Znhit2	1.23	3.68E-04
Trappc6a	1.92	7.86E-05	4933434E20Rik	-1.93	2.06E-03	Slc8a2	1.22	2.00E-02
Tomm40l	1.92	6.15E-05	Hyi	-1.93	3.10E-03	Wfikkn2	1.22	3.22E-04
Enho	1.91	5.01E-05	Fam181b	-1.92	1.10E-02	Tmem160	1.22	4.53E-05
Vps37d	1.91	1.01E-03	Ccdc153	-1.92	7.07E-03	Lzts2	1.22	1.77E-06
6030407O03Rik	1.91	4.79E-03	Glrx3	-1.91	2.26E-03	Pdlim7	1.21	1.43E-05
C1qb	1.90	4.45E-05	Phf11b	-1.91	4.12E-02	Ifitm10	1.21	3.52E-02
Snhg20	1.90	5.35E-03	Wnt4	-1.91	4.12E-02	Il17rc	1.21	6.37E-03
S100a14	1.88	4.23E-02	Sdc1	-1.91	4.41E-02	Nos1	1.20	2.97E-03
Hspb2	1.88	1.51E-02	2410015M20Rik	-1.90	2.20E-03	Celf4	1.20	1.28E-03
Zfp444	1.87	1.25E-04	Apex1	-1.90	3.12E-03	Igfbp6	1.19	4.23E-02
Nudt6	1.87	2.95E-03	C1qb	-1.88	2.29E-03	Ltc4s	1.19	3.77E-02
Chchd1	1.87	7.70E-05	Gm14403	-1.87	4.92E-02	Cox17	1.18	8.84E-03
Bcl7c	1.86	1.01E-04	Vcpkmt	-1.86	1.11E-02	Zfp628	1.17	4.69E-03
Golga7b	1.86	2.53E-03	Nov	-1.86	6.39E-03	Zfp219	1.17	3.60E-06
Gm15972	1.85	4.61E-02	Emc8	-1.86	3.10E-03	Ppp1r14a	1.17	1.93E-05
Bbc3	1.85	6.85E-04	Angptl6	-1.85	1.10E-02	Prkcg	1.17	3.16E-02
Tmem160	1.85	1.24E-04	Bax	-1.85	2.92E-03	Gadd45g	1.16	2.39E-05
Il11ra1	1.85	1.19E-04	Ppp1cc	-1.84	9.29E-03	Ankrd9	1.16	2.05E-02
Grin2a	1.84	1.45E-02	1110038B12Rik	-1.83	4.95E-03	Arhgef33	1.15	3.91E-02
Rabac1	1.84	8.07E-05	Rgs1	-1.82	1.74E-02	1110017D15Rik	1.15	5.02E-02
Rita1	1.84	4.04E-04	Acbd4	-1.82	5.91E-03	Epn3	1.14	1.41E-02
Olfm3	1.83	1.33E-03	Pkdcc	-1.81	3.50E-02	Csf2ra	1.13	1.81E-03
Gm14306	1.83	3.08E-02	Wfdc17	-1.81	5.77E-03	Rplp1	1.13	1.20E-06
Rpl27	1.82	1.56E-03	Drap1	-1.81	3.34E-03	Dlk1	1.12	1.59E-05
Gm17750	1.82	4.55E-04	Taf1d	-1.80	3.09E-02	Chpf	1.12	1.14E-05
Lyrm4	1.82	2.10E-04	Znrf2	-1.80	8.16E-03	Macrod1	1.12	8.55E-04
Card11	-1.82	4.94E-02	Lyrm4	-1.79	1.03E-02	Gm5617	1.11	1.20E-02
Rapsn	1.81	2.40E-02	1110065P20Rik	-1.79	4.72E-02	Bsn	1.11	1.07E-02
Hpca	1.81	2.98E-03	Zfp444	-1.78	1.60E-02	Slc29a4	1.11	9.58E-03
Rasl2-9	1.81	3.73E-02	Sirt6	-1.77	4.55E-02	Rgs8	1.11	1.55E-02

Tenm1	1.80	5.39E-03	Atp6v0e	-1.76	4.38E-03	Sv2b	1.11	1.45E-02
Kcnip2	1.80	5.47E-02	Lage3	-1.76	6.84E-03	H19	-1.10	4.53E-03
4933434E20Rik	1.80	1.19E-04	Mrps12	-1.76	5.19E-02	Rps26	1.10	2.18E-05
Gm10687	1.80	2.33E-04	Rita1	-1.76	4.15E-02	Tmem121	1.09	1.87E-02
Mrps24	1.79	1.73E-04	9130401M01Rik	-1.76	1.41E-02	Fat2	1.08	1.92E-03
2810428I15Rik	1.79	1.95E-04	Mea1	-1.75	5.39E-03	Id3	1.08	3.15E-06
Susd3	1.79	2.45E-04	Mrps24	-1.75	1.20E-02	Pifo	1.07	4.96E-02
Samd1	1.79	1.74E-04	Atp1a3	1.74	5.81E-03	Pou3f1	1.07	2.19E-02
Mea1	1.78	3.00E-04	Tomm40l	-1.74	5.26E-03	Plk5	1.07	2.27E-02
Rbm7	1.77	1.60E-04	Gdf10	1.74	1.28E-02	Akt1s1	1.07	3.80E-05
Galk1	1.77	2.27E-04	Lyrm9	-1.73	3.63E-02	Lmtk3	1.07	1.39E-02
Crlf2	1.77	8.50E-04	Cbx8	-1.72	5.12E-02	Nfkbib	1.06	5.43E-04
Ptpn18	1.77	7.32E-04	Macrod1	-1.72	7.83E-03	Mrps12	1.06	7.22E-04
Kctd8	1.77	9.51E-03	Tradd	-1.72	2.19E-02	Btbd17	1.06	5.75E-04
Crls1	1.77	1.85E-04	Clstn3	1.72	1.48E-02	Bahcc1	1.05	1.28E-03
Ankrd39	1.76	1.32E-03	Ms4a6d	-1.70	6.73E-03	Fam109a	1.05	3.16E-03
Hspbp1	1.76	1.83E-04	Rgs4	-1.70	4.49E-02	2810410L24Rik	1.05	4.46E-03
Rps15	1.76	1.56E-04	Nr2f6	-1.70	1.69E-02	Mrpl34	1.05	7.80E-04
Macrod1	1.74	4.14E-04	Gm11974	-1.70	3.40E-02	Tmem132a	1.04	6.18E-04
Avpi1	1.74	4.56E-04	Cenpk	-1.69	3.81E-02	Sh2b2	1.04	6.80E-03
C1qtnf5	1.74	3.44E-03	Plscr2	-1.69	1.01E-02	Fam171a2	1.04	2.99E-03
Ccne2	1.73	2.39E-03	2810428I15Rik	-1.68	8.35E-03	1110001J03Rik	1.04	2.12E-03
Atad3aos	1.72	1.50E-02	Nudt22	-1.67	1.31E-02	Id1	1.04	6.95E-05
Bax	1.72	2.31E-04	Snap25	1.66	1.14E-02	Dok3	1.03	4.45E-02
Plscr2	1.72	3.43E-04	Mrps26	-1.66	1.47E-02	1500015O10Rik	1.03	1.97E-04
Apex1	1.71	4.07E-04	Plekho1	-1.66	9.81E-03	Ckb	1.02	5.45E-06
Ryr2	1.71	5.17E-03	Tmem141	-1.66	2.29E-02	Avpi1	1.01	1.75E-03
mt-Co3	1.71	4.70E-03	Plekhj1	-1.65	9.20E-03	Ace	1.01	2.93E-04
Csrp2	1.71	2.54E-03	Ppp1r14b	-1.65	1.40E-02	Apba3	1.00	8.40E-04
Runx3	-1.70	5.26E-02	Dusp15	-1.65	7.97E-03	Abca4	1.00	2.50E-02
Tpt1	1.70	2.47E-04	Snrpd2	-1.65	8.58E-03	1500011K16Rik	1.00	2.36E-04
Cgref1	1.70	5.89E-04	Ctla2b	-1.64	1.57E-02	F13a1	1.00	3.57E-02
Rpl13	1.70	4.13E-02	Lsm5	-1.64	1.39E-02	Mt1	1.00	7.64E-06
Gt(ROSA)26Sor	1.70	5.93E-04	Gng13	1.64	4.80E-02	Chchd10	1.00	5.27E-05
Cacna1e	1.70	4.42E-03	Ly96	-1.63	2.19E-02	1700003E16Rik	1.00	1.39E-02
Ift20	1.69	3.36E-04	Cd5l	-1.63	1.15E-02	Gtpbp6	1.00	1.88E-02
Tmem243	1.69	4.66E-04	Slirp	-1.63	8.53E-03	Wdr86	1.00	5.30E-02
Tagln3	1.69	3.03E-04	Cstb	-1.63	9.17E-03	Pigyl	0.99	8.00E-04
Fam71e1	1.68	1.93E-02	Ap1s1	-1.63	8.68E-03	Ahdc1	0.99	5.18E-04
Dgkg	1.68	5.25E-02	Swi5	-1.62	8.15E-03	Galk1	0.99	5.68E-04
Gnb2l1	1.68	2.88E-04	Clic1	-1.62	8.35E-03	Dao	0.99	1.97E-02
Pdcd2l	1.68	4.94E-04	Cebpzos	-1.62	9.85E-03	Hlx	0.98	5.36E-02
Cebpzos	1.67	5.17E-04	Ccdc12	-1.62	1.03E-02	Tbcc	0.98	2.36E-03
Pafah1b3	1.67	8.15E-04	Pcp2	1.61	4.33E-02	Mdfi	0.97	2.38E-03
Zfp931	1.67	7.13E-04	Gnb2l1	-1.61	8.36E-03	Mpst	0.97	2.35E-04
Lsm5	1.67	7.22E-04	Ccdc90b	-1.61	9.96E-03	Comtd1	0.97	3.35E-02
Xlr	1.67	9.70E-04	Ssbp4	-1.61	9.35E-03	Nat14	0.97	6.08E-04
1010001B22Rik	1.67	2.04E-02	Mrps28	-1.61	1.63E-02	Psmg4	0.96	1.39E-02
Tmem240	1.67	1.65E-02	Metrn	-1.60	8.73E-03	Nckap5l	0.96	3.73E-02
Cyc1	1.66	3.47E-04	S100a4	-1.60	1.15E-02	Pgp	0.95	1.75E-03
Rpl13a	1.66	3.40E-04	Rgs17	-1.60	4.77E-02	Lrrc4b	0.95	1.30E-04
Lage3	1.66	4.54E-04	Josd2	-1.59	1.08E-02	Dmrta1	-0.95	1.89E-03
Atp6v0b	1.65	3.73E-04	Sirt7	-1.59	1.73E-02	Cdkn2a	0.95	2.41E-02
Pou2f1	1.64	2.59E-02	1110046J04Rik	-1.58	2.48E-02	Mdk	0.95	1.94E-03
Mdfi	1.64	9.52E-04	Gin1	-1.58	4.86E-02	Rara	0.95	3.44E-02
Actr6	1.64	5.77E-04	Dnajc19	-1.58	1.39E-02	Dgcr6	0.94	1.72E-02
Sep_15	1.64	3.98E-04	Tstd3	-1.58	4.25E-02	Map3k10	0.94	7.23E-04
Ramp3	1.64	2.84E-02	Galk1	-1.58	1.45E-02	Egln2	0.94	2.16E-04
1700016K19Rik	1.63	1.45E-02	Tmem160	-1.57	1.62E-02	Stmn3	0.94	2.73E-04
Snrpc	1.63	9.04E-04	Snhg6	-1.57	1.52E-02	Arhgef19	0.94	2.10E-04
RP24-80F7.5	1.62	2.11E-02	Tmf1	-1.57	1.74E-02	Zfp579	0.94	6.42E-03
Fam174a	1.61	5.77E-04	Sap30	-1.57	2.28E-02	Gm13111	0.94	4.98E-02
Ms4a6d	1.60	6.23E-04	Atp6v0b	-1.57	1.04E-02	2410006H16Rik	0.93	1.77E-03
Pop5	1.60	7.37E-04	Pdcd2l	-1.56	1.78E-02	Adgrb1	0.93	2.38E-03
C630043F03Rik	1.60	2.41E-03	Snhg12	-1.56	3.29E-02	Itpr1	0.93	1.62E-04
Cytip	1.60	4.27E-02	Sdf2l1	-1.56	2.13E-02	Cactin	0.93	3.01E-03
Stard6	1.60	4.27E-02	Agpat2	-1.55	4.08E-02	Zfp444	0.93	2.95E-03
Slirp	1.60	6.86E-04	Ppil3	-1.55	1.40E-02	Sema6b	0.93	5.52E-03
Ucma	1.60	1.10E-03	Pdlim2	-1.54	1.25E-02	Irf2bpl	0.92	2.39E-04
1700047M11Rik	1.59	1.10E-03	Crls1	-1.54	1.51E-02	Zfp428	0.92	1.04E-02

Coro1a	1.59	6.54E-04	Rrp9	-1.54	1.78E-02	St6galnac2	0.92	2.52E-02
Clic1	1.59	6.19E-04	Coro1a	-1.54	1.28E-02	Cbln3	0.91	3.99E-03
Uqcrq	1.58	7.08E-04	1700047M11Rik	-1.54	3.66E-02	Sf3b5	0.91	1.26E-03
Zfp771	1.57	3.74E-03	Fkbp8	-1.54	1.22E-02	Hspbp1	0.91	3.07E-04
Acbd4	1.57	1.06E-03	Rps15	-1.53	1.23E-02	Klhl36	0.91	1.82E-02
Isoc2b	1.57	1.79E-03	Coa3	-1.52	3.27E-02	Atp13a2	0.91	3.08E-04
Ly96	1.57	2.67E-03	Arhgdig	-1.52	4.14E-02	Dohh	0.90	1.18E-03
Tma7	1.57	8.65E-04	Amdhd2	-1.52	1.55E-02	Mex3d	0.90	5.64E-03
Lmo1	1.57	4.87E-02	Sptbn2	1.52	3.56E-02	Cplx1	0.89	1.22E-02
L3hypdh	1.56	5.05E-03	Dpf1	-1.52	5.17E-02	Alkbh7	0.89	8.86E-03
Upp2	1.56	2.50E-03	Rbm7	-1.52	1.68E-02	Ifi27l2a	0.89	1.43E-03
Crtam	1.56	8.09E-03	Slc12a5	1.52	3.86E-02	Spint2	0.88	8.26E-03
1810026B05Rik_1	1.56	4.26E-03	Sh3gl2	1.52	2.93E-02	Fbl	0.88	5.36E-02
Tnfrsf12a	1.56	1.04E-03	Chchd1	-1.51	1.69E-02	Snx21	0.88	8.02E-03
Pvalb	1.55	1.02E-03	Sep_15	-1.50	1.37E-02	Thap3	0.88	2.14E-02
1110008P14Rik	1.55	6.47E-03	Tbca	-1.50	1.80E-02	Adcy1	0.87	1.85E-03
Gabra6	1.55	2.09E-03	Mrpl54	-1.50	3.21E-02	Tcf3	0.87	9.20E-04
Usmg5	1.55	1.01E-03	Lyrm2	-1.50	2.31E-02	Shf	0.87	3.94E-02
Gm14418	1.55	2.93E-02	Snrpe	-1.49	1.83E-02	Hmg20b	0.87	4.70E-03
Clec2d	1.55	9.99E-03	Igfbp2	-1.49	1.91E-02	Rnf126	0.87	9.00E-03
Dpm3	1.55	1.63E-03	Pafah1b3	-1.49	2.85E-02	Ppia	0.86	3.82E-04
Serp2	1.55	4.91E-03	Dnm1	1.48	2.75E-02	6030419C18Rik	0.86	1.60E-02
A430005L14Rik	1.54	1.49E-03	Dao	1.48	4.92E-02	Tesc	0.86	3.26E-02
Itpka	1.54	3.20E-02	Snrnp25	-1.48	2.47E-02	Ubxn10	0.86	4.22E-02
Snrpe	1.54	1.14E-03	Rpl13a	-1.48	1.50E-02	Med25	0.86	5.18E-04
Fam96b	1.54	1.12E-03	Abhd16a	-1.48	1.58E-02	Papss2	-0.85	4.20E-02
1500011K16Rik	1.54	1.17E-03	Gria1	1.48	1.53E-02	Numbl	0.85	1.08E-02
Cnr1	1.53	1.94E-03	Ak1	-1.46	1.88E-02	Fance	0.85	6.55E-03
Abhd16a	1.53	9.86E-04	Bad	-1.46	2.58E-02	Irf8	0.84	2.91E-02
Efna3	1.53	4.54E-02	Nt5c	-1.46	2.21E-02	Uqcr11	0.84	5.63E-04